TÉCNICO LISBOA

Development of Raman spectroscopic methodology for *in vivo* determination of skin penetration and permeation of topically applied compound

Patrícia Robalo Curto

Thesis to obtain the Master of Science Degree in

Biological Engineering

Supervisors: Dr. Gerwin Puppels / Professor Luís Filipe da Silva dos Santos

Examination Committee

Chairperson: Professor Duarte Miguel de França Teixeira dos Prazeres

Supervisor: Professor Luís Filipe da Silva dos Santos

Member of the Committee: Dr. Peter Caspers

June 2018

Preface

The work presented in this thesis was performed at the RiverD International B.V. (Rotterdam, The Netherlands), during the period September 2017 to February 2018, under the supervision of Dr. Gerwin Puppels. The thesis was co-supervised at Instituto Superior Técnico by Prof. Luís Santos.

RiverD has the mission to market innovative solutions for unmet diagnostic needs based on Raman spectroscopic analysis of cell and tissues. The company is a spin-out of the Erasmus Medical Center in Rotterdam, the Netherlands.

Acknowledgements

First and foremost, I would like to thank Dr. Gerwin J Puppels for this unique opportunity to join his highly motivated group at RiverD International and to always motive me to achieve better results.

I would like to thank all the professionals and colleagues at RiverD International for the great mentoring and friendship that help me to grow in this project.

I would like to express my deep gratitude to Dr. Peter Caspers that challenged me with new ideas and great discussions, so this project could move forward with the most promising results.

Finally, I would like to express my gratitude to Prof. Luís Santos, who supported the work as the official supervisor at IST Lisbon and was an essential help in the last phases of this thesis.

To all my friends and family that supported me throughout these years, I thank for all the great memories and experiences shared.

A special gratitude to my parents that supported me and always believed in me. You push me to thrive in every aspect of my life, it's been a long way, but I couldn't do it without you.

Abstract

The Raman spectroscopic methodology developed in this study provides reliable quantitative information for a wide range of applications in skin for different active pharmaceutical ingredients (APIs) in topical skin products.

The method premise is based on a quantitative calibration for these APIs, that relates the mass ratio of a set of API solutions with the intensity ratio of the Raman signals of these solutions. A set of different calibrated solvents were added to the library methodology that enable the method to be universal, in theory, for any API that can be dissolved in this solvent database.

The starting point of this methodology states that bovine serum albumin can be use as approximation to keratin in the stratum corneum, with an error of approximately 15%, due to spectral similarities in shape and intensity. Thus, dissolving BSA in water and doing a calibration of these solutions enables water to be related to keratin and to be the first solvent added to the method, with a quantification factor of $3{,}294 \times 10^{-5}\ mg_{water}/g_{keratin}$ and a relative error of $\pm 19{,}80\%$.

New water-soluble APIs and solvents can be calibrated and added to a library for *in vivo* studies in skin, their addiction to a methodology library expands the possibility of calibrating other APIs that are insoluble in water. And in fact, most APIs in this thesis present higher solubility in ethanol.

Ethanol in water calibration has a quantification factor of $1{,}409 \times 10^{-6}\ mg_{ethanol}/g_{keratin}$ with a relative error of $\pm 22{,}53\%$.

Moreover, the premise that this method is not limit to water and ethanol-soluble APIs was validated, since acetone (quantification factor of $1{,}167 \times 10^{-6}\ mg_{acetone}/g_{keratin}$ and relative error of $\pm 24{,}59\%$), and MCT oil (quantification factor of $1{,}838 \times 10^{-6}\ mg_{MCT\ Oil}/g_{keratin}$ and relative error of $\pm 27{,}33\%$) were also calibrated and tested with different APIs.

In vivo skin studies with salicylic acid, ibuprofen, caffeine and oleic acid were done to test the application of this method to topically applied compounds in skin.

Keywords: Raman spectroscopy; *In vivo*; Skin Penetration; API; Multiple Least Squares Regression

Thesis Outline

The objective of this thesis is to develop an optimized Raman spectroscopic methodology for *in vivo* determination of skin penetration and permeation of topically applied compounds. This thesis is divided in five different chapters.

Chapter 1: Introduction

The first chapter starts by giving context to the thesis theme, by explaining the applications and importance of the work developed, as well as the advantages of using this method compared to others.

This chapter also gives an insight of the theoretical background of the method used in this thesis, starting by explaining the general approach of the method and then elucidating the number of premises and approximations that were done to have a viable methodology.

Chapter 2: Literature Review

A literature review of the basic principles of the main subjects discussed is presented as well as different approaches of calibration methods used in Raman spectroscopy.

Chapter 3: Materials and Methods

This chapter gives an insight of all the instrumentation and software used for all the Raman experiments, as well as a detailed description of three variations of the API calibration method optimized in this thesis: calibration of BSA in water; calibration of ethanol in water and a general API calibration.

Chapter 4: Results and Discussion

The chapter of the results is compiled with its discussion. The chapter is mainly divided by two parts: one with all the material calibrations done in this thesis and another with the results of applications of the method developed: *In vivo* Skin Measurements.

The material calibrations are the core of this thesis, since the method had to be optimized, validated and updated. Therefore, the results of calibration presented are divided by the solvent chosen to calibrate each API. There are four subchapters: APIs in Water; APIs in Ethanol; APIs in Acetone and APIs in MCT oil.

Chapter 5: Conclusions

This last chapter summarizes the work done and indicated future work proposals.

Contents

List of Figures

List of Tables

List of Abbreviations

API	Active pharmaceutical ingredient
A.U.	Arbitrary Units
β	Fit coefficient
BSA	Bovine serum albumin
c	Calibration constant
CCD	Charge Coupled Device
CLS	Classical least squares
f	Scale factor
ILS	Inverse least squares
IR	Infrared spectroscopy
LSR	Least squares regression
m	Mass
MCT oil	Medium-chain triglyceride oil
MLR	Multiple linear regression
MLSM	Multiple least squares method
NIR	Near-infrared spectroscopy
NMF	Natural moisturizer factor
OLS	Ordinary least squares
PCR	Principal component regression
PG	Propylene glycol
PLS	Partial least squares
R	Raman spectrum
SA	Salicylic acid
SC	Stratum corneum
SNR	Signal to noise ratio
UV	Ultraviolet
VE	Viable epidermis

Chapter 1

Introduction

1.1. Background and Applications

Application of topic compounds is a widely used method in cosmetics and in the treatment of different skin conditions, which are driven by an affluent industry that is expanding its market every day. Moreover, dermal toxicology is a field of great interest to study skin exposures to toxins and toxicants.

The medical and cosmetic industries have been interested in the study of human skin, namely its molecular composition, as well as the different pathological and cosmetic conditions. Skin penetration and permeation of different topically applied compounds is a major tool for *in vivo* skin studies.

Non-invasive techniques that provide information about molecular composition, structure, and interactions are crucial to understand the relation between skin disease and biochemical changes in skin, as well as for the development of penetration enhancers for transdermal drug administration. [1]

Raman spectroscopy has been used in the biomedical field and it has a great potential for skin studies. It has been demonstrated that changes in molecular structure and composition on the skin can be detected in the Raman spectra, without altering the chemical composition of living biological tissues.

Topically applied compounds in human skin must permeate through a highly effective barrier to water, chemicals, and microbes. The first barrier is known as stratum corneum, SC, which is the outermost layer of the epidermis and it's known to play a dominant role in this barrier skin function. In the field of transdermal delivery, the dermis provides a minimal barrier to the delivery of most polar drugs, while the SC is viewed as a separate membrane in topical and transdermal drug delivery studies. [1]

Raman and Infrared, IR, spectroscopies are complementary techniques that can be used to study the mechanisms involved in this barrier function. Yet, Raman spectroscopy has certain advantages, such as its relative insensitivity to water, that justify its increasing popularity for skin characterization. [2]

Although, near-infrared, NIR, and IR spectroscopy analysis can offer spectroscopic ''fingerprint'' information similar to Raman spectroscopy, these methods have significant more disadvantages. NIR doesn't provide specific molecular identification information inherent to IR and Raman spectroscopy, and it isn't sufficiently spatially resolved to offer composition profiles as a function of depth. [3]

IR has been used for *in vivo* studies of SC hydration and permeability, due to the strong absorption of mid- and far-IR radiation by water. However, the penetration depth in a naturally hydrated tissue such as the skin is limited to a few micrometres. Therefore, in an *in vivo* IR spectroscopy experiment only the outermost layer of the SC is sampled. [4]

In contrast, Raman spectroscopy can be applied to obtain information regarding the molecular composition of the skin down to several hundred micrometres below the skin surface. Therefore, the positions, relative intensities, and shapes of the bands in a Raman spectrum carry information about the molecular composition of a sample and about molecular structures and interactions present. [4]

There've been several different methods used to study *ex vivo*, which require material to be removed from the skin and analysed *in vitro*. A drawback of these is that they're invasive, inherently influence the skin—regeneration stops, immune response ceases, and metabolic activity is usually lost. They alter the system under investigation either by extraction of compounds from the skin or by physical disruption of cell layers, these invasive processes may not translate directly to the *in vivo* situation. [1]

Pharmaceutical skin products in the market have two different components, an active pharmaceutical ingredient, API, and the excipients. API is the main ingredient present, mainly for therapeutic purposes, while excipients can enhance the permeation of the API into skin.

Prior to the advent of *in vivo* Raman spectroscopy, a number of other methods have been used to monitor possible paths of APIs or other substances as they penetrate the skin, or to detect and follow reactions of interest in skin tissues. Some of the major methods include: Franz cells, ^{14}C labelling, biopsies, tape stripping, NIR and IR spectroscopy. [3]

Microspectroscopic Raman measurements on tissues are used for in vivo clinical studies, but require an optimized instrumentation for the application. Recently, specific Raman instrumentation has been developed to skin studies and made commercially. [5]

All the measurements in this thesis were carried out in a NIR-Raman microspectrometer, it's the most sensitive system on the market and it's RiverD's second generation Skin Composition Analyzer (gen2-SCA, RiverD International B.V., Rotterdam, The Netherlands). This microspectrometer enables non-invasive *in vivo* measurements with a method that can provide detailed information about the molecular composition of the skin and concentration gradients in the skin. [1], [6], [7]

This thesis focuses on the optimization of a method that can quantify the concentration of APIs in the skin, relative to keratin mass in the SC (e.g., mol / g keratin or g / g keratin), since components in the SC are in an environment that predominantly consists of the protein keratin and water. The APIs tested in this thesis are used for a wide range of applications, since they can be classified as: corticosteroid; chemical UV filter; local anaesthetic; nonsteroidal anti-inflammatory drug; sex hormone; etc.

Although, this method is focused on skin penetration and permeation of different APIs, it's not limited to those. Skin product excipients can be studied as well, enabling a more complete approach to study a skin product, since there's are ingredients that can interact with each other and with skin.

APIs quantification using Raman spectroscopy should use an internal standard, relative to which the concentration is determined. This standard can be a quantification of a soluble component relative to its solvent, resulting in known mass ratio that can be directly link to Raman intensity in a spectrum.

After optimization of this quantification method that enables the calibration of a library of different APIs, an application example is presented in the Chapter 4.6, where four skin products were tested by a non-invasive *in vivo* optical monitoring of the penetration of the active molecules through the skin.

The method has the capacity to provide qualitative, semi-quantitative and quantitative information. Qualitative information since it can answer questions such as: "did the product penetrate into the skin?"; "how far into the skin?"; "how fast?"; "how long does it stay in the skin?". On the other hand, quantitative information can state how much product penetrate into the skin ($\mu g/cm^{-2}$) or what was the flux of that product penetration ($\mu g/s^{-1}.cm^{-2}$). Moreover, the semi-quantitative information provides comparison of efficiency of delivery for different APIs formulations and its delivery for different application times.

1.2. Thesis Premise

API calibration using Raman spectroscopy has the premise that the concentration of a compound is proportional to its Raman intensity in a spectrum. Therefore, the Raman signal is concentration dependent function enabling its quantitation in set of APIs solutions.

Any quantitative analysis involves measurement of a test sample and comparison with standards of known concentration. The resulting calibration plot reproduces the relationship between the Raman intensity ratio and the analyte concentration. Provided appropriate standards for calibration of an analytical method selected, vibrational spectroscopy is a valuable potential technique for quantitative analysis. [8]

Moreover, vibrational spectroscopy has different advantages, such as: it has a wide variety of different states of matter of the sample studied; it can clearly separate peaks that are often found in the Raman spectra; it has unique bands that frequently allow multicomponent analyses of mixtures; typically, the sample preparation is relatively simple for analysis. [8]

The intensity of a Raman signal is characterized by a number of factors, including incident laser power, frequency of the scattered radiation, efficiency of the grating (in the case of dispersive instruments) and detector, absorptivity of the materials involved in the scattering, molar scattering power of the normal mode, and the concentration of the sample. [9]

In this method, the Raman intensity in a spectrum of an API can be characterized by equation 1.1, where k_{API} is an API coefficient which depends its molecular structure and Raman signal and ρ_{API} is the density of the API. The remaining variables are instrument and experiment dependent, where I_{laser} is the laser power, $f(\Omega, V)$ is a function dependent on the volume of measurement, V, and the solid angle of detection. Lastly, $e(z)$ is dependent on the depth of the measurement, since for higher depths there can be less Raman signal detected due to increasing reflection and scattering of the Raman signal.

$$R_{API} = [k_{API} \times e(z) \times I_{laser} \times f(\Omega, V)] \times \rho_{API} \tag{1.1}$$

Quantification of molecular species using Raman spectroscopy almost uses an internal standard, relative to which the concentration is determined. The only exception is when the exact geometry and collection efficiency of the system are known, which would enable a direct measurement of the number of scattering molecules. This approach never applies to *in vivo* Raman measurements.

A practical solution can be the quantification of a soluble component relative to its solvent, since the mass ratio is also known, presented in equation 1.2. The density of a material is equal to its mass divided by the volume of measurement, and since this volume is the same between the two materials it can be discarded. Moreover, the rest of the variables that are material, experiment and instrument dependent cancel out of the equation, resulting in just one constant, and the ratio of the two material constants $c_{API}/c_{Solvent}$ is called the calibration constant.

$$\frac{R_{API}}{R_{Solvent}} = \frac{[k_{API} \times e(z) \times I_{laser} \times f(\Omega,V)] \times \rho_{API}}{[k_{Solvent} \times e(z) \times I_{laser} \times f(\Omega,V)] \times \rho_{Solvent}} \leftrightarrow$$

$$\frac{R_{API}}{R_{Solvent}} = \frac{c_{API} \times (m_{API}/V)}{c_{Solvent} \times (m_{Solvent}/V)} = \frac{c_{API}}{c_{Solvent}} \times \frac{m_{API}}{m_{Solvent}} \tag{1.2}$$

The use of an internal normalization standard makes the expression invariant to instrument, laser power, measurement volume, etc. Therefore, equation 1.2 represents a linear function where the calibration constant is equal to the slope of the Raman intensity ratio plotted versus the mass ratio.

The goal of every API calibration is first to create a so-called fit model that's specific to the API that is being calibrated and it's going to be used in the multiple least squares fit method, MLSM, described in

detailed in chapter 3.3.3. The accuracy of this fit model with the combination of good quality measurements of the data set determines the precision of the calibration.

This method is robust and can be easily automated. The fit model is created with the maximum components that can be differentiated within a Raman spectrum of an API solution. All these together must give an optimal fitting result of each solution spectrum, that is an optimal representation of all components in a solution spectrum.

This fitting using MLSM results in an estimation of the fit coefficients of each component represented in the fit model. The fit coefficients of the API and the solvent represent an approximation to R_{API} and $R_{Solvent}$. Since, each fit coefficient is in fact a scale factor that enables the scaling of the reference spectrum to its Raman intensity in the solution spectrum.

The fit model of calibration has two components that are chosen by the user in the calibration experiment, the reference spectrum of the API and a reference spectrum of the solvent.

The API reference spectrum shouldn't be the raw material itself, since crystal spectra has too many differences compared to the API dissolved in the solutions, resulting in poor fitting. Thus, this spectrum must always be processed from a solution with the highest API Raman signal. To achieve a reference spectrum of every API, the extraction of intensity contribution of the API in the solution must be processed manually, leading this approach to have an intrinsic error.

Ideally, the API reference spectrum should be processed automatically. However, no mathematical method was yet developed to optimize such requirement, the error in this step was too high to consider any feasible automatic approach.

This fitting has the premise that a good calibration doesn't have spectral changes between the API reference spectrum and the solutions used in the experiment. However, the range of concentrations in the calibration data set must be chosen to achieve an optimal calibration. Since, there're spectral changes with the increase of an API concentration in solutions due to interactions with the solvent that might result in low quality calibrations, discussed in chapter 4.

The quantitation of different materials has the starting point of a generic methodology for water-soluble and ethanol-soluble materials. However, the method should, in theory, be evolved and applied to other solvents as well, as long these solvents are calibrated as well.

The application of the calibration method in this thesis is to quantify Raman signals of APIs in the SC, into actual concentrations of the API in skin in units of $mg\ API/g\ keratin$.

Components in the SC are in an environment that predominantly consists of the protein keratin and of water. In this case, the quantification determines the amount of an API relative to the wet or dry weight of the SC. However, keratin is insoluble in most common solvents used in this study, which hinders the use of calibration solutions with keratin and a solvent in various concentrations.

An alternative protein, bovine serum albumin (BSA) has been used as an approximation in the method, since it dissolves in water. It was chosen due to similar amounts of BSA and keratin in *V* give similar Raman signals, both in intensity and spectral shape. [5] Since BSA is soluble in water, this method has been used to quantify water in the SC, in which the Raman signal of water is determined relative to the Raman signal of keratin.

The quantification of an API in skin, the relation between an API and keratin is given by equation 1.3.

$$\frac{R_{API}}{R_{keratin}} = \frac{c_{API}}{c_{keratin}} \cdot \frac{m_{API}}{m_{keratin}} \tag{1.3}$$

If the API is water-soluble, its calibration constant is determined by several intermediate steps derived from different calibrations constants, equation 1.4.

$$\frac{c_{API}}{c_{keratin}} = \frac{c_{API}}{c_{water}} \times \frac{c_{water}}{c_{BSA}} \times \frac{c_{BSA}}{c_{keratin}} \quad (1.4)$$

However, if an API isn't soluble in water, another solvent must be chosen to dissolve it, and its calibration constant as to be linked, ultimately, to keratin to be quantified in skin, equation 1.5.

$$\frac{c_{API}}{c_{keratin}} = \frac{c_{API}}{c_{solvent}} \times \frac{c_{solvent}}{c_{water}} \times \frac{c_{water}}{c_{BSA}} \times \frac{c_{BSA}}{c_{keratin}} \quad (1.5)$$

Every calibration is subjective because of the user dependent step of choosing the references in the fit model. Moreover, an API quantification in skin is going to have a chain of errors that is dependent on the mathematical method chosen and the library used to estimate the calibration constant to keratin.

In summary, in theory a database can be created for a large collection of different materials. It also means that the results of different penetration experiments can be compared and can be reproducible, even if the measurements have been done on different Raman instruments.

1.3. Thesis Contribution

The methodology in this thesis was already developed by RiverD International in previous studies, especially for ethanol and water-soluble APIs. There are several *in vivo* studies done for an API quantification in skin in units of normalized concentration. [1], [7] Or even in arbitrary units. [10] More recent ones with this methodology involve the quantification in units of $mmol_{API}/g_{keratin}$. [11]

Nevertheless, the previous method needs to be updated and optimized. Moreover, new premises were tested and validated, enabling an extension and evolution of the calibration method.

The previous API and solvent library used in the previous method was done in an older RiverD's device. RiverD is commercializing a new device that results in more accurate Raman measurements, and since this method is a new service available by the company, it needed to be updated with new data.

In the previous calibration method, the results had some difficulty on being reproducible with different calibration experiments, since small variations with the data analysis resulted in variations of up to 25% in the calibration constants, therefore the method wasn't robust enough.

The calibration of BSA-water, ethanol-water and the *Quanti* tool of the general API calibration method were optimized, as indicated in chapter 3.3.2. The most important feature implemented in this calibration was a normalization of the spectra in the fit model. Different types of normalizations were studied and the one chosen was crucial to enable the method to be more reproducible and robust.

The *Quanti* tool was updated to have a new feature, the API reference spectrum was automatically processed before, however since this approach wasn't viable, the tool now has the option to insert the final reference after its manual processing. A new Matlab tool was created to automatically add new calibrated solvents to the *Quanti* tool library.

Validation models for these calibrations were studied as well, permitting the method to have a valid relative error for the first time. Moreover, this thesis validated the premise that new solvents can be included in this methodology, not only water and ethanol, but also other organic solvents and oil.

In summary, an optimization of API calibration method was concluded and a relative error of the method was estimated. New data was collected which resulted in a library that includes 6 solvents of choice and 18 APIs calibrated, which is a starting point for a method with great potential in the pharmaceutical and cosmetic market.

Chapter 2

Literature Review

2.1. Raman Spectroscopy

2.1.1. Vibrational Spectroscopy

Spectroscopy has a broad number of different techniques that use radiation to study the structure and properties of matter, by measuring and interpreting spectra that arise from the interaction of electromagnetic radiation with matter. In summary, spectroscopy is an experimental subject that studies the absorption, emission or scattering of electromagnetic radiation by atoms or molecules. [12]

Several spectroscopic techniques have been developed, covering different ranges of the electromagnetic spectra that can be defined as a function of wavelength, Figure 2.1.

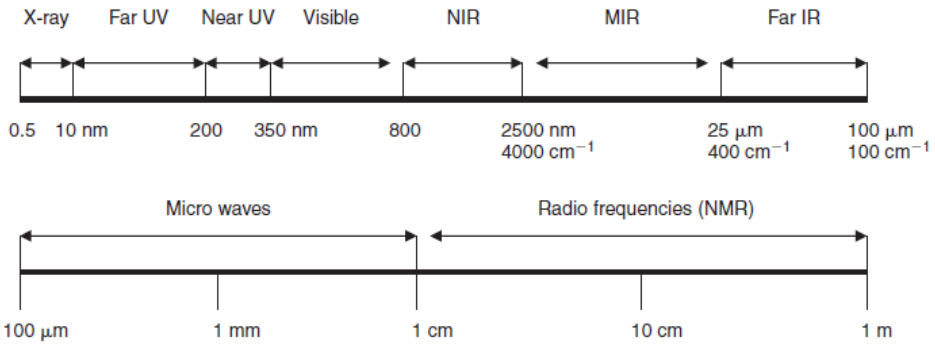

Figure 2.1 - Spectral regions of interest for analytical purposes, as a function of wavelength. [13]

Vibrational spectroscopy is a branch of molecular spectroscopy that includes several different techniques to detect vibrations in molecules for the elucidation of its structure, the most important of which are mid-infrared (IR), near-IR, and Raman spectroscopy.

They are widely used to provide information on chemical structures and physical forms, to identify substances from the characteristic spectral patterns ('fingerprinting'), and to determine quantitatively or semi-quantitatively the amount of a substance in a sample. Samples can be examined in a whole range of physical states or in bulk, as microscopic particles, or as surface layers. [8], [12]

IR spectroscopy was the first structural spectroscopic technique widely used by organic chemists. In the 1930s both IR and Raman techniques were experimentally challenging with only a few users.

The phenomenon of inelastic scattering of light was first postulated by Smekal in 1923 and first observed experimentally in 1928 by Raman and Krishnan, discovering the Raman scattering by explaining the shift in wavelength of a small fraction of radiation scattered by molecules, having different frequency from that of the incident beam. [8], [14]

2.1.2. Basic Principles

For electromagnetic radiation, important parameters are: wavelength (λ), frequency (ν), and wavenumber, $\bar{\nu}$, number of waves per unit length), related by equation 2.1, where *c* is the speed of light and *n* the refractive index of the medium it is passing through.

$$\bar{\nu} = \frac{\nu}{(c/n)} = \frac{1}{\lambda} \tag{2.1}$$

Two fundamental studies performed by Planck on black-body radiation and Einstein on the photoelectric effect show the quantum nature of light energy. [13] Radiation is emitted from a source in discrete units called photons where the photon frequency, ν, and photon energy, *Ep*, are related by equation 2.2, where *h* is the Planck's constant.

$$E_P = h\nu \tag{2.2}$$

When light interacts with matter, the photons which make up the light may be absorbed, scattered or may not interact with the material and may pass straight through it.

It is possible for a photon to interact with the molecule and scatter from it. The scattered photons can be observed by collecting light at an angle to the incident light beam, the efficiency increases as the fourth power of the frequency of the incident light. [14]

2.1.3. Raman Scattering

Light scattering phenomena may be described in terms of electromagnetic radiation produced by oscillating dipoles induced in the molecule by the electromagnetic fields of the incident radiation. In a typical Raman experiment, a laser is used to irradiate the sample with monochromatic radiation. Laser sources are available for excitation in the UV, visible, and near-IR spectral region. [8]

There's two types of light scattering, elastic and inelastic. In elastic scattering there's essentially no appreciable change in energy, and it's at the same type the most intense form of scattering, since it occurs when the electron cloud relaxes without any nuclear movement. This is also known as Rayleigh scattering. [14] In terms of energy states, when light is incident on a molecule, it can interact with the molecule but there's no net exchange of energy, $E = 0$, so the frequency of the scattered light is the same as that of the incident light, $E = E_0$, presented in Figure 2.2.

Inelastic scattering of light, also called Raman effect, results in a shift in wavelength of radiation scattered by molecules, which has a different frequency from the incident beam. When a light wave, considered as a propagating oscillating dipole, passes over a molecule, it can interact and distort the cloud of electrons around the nuclei. This energy is released in the form of scattered radiation. [15]

The induced dipole moment occurs as a result of the molecular polarizability, where the polarizability is the deformability of the electron cloud about the molecule by an external electric field. [8]

Raman scattering is a two-photon event, since it's the change in polarizability of the molecule with respect to its vibrational motion. The interaction of the polarizability with the incoming radiation

creates an induced dipole moment in the molecule, and the radiation emitted by this induced dipole moment contains the observed Raman scattering. [16]

This shift in photon frequency due to excitation or deactivation of molecular vibrations results in the photon losing some amount of energy or gaining energy. [15] Thus, this shift depends upon the chemical structure of the molecules responsible for scattering. Raman spectroscopy uses scattered light to gain knowledge about molecular vibrations which can provide information regarding the structure, symmetry, electronic environment and bonding of the molecule.

Raman scattering can be divided in two types of scattering, Stokes and Anti-Stokes scattering, presented in Figure 2.2. The light can interact with the molecule and the net exchange of energy is the energy of one molecular vibration. If the interaction causes the light photon to gain vibrational energy from the molecule then the frequency of the scattered light will be higher than that of the incident light ($E = E_0 + E_v$), known as anti-Stokes Raman scattering. However, if the interaction causes the molecule to gain energy from the photon then the frequency of the scattered light will be lower than that of the incident light ($E = E_0 - E_v$), this process is known as Stokes Raman scattering. [15]

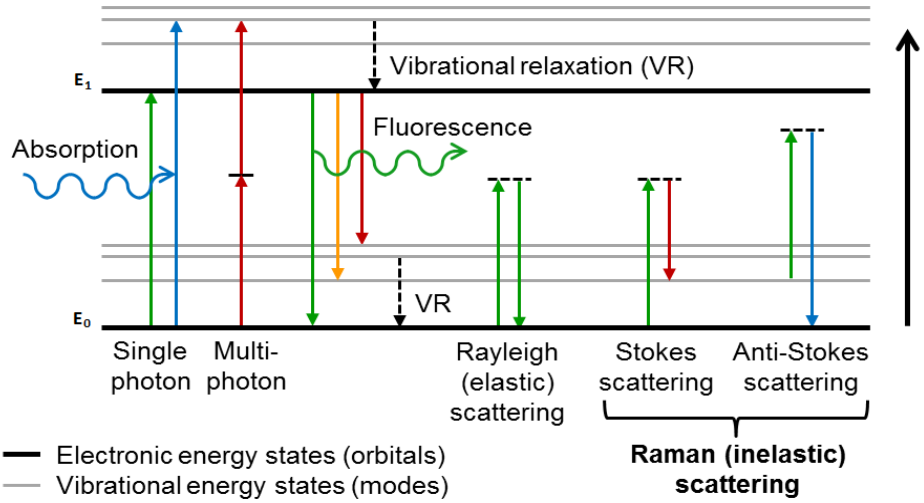

Figure 2.2 - Mechanism of Absorption, Fluorescence and Raman scattering. [17]

The dipole moment oscillations of a molecule can emit scattered radiation with the same frequencies as Rayleigh, Raman anti-Stokes and Raman Stokes frequencies. If a molecular vibration doesn't cause a change in the polarizability, then there's no amplitude modulation of the dipole moment oscillation and there's no Raman Stokes or anti-Stokes emission, no Raman bands can be observed. [8]

2.1.4. Raman Spectra

A Raman spectrum can be studied in two different regions, the region of group frequencies which gives increase to strong bands above the 2500 cm^{-1} range, and the fingerprint region featuring bands below 2500 cm^{-1} that can be weaker. Nevertheless, this thesis focuses all API calibration in the fingerprint region of the spectra, since it's the region that can give more information about the molecules studied.

A Raman experiment can result not only in Raman signal, but some noise or background can appear in the spectra. The quality of a spectrum is often characterized by its signal to noise ratio (SNR), an optimization parameter which aims to increase the signal and reduce the noise. This parameter depends on the instrument being used, especially from the charge-coupled device (CCD) present, and the conditions set for the Raman experiment. The processing of a spectrum often includes a spike filter, due to background light such as cosmic rays, which can hit the instrument detector.

As it was explained, analysing a spectrum with a division of regions by band's shape and position can give information about a molecular structure, however this is a limited feature. For a broad interpretation of Raman spectra, Appendix I has a table of functional groups by region of the spectrum.

2.2. Human skin

Human skin is the largest organ of the integumentary system, it's known to have several vital different functions, such as: protection; heat regulation; absorption; water resistance; immunity; etc. It's composed by three primary layers: the epidermis, the dermis and the hypodermis.

The epidermis is a stratified epithelium of cornified cells, which the most important function is to produce the SC that forms the primary barrier to water loss and invasion of microbes and chemicals. The epidermis is lying on top of a fibroelastic tissue, also known as dermis, which gives the skin tensile strength. The layers are connected to the body by a fatty subcutaneous connective tissue, hypodermis, which dissipates mechanical stress and allows the skin to follow the motions of the body. [5]

2.2.1. Epidermis

The epidermis generates protective and defensive functions mediated by its unique differentiation end product, the stratum corneum – SC. One of the most important functions is the permeability barrier, which retards transcutaneous evaporative water loss, allowing survival in a potentially desiccating external environment.

The epidermis is a stratified epithelium composed of keratinocytes, containing filaments of the protein keratin, which give the cell its structural stability that are formed by division of cells in the basal layer and give rise to several distinguishable layers as they move outwards and progressively differentiate. Within the epidermis, there are several other cells, such as: melanocytes, which donate pigment to the keratinocytes; Langerhans' cells, which have immunological functions and Merkel cells. [18]

In the final stage, the keratinocyte is fully cornified and desquamates at the skin surface. The complete differentiation process from basal cell until desquamation takes about 15-30 days. [5]

Melanocytes are in the basal layer of the epidermis and produce pigment granules called melanosomes containing melanin. These melanosomes are transferred from the melanocytes to the epidermal keratinocytes, which can protect skin from ultraviolet light. The melanin synthesis and transfer of melanosomes occurs continuously as the epidermis renews itself.

On the other hand, Langerhans cells are dendritic immune cells that give an immune barrier of the epidermis and also participate in contact allergy. [19]

The total thickness of the epidermis lies between 50 and 150 μm with distinct four sub layers, which represent the successive stages of differentiation of the keratinocytes, Figure 2.3. The differentiation process starts at the stratum basale, which is the innermost layer of the epidermis, separated from the dermis by a continuous basal membrane.

The migration and differentiation process, starts by enter the stratum spinosum, comprised of polyhedral cells with a spine-like appearance caused by bundles of tonofilaments that are in contact with adjacent keratinocytes. The following layer is the stratum granulosum, comprised of several layers of flattened cells filled with keratohyalin granules. Keratohyalin granules are the precursor of protein filaggrin, which plays a role in the aggregation of keratin filaments within the cornified cells.

In the upper part of the stratum spinosum there's an abundance of submicroscopic granules, the origin of which is thought to be the Golgi apparatus. These granules exhibit a lamellar structure comprised of lipids (sterols, phospholipids and cerebrosides) and several hydrolytic enzymes. [5], [20]

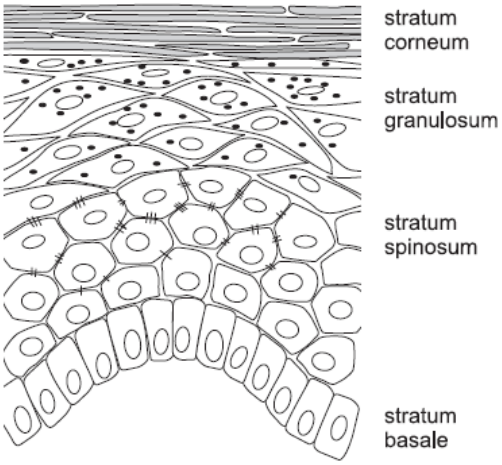

Figure 2.3 - Schematic drawing of the epidermis. Four major layers of cells are distinguished: the basal layer (stratum basale); the spinous layer (stratum spinosum); the granular layer (stratum granulosum); and the stratum corneum. [5]

In the last step of differentiation, the keratinocytes transform into flat cells, fully keratinized, to form the SC, flattened cornified cells. Thus, the development and maintenance of the SC are the key to its ability to defend the body against both chemical and microbiologic attack as well as dehydration. [21]

2.2.2. Stratum Corneum

The thickness of the SC is approximately 15 µm on most parts of the body, which the most important components are: keratin, lipids, natural moisturizing factor (NMF) and water. These flat cells are embedded in a matrix of lamellar lipids renders an almost impermeable barrier that keeps water in and harmful substances and microorganisms out of the body. [5]

The most important lipids found in the SC can be: ceramides, free fatty acids or cholesterol. The lipid synthesis is believed to take place in the stratum granulosum where small cytoplasmic inclusions are formed and packed in multi-layered stacks. At the interface between the SC and stratum granulosum, lamellar body exocytosis takes place to form the lipid lamella. [22]

The SC is often described as a brick wall, in which the corneocytes are the resistant cell envelopes and keratin microfibrils are considered to be the bricks, linked by desmosomes, while the layers of lipids found between the cells are considered to be the mortar. The permeability of lipid soluble molecules is considered to diffuse through the lipid mortar passing around the corneocyte bricks. Both the bricks and the mortar of the SC are produced by keratinocytes, which release the lipids of the mortar into the space between the cells as they are being transformed into the corneocytes. [21]

The SC is, approximately, 60% keratin by dry weight, which is the major structure protein present in the epidermis, but it can also be found in hair and nails. [21] Keratins are part of a family of proteins called intermediate filaments that form part of the cytoskeleton of nucleated cells, they've a variety of different classifications, according to molecule mass, acidity, structure and cysteine content [5]

The level of acidity can determine if the protein is acidic type I keratin or basic type II keratin, which depends on the charge of amino acid side chains in keratin. [21] Alternatively, the amount of cysteine present is in fact link to the sulfur content of a protein, since sulfur rich amino acids contribute to the rigidity of the fibers by forming disulfide links, which result in different types of keratin. [5]

Keratins have the capacity to have a helical structure, that when two helices interact with each other formed coiled-cols structures that are the core of the structure function responsible in keratinocytes. At the stratum granulosum, as keratinocytes transformed into the corneocytes, the coiled-coils aggregate to form structures called microfibrils, which are thought to lie parallel to the surface of the skin serving to reinforce the corneocytes and limit SC swelling in the plane of the skin surface. [21]

Keratin can be divided into α- and β-keratin, according to the α-helical or β-sheet secondary conformation. The human SC has about 90% composed of α-keratin and for 10% of β- keratin. [5]

Filaggrin is a filament-associated protein that participates in the aggregation of the keratin coiled-coils in epithelial cells. After this function, filaggrin is modified to come off the keratin microfibrils and is then digested by proteolytic enzymes to produce the amino acid components of the natural moisturizing factor (NMF). NMF consists of lactate, amino acids from filaggrin breakdown, and pyrrolidine carboxylic acid formed from the amino acid glutamine. [21]

The function of NMF is to maintain an optimal level of hydration in the SC, by being natural moisturizers, allowing it to be flexible and to desquamate properly. The chemical constituents of NMF are highly water soluble and hygroscopic, which is the reason that the SC can maintain water.

2.2.3. Dermis

Most of the dermis is formed by mesenchymal cells that migrate from other mesodermal areas, which makes for a fibroelastic connective tissue that gives the skin tensile strength, responsible by proteins such as collagen and elastin.

Collagen is the major structural protein and represents 75% of the dry weight and 90% of the total protein content of the dermis. The molecule consists of three polypeptide chains, wrapped around one another in a triple helix. In adult skin 80% of the total collagen is of type I, 15% of type III and the remaining 5% exists of type IV, V, VI and VII. [5]

These mesenchymal cells give rise to the whole range of blood and connective tissue cells, including the fibroblasts and mast cells of the dermis and the fat cells of the hypodermis. [21] Moreover, it can contain nerves, lymph vessels, muscles, hair follicles, sweat glands and sebaceous glands. The total thickness of the dermis varies from 1 mm to a maximum of 4 mm on the back. [5]

2.3. Chemometric Approach

Calibration is the association by a mathematical relationship between the values provided by a measuring instrument and those known for the measured material object is established. In Raman spectroscopy, quantitative analysis methods can include both classical and chemometric analysis.

The intensity of the Raman scattered radiation, I_R, is given by equation 2.3, where I_o is the incident laser intensity, N is the number of scattering molecules in a given state, ν is the frequency of the exciting laser, α is the polarizability of the molecules, and Q is the vibrational amplitude, and the parameter $(\partial\alpha/\partial Q)$ is the Raman cross section. [8]

$$I_R \propto v^4 I_0 N \left(\frac{\partial \alpha}{\partial Q}\right)^2 \quad (2.3)$$

The Raman cross section is a constant specific for the material at a specific wavelength of the Raman experiment. Thus, since the Raman cross section and the incident laser intensity remain constant, the intensity of the Raman band is directly proportional to the sample concentration.

However, in Raman experiment, the exact experimental parameters that determine the signal intensity are difficult to control. Thus, a ratio of an analyte band is often normalized against another component to eliminate these sources of variation, enabling the experiment to be insensitive to the Raman instrument. [8]

Classical analytical methods can use the ratio method with peak heights or integrated peak areas that often provide a robust calibration.

The selection of the peaks in the spectrum are chosen as the inputs for the quantitative analysis based on the spectral separation and knowledge of underlying vibrational modes.[8] Using band intensity ratios and peak position was demonstrated as being a viable calibration.[23]–[25] However, these calibrations are specific to a certain range of the spectra and it doesn't consider all the peaks of the material.

For high concentrations, molecular interactions of the components in the sample can often result in non-linearity behaviour. However, if the calibration takes such non-linearity into account, it will not affect the quantitative accuracy of the analytical method. An alternative is the use of a class of semi-empirical equations and linear fractional transformations. [8]

Therefore, most analytical methods use this direct relationship between measured signals and concentrations for quantitation purposes, only if it depends exclusively on the concentration of the specific analyte. Calibration models for these techniques are usually based on the least squares regression (LSR) of the absorbance values for a set of standards against their concentrations. [13]

However, there're a few different types of Raman experiments that might use several analytes or even a sample matrix, which must use a multivariate calibration, since the LSR isn't able accurately predict analyte concentrations. Multiple linear regression (MLR), is an extension of linear regression, using more than one variable in order to predict the concentration of one or more analytes. [13]

MLR has two known specific restrictions, since one is related to the number of variables used, that can't exceed the number of samples, and the other is also a mathematical limitation that the matrix containing the responses of the different variables and its transpose should be mutually related, otherwise, the matrix of the product of both cannot be inverted. Although, the theory of a Raman experiment should expect a visible outcome of the MLR, sometimes Raman experiment can be noisy, which leads to unstable inverted matrix. [13]

There's two types of calibration methods, classical or inverse calibration methods. In the MLR, classical calibration methods can be ordinary or classical least squares (OLS or CLS). On the other hand, inverse calibration methods include: inverse multiple linear regression (inverse MLR); principal component regression (PCR) and partial least squares (PLS).

The limitation of both classical methods is that, for the most part, there are only useful for the prediction of concentration and they require that the user to know the concentrations of all interfering species present in the sample. [16]

The classification of inverse method is due to the model using the inverse form of Beer's law where the concentration is expressed as a function of the absorbance. [16]

When MLR is used to construct a predictive model based on signals from the Raman instrument as inputs and a property of interest, such as concentration of a component, as output, the method is referred to as inverse linear regression or inverse least squares (ILS). [13]

This thesis uses the ILS model, presented here as the multiple least squares fit method. The most salient implication of the ILS method is that it assumes the error of the model to be present, and this model minimizes the square of the errors as it determines a single component in a complex mixture. The most important advantage of the method is that is the simpler to use of all analytically useful multivariate calibration methods. [13], [16]

One disadvantage of ILS is that it requires a number of samples that excides the number of variables in the model, that is the target variables must be chosen with careful consideration. In fact, ensuring acceptable results with ILS entails careful small selection of the target wavelengths, otherwise the number of calibration samples can go beyond practical limits of the method. Therefore, ILS cannot benefit from increased precision and the use of full spectra. [13]

This has made the ILS method widely popular, especially for IR and Raman spectroscopy; recently, however, it has been gradually superseded by variable-compression methods such as PCR and PLS.

Not all spectroscopy experiments result in a linearity behaviour, therefore there're several traditional methods that fail on obtaining a calibration of linear signals.

Non-linear responses can be of instrumental, physical and/or chemical origin, and result in a curved response–concentration line by effect of a non-linear detector response, straight light generated at high optical densities, baseline drift (e.g. due to physical scattering of the light by solid particles), and shifts in the positions of bands or changes in their widths by effect of changes in temperature or the nature of the solvent. [13]

There're still a few multivariate calibration methods that can model some slight deviations from linearity at the expense of an increased complexity, and this is the reason that PCR and PLS are been used increasingly compared to the ILS. One the other hand, some complete non-linear methods, such as artificial neural networks, are more complex but can fully describe these nonlinear experiments.

In summary, multivariate calibration methods give reliable results for unknown samples since there is a combination of new pre-processing and analysis techniques that are based on standard approaches.

These chemometric approaches have the capacity to give a reliable quantitative determination of different Raman spectra, based on the information extracted from spectral changes, such as: Raman intensity; band shape; band position and some property of the material (e.g. concentration). [13], [16]

Chapter 3

Materials and Methods

The following chapter will present a description of the experimental data sets and the respective methodology, equipment and software used for the data analysis. It also includes two different variations of the calibration methodology developed in this thesis to calibrate materials.

Bovine serum albumin/water and ethanol are three materials that required a different type of calibration, the method had to more personalized and detailed, since these materials are the starting point of the methodology and new APIs are linked to these.

For this reason, there're going to be described first in this chapter and a general API calibration is going to be described in the end for all other solvents and APIs.

3.1. Materials

This chapter includes all the APIs that were studied for this thesis, as well as, the solvents necessary for the dissolution of each API, a summary table is presented in Appendix II.

An overview of the experimental data sets is in the chapter 3.4. Chemicals that were used in these experiments didn't require any further purification.

For *in vivo* measurements in skin, four different types of products were used to test the calibration method develop in this thesis, presented in Table 3-1.

Table 3-1 - Products that were used for in vivo measurements in skin to test methodology for penetration and permeation of topically applied compound with APIs.

Type of Products	API	Name of Product
Ibuprofen and Levomenthol gel	5% ibuprofen	Product A
Acne Treatment Cream	2% Salicylic Acid	Product B
Marula Oil	Oleic Acid	Product C
Caffeine Oil	5% Caffeine	Product D

3.2. Instrumentation

3.2.1. The gen2-SCA System

Spectroscopic measurements in this thesis were carried out in a near Infrared Raman microspectrometer - gen2-SCA, presented in Figure 3.1, which has two main system components: Skin Analyzer and a personal computer.

Figure 3.1 – The gen2-SCA system: RiverD's second generation Skin Composition Analyzer.

The Skin Analyzer is the measurement unit and it's operated via a computer with the RiverICon instrument control software. The Analyzer has a built-in high performance Raman module with a CCD detector, two built-in lasers and a confocal microscope measurement stage.

The Analyzer incorporates two continuous wave Class 3B lasers, operating at wavelengths of 671nm and 785nm. Light of 671nm is red, whereas radiation at 785nm is in the near-infrared and is (nearly) invisible. The laser power levels, the wavelengths used, and the geometry of the system, result in classification of the gen2-SCA as a Class 2M laser device and comply with the Maximum Permissible Exposure levels for skin.

Measurements in skin and solutions were placed on a fused silica window. The backscattered Raman light from the sample measured is collected by the objective and is focused back to the entrance of the pinhole of the spectrograph. The microscope objective is mounted on a precision translation table, enabling this objective to focus the laser light at a selected laser depth above the window. Since the instrument is optimized for rapid *in vivo* measurements of human skin, it offers an axial spatial resolution of less than 1 μm. An illustration of the gen2-SCA system and a more detailed design of Skin Analyzer is presented in Figure 3.2.

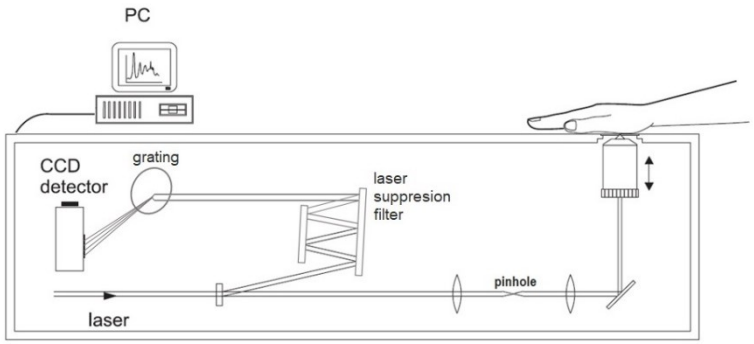

Figure 3.2 - Confocal Raman setup for in vivo experiments. Laser is transmitted and focused in the skin by a microscope objective. Raman scattered light is collected by the same objective and passes through a pinhole and a laser suppression filter before going into grating to be detected by a CCD.

The spectrometer allows measurements in the high wavenumber region (2400-4000 cm^{-1}) and the fingerprint region (340-2450 cm^{-1}) of the Raman spectrum. The high wavenumber region is obtained using the 671 nm laser excitation, bringing this part of the spectrum into the more sensitive region of the CCD detector, while the fingerprint region is obtained using the 785 nm excitation to minimize any possible fluorescent problems. The maximum spectral resolution is 5 cm^{-1} throughout the entire spectral range.

The Analyzer has a built-in video camera that allows for the skin surface / sample inspection on the window, enabling the selection of the measurement spot. The space between the measurement window and the microscope objective was filled with immersion oil. This way, refractive index mismatch is minimized.

3.2.2. Other instrumentation and Software

All the solutions measured were prepared with an electronic balance (type ABJ 120-4M, KERN & Sohn GmbH, Germany) with a capacity of 120 g and with an error of 0,1 mg.

For data analysis, Matlab R2017a v. 9.2.0.556344 (The MathWorks AS, Massachusetts, USA) was used to perform all the routines together.

Moreover, to collect Raman spectra there's an instrument control software, RiverIcon (RiverD International, The Netherlands), the version of the software used for all the measurements on this thesis was RiverIcon 4.0.171017.

RiverICon is a comprehensive software application that is used to operate the gen2-SCA system, which performs Raman experiments. It also offers templates, which enable the operator to quickly perform various types of Raman measurements, such as single point measurements or automated profile measurements. Raman data analysis models are included and provide real-time analysis and display of concentration profiles of various skin constituents, while the Raman spectra are being captured.

The Skin Analyzer requires one calibration of the device per day and if the corresponding calibration in the data processing panel is active a copy of the measured spectrum is saved in a pre-processed, calibrated format.

RiverICon allows the spectra to be always saved in raw, unprocessed format as Matlab files. Spectra can be imported, visualized, processed and exported to tab delimited text files using the data analysis software SkinTools (RiverD International, The Netherlands).

SkinTools 2.0 enables the user to process highly multidimensional experimental data in a fast and efficient way. Important features in this tool are:

i. automatic, customizable outlier detection;
ii. calibrate unprocessed spectra;
iii. plot the difference between two different spectra with a manually chosen scale factor;
iv. automatic and precise calculation of the skin surface location, by interpolation of the depth composition profiles, as well as, analysis methods with components other than the endogenous skin constituents.

3.3. General Procedure for API Calibration

A complete calibration of a new material should include several steps, which same of them are further explained in chapter 3.3.1 and 3.3.2:

I. Calibration of gen2-SCA system;
II. API solutions preparation;
III. Raman measurements of API solutions and solvent;
IV. Extract API reference spectrum;
V. Data analysis of the API experimental data set;
VI. Evaluate calibration results of data analysis;
VII. Add quantified API reference spectrum to the library.

3.3.1. API Solutions Preparation & Measurements

A general protocol was standardized for data collection for an API calibration experiment, which all the detailed steps are presented in Appendix III. A general approach to solutions preparations used a weighting method, where the API mass was first measured and then the total solution mass to achieve the chosen mass ratio, considering the purity of the API, described by equation 3.1.

$$Mass\ Ratio_{API\ Solution} = \frac{m_{API}}{m_{solvent}} = \frac{m_{API}}{m_{solution} - m_{API}} \quad (3.1)$$

After all Raman measurements were collected, usually with 5 seconds exposure time and 100 to 200 frames, the data set should be evaluated to see if it meets quality standards to be use for calibration.

3.3.2. API Calibration Method

The premise of the calibration method studied in this thesis was explained in chapter 2.1. The method enables a quantification of Raman signals of materials in the SC, by relating the API to keratin in the SC. The first step required is the calibration of BSA, which is soluble in water. Thus, water is the first solvent to be calibrated and added to the methodology library.

Ethanol was the second solvent to be added to the library, since most APIs studied in this thesis needed to be dissolved in ethanol. Therefore, ethanol was also part of the starting point of the methodology.

BSA/water and ethanol calibration are an exception to the general method because there was a need for a personalized Matlab script to optimize both calibrations. Since both calibrations are the foundation of this method, there're going to be described first. A general API calibration is going to be detailed in the end of the chapter.

Bovine Serum Albumin Calibration

Every new material quantified to keratin will be related intrinsically to BSA, equation 1.5. To decrease the propagation of the error in the BSA calibration method and to increase the robustness and reproducibility of the methodology, all the different components in this calibration were taken into account individually.

The calibration studied in this chapter has two different parts: the calibration of BSA to water and the calibration of BSA to keratin in the SC. A general overview of BSA/water calibration is presented in Figure 3.3.

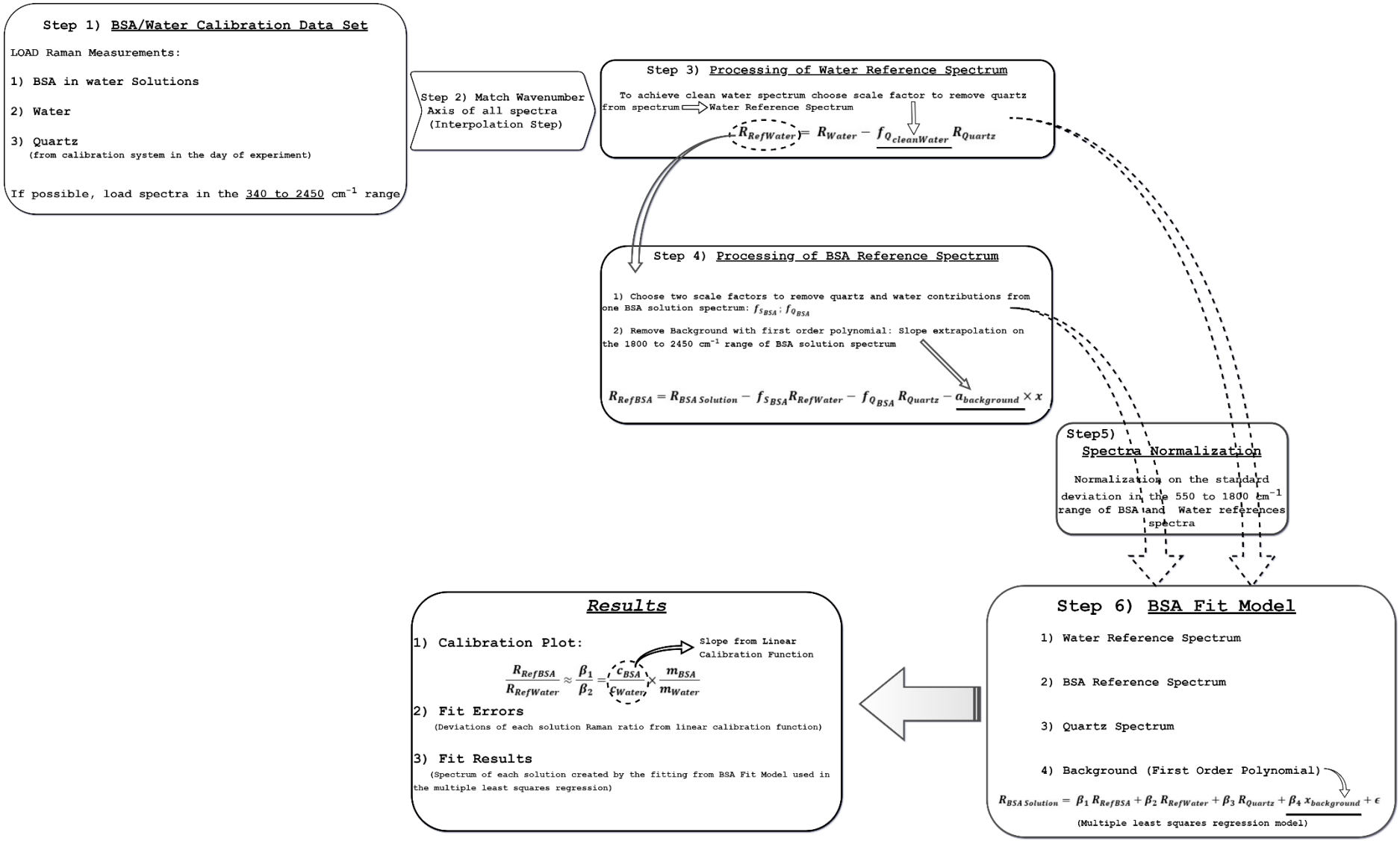

Figure 3.3 – BSA in water calibration – general overview diagram.

In step 1, the calibration data set of BSA/water should be evaluated before a calibration analysis. An optimization of quality of any Raman measurements can and should be done with different experimental sets, if a data set doesn't meet the quality requirements. The gen2-SCA system has a calibration each day, which includes a quartz spectrum (R_{Quartz}) that should be use for this calibration.

In step 3, the reference water spectrum ($R_{RefWater}$) to be used in the fit model should be clean of quartz. There's a subtraction of a scaled quartz spectrum from the water measured in the day of experiment - R_{Water}, by choosing a scale factor $f_{Q_{cleanWater}}$, described by equation 3.2.

$$R_{RefWater} = R_{Water} - f_{Q_{CleanWater}} R_{Quartz} \quad (3.2)$$

This reference water processed is going to be saved in the methodology library as the first solvent available with all the quantification constants, after the calibration is completed.

Step 4 includes the extraction of BSA Raman signal from a BSA solution that's chosen by the user. The highest BSA concentration of the calibration data set should give the best API Raman signal, thus is the best solution to use. One requirement of choosing this solution is that it should have a comparable contribution of Raman intensities between BSA and water, to achieve comparable fit coefficients in the multiple least squares fit, decreasing the error of estimating the BSA fit coefficient $\beta_1 \approx R_{RefBSA}$.

Consequently, it's necessary to be aware that the spectrum of a BSA solution has different contributions of intensity from different sources. Each solution has contributions from: BSA, water, quartz and some background from the Raman experiment itself.

The water reference spectrum and quartz spectrum are scaled by multiplying each one with two scaling factors, $f_{S_{BSA}}$ and $f_{Q_{BSA}}$, respectively. By manually choosing these factors, an optimized subtraction of water and quartz Raman contribution from the BSA solution spectrum is achieve, described by equation 3.3. Finally, there's some background observed, which might be due to fluorescence, that needs to be subtracted, described by equation 3.3 as well.

$$R_{RefBSA} = R_{BSA\,Solution} - f_{S_{BSA}} R_{RefWater} - f_{Q_{BSA}} R_{Quartz} - a_{background} \times x \quad (3.3)$$

The range 1800 to 2450 cm^{-1} in the BSA solution after the water subtraction should be flat and close to zero in Raman intensity, which doesn't happen because of this background presence. Therefore, a slope was extrapolated from the intensity in this range of the spectrum. This slope is used for a first order polynomial, and this polynomial is then subtracted from the spectrum.

The normalization process in Step 5 is an essential for the calibration method, since the method will be reproducible and enables the comparison between different calibrations. It's done on the standard deviation of the intensity on the 550 cm^{-1} to 1800 cm^{-1} range of the spectra.

Step 6 is the goal of every calibration, a fit model is created to be specific to the calibration data set chosen. The model uses a multiple least squares regression to estimate each fit coefficient – β – which is in fact a scale factor of each component that reproduces each BSA solution spectrum of the data set.

A fit result of a spectrum is originated by the sum of every contribution in the model times each scale factor. Since the multiple least squares fit works by minimizing the residuals ε, a viable calibration takes into consideration that the fitting results should have almost no detectable residuals, validating the hypothesis that the fit model is able to reproduce any BSA solution in the data set.

The results of BSA/water calibration include a calibration plot, which the slope estimated in the linear function it's a representation of the fit results of the multiple least squares fit model. The calibration function has in x-axis the mass ratios of each solution of the data set and the y-axis has the ratio of the fit coefficients between BSA and water in the model. In the end, calibration constant c_{BSA}/c_{water} is the slope estimated.

The second part of this calibration is linking BSA to keratin in the SC by determining the calibration constant $c_{BSA}/c_{keratin}$. This step is essential to quantify any API in units of $mg\ API/g\ keratin$, which enables the API quantification values to be comparable and reproducible for different experiments.

The standard spectrum of keratin in SC, present in RiverD library was measured with the instrument HPRM 2500 high-performance Raman module (RiverD International, The Netherlands) in 22/06/2004 with 10 seconds exposure time in a single frame.

Since the BSA was used as an approximation to keratin, it's considered that the mass ratio between the two is 1:1. Then, the calibration constant is only dependent on the Raman ratio between the two reference spectra. The multiple least squares regression fit is used to fit BSA reference spectrum to keratin spectrum, the fit coefficient from the fitting results is the calibration constant $c_{BSA}/c_{keratin}$.

The link to BSA is an intermediate step necessary of this method, but not a necessary step to be always mentioned for the calibration of new materials. The calibration constants of BSA in water and BSA to keratin are fixed constants in this method, after this step new materials need only to be linked to water, subsequently water is linked to keratin with only one constant, $c_{water}/c_{keratin}$, equation 3.4.

$$\frac{c_{water}}{c_{keratin}} = \left(\frac{c_{BSA}}{c_{water}}\right)^{-1} \times \frac{c_{BSA}}{c_{keratin}} \tag{3.4}$$

Ethanol Calibration

Since there is a large percentage of APIs that are insoluble in water, the calibration method if it just included water as the only solvent available it would be a very restricting method. Organic solvents can be used for water-insoluble APIs and most APIs studied in this thesis have a high solubility in ethanol. There were already experiments done with ethanol that can be comparable to new calibrations, thus ethanol was chosen to be first organic solvent to be added to this methodology.

Ethanol had the same type of calibration as BSA in water, since all different Raman contributions in the fit model of calibration were processed manually to optimize the final calibration constant with a personalized Matlab script. A general overview of ethanol calibration is presented in Figure 3.4.

Since the calibration of ethanol follows the same steps as the BSA, just a few remarks must be taken into account to study the difference between the two calibration analysis.

The main difference between the two is how the water spectrum is processed to be used in the ethanol fit model in step 3. There's still a need to subtract the quartz contribution from the water spectrum measured in the day of the calibration experiment, by manually choosing the scale factor $f_{Q_{cleanWater}}$.

This clean water processed spectrum needs a different normalization. The normalization is going to be done on the standard deviation of the water reference spectrum (saved in the library from BSA/water calibration, since this is the water spectrum that is quantified to keratin). The spectrum must be divided by the fit coefficient β_1 that scales the clean water spectrum to the water reference by using the multiple least squares regression with a fit model compose by equation 3.5.

$$R_{clean\ water} = \beta_1 \times R_{RefWater} + \beta_2 \times R_{quartz} + R_{background} \tag{3.5}$$

In step 4, the processing of ethanol reference is the same as BSA, both scale factors are manually chosen to optimize the subtraction of water and quartz. However, the background observed was in a different range, that is the slope was calculated from the spectrum in the range 1750 to 2050 cm^{-1}, since this range should be close to zero in intensity. This slope is then used on first order polynomial that is going to be subtracted from the spectrum.

The linear calibration function estimates directly the calibration constant $c_{RefEthanol}/c_{RefWater}$ of the processed ethanol reference spectrum to water reference spectrum from library, since the clean water spectrum in the fit model is already linked to the library reference with the normalization step.

After the calibration constant is determined, ethanol can be linked to keratin with the calibration constant $c_{Refethanol}/c_{Refkeratin}$ that was estimated by equation 3.8. After the calibration of ethanol is finalized, ethanol can be added to the reference library as a solvent option for new APIs calibration.

$$\frac{c_{RefEthanol}}{c_{RefKeratin}} = \frac{c_{RefEthanol}}{c_{RefWater}} \times \frac{c_{Refwater}}{c_{RefKeratin}} \tag{3.6}$$

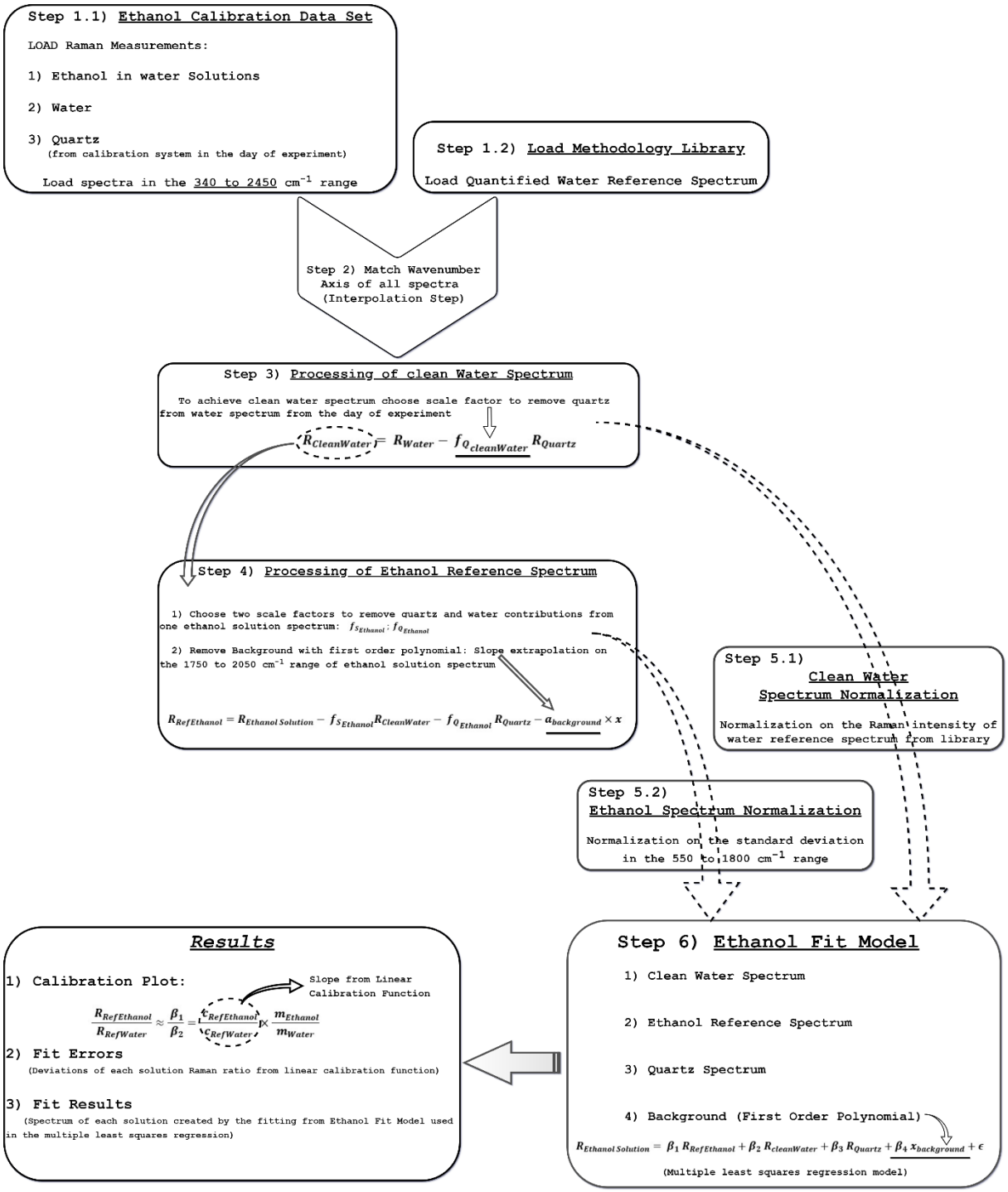

Figure 3.4 - Ethanol in water calibration – general overview diagram.

Calibration of new APIs

Any other solvent that must be added to the reference library for future quantification of APIs, needs primarily to be processed as a new material. Just like ethanol was first considered to be a new material. If a new solvent isn't linked to water by calibration constant $c_{solvent}/c_{water}$, the only calibration constant that is determined is $c_{API}/c_{solvent}$, and there is no intermediate step to relate it to keratin.

The new solvent doesn't need to be water-soluble, since there is an unlimited number of intermediate steps that can be added before there's a link to water. However, dissolving a new solvent in water should be the preferred method. Even though, in theory, there's unlimited intermediate steps to link the solvent to water, the more steps the calibration has the higher the error of the solvent quantification will have, due to the propagation of the error of all the intermediate constants.

This line of though is the same for any other new API, ideally an API should be first dissolved in water and only if it's insoluble a new solvent can be considered for its dissolution.

For the calibration of a new API, the approach is more straight forward than before, since there is only the need to calibrate the solutions to get the constant $c_{API}/c_{solvent}$, as long as this solvent was previously calibrated. BSA/water and ethanol calibration enable, immediately, a wide range of different APIs that could be calibrated in a simple and straight forward way.

This methodology has three different parts that can be used by a non-proficient user in Matlab or Raman spectroscopy. These steps include three Matlab tools that enable the calibration of any API or even add new solvents to the references library. A general overview is presented in Figure 3.5 and 3.6.

Part I starts with an evaluation of quality of the calibration data set chosen. The data set with the best quality has the least amount of noise and artefacts in the spectra, the Raman conditions are the same throughout all Raman measurements.

The first tool used is "Calibrate Unprocessed Spectra" from SkinTools. It's used to change the wavenumber range to 340-2450 cm^{-1}, to extend raw spectra to full range. In the end of Part I, the calibrated API solution and solvent spectra is in the range required of a good quality calibration, since the standard range 400-1800 cm^{-1} has more uncertainty in the final calibration results.

Part II of this methodology is the API reference spectrum processing. It starts by using SkinTools tool "Difference Spectrum" to load the chosen the API solution that will be used to extract the API reference spectrum and the respective solvent used to prepare the solutions, from Part I.

The main difference in this step compared to BSA and ethanol references, besides that it's done in an easy to use tool, is that the extraction of API Raman signal from the API solution doesn't take into consideration the quartz and solvent contribution separately in the API solution spectrum.

There is only one scale factor – f – manually chosen to obtain the API reference spectrum – R_{RefAPI} – by subtracting the solvent Raman contribution – $R_{Solvent}$ – from API solution spectrum – $R_{API\ Solution}$, described in equation 3.7.

$$R_{RefAPI} = R_{API\ Solution} - f \times R_{Solvent} \tag{3.7}$$

It's implied that the quartz contribution is, approximately, the same between the solvent and API solution spectra. Which, in fact, the BSA/water and ethanol calibration results in chapter 4 have proved that it isn't. This direct subtraction of the solvent measurement might introduce a positive or negative contribution of quartz in the API reference spectrum, but it's considered to be negligible.

If the API reference spectrum has enough quality, it should be saved and used further in the API calibration. If not, there's a few processing techniques that can used in Matlab to achieve the best quality possible. The quality requirements and a few remarks are detailed in Appendix IV.

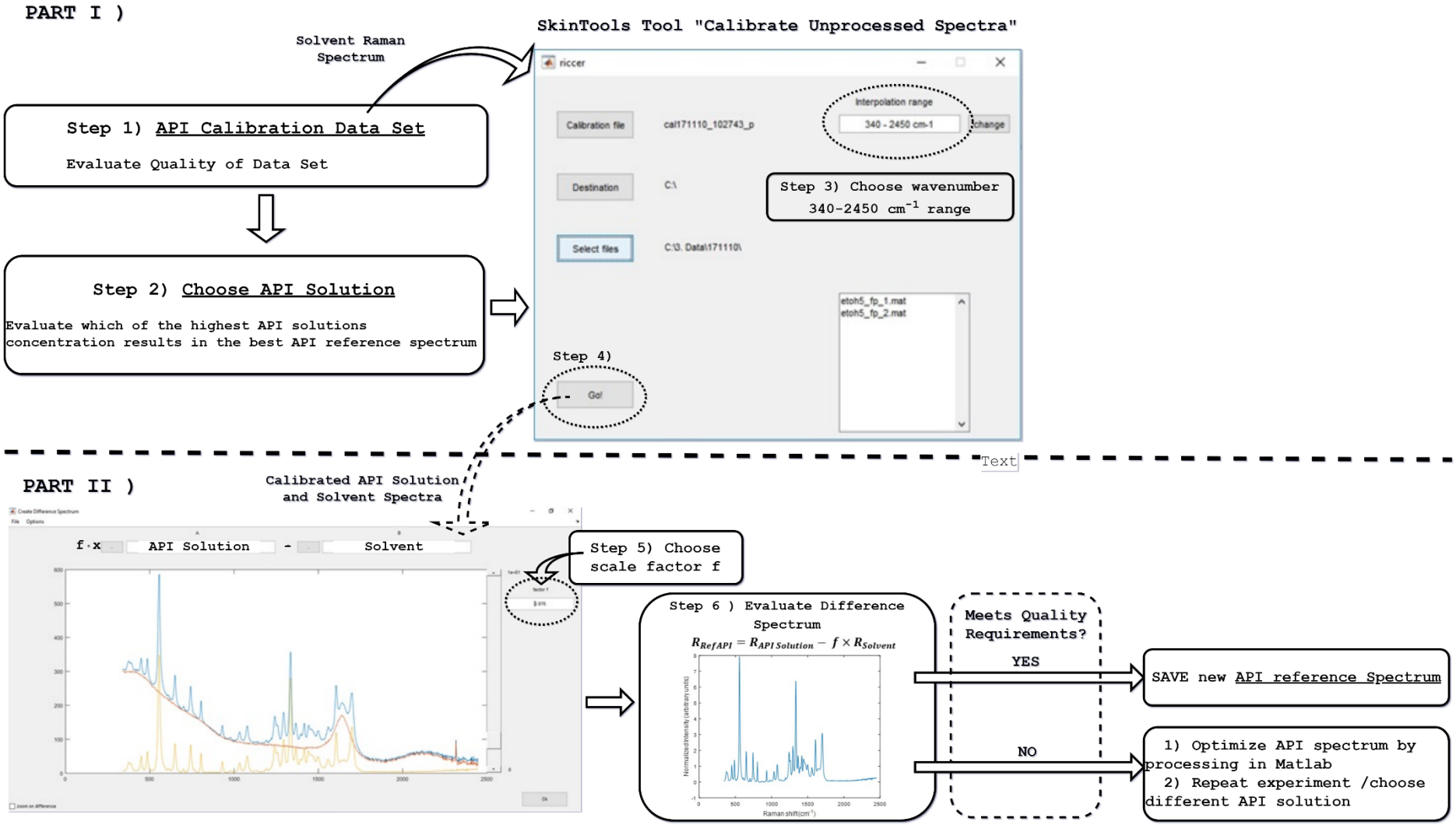

Figure 3.5 – Part I and II of the calibration methodology used in a standard API calibration.

Part III is the final part of the methodology, which uses the Quanti tool to do the automatic API calibration analysis. It was designed to calibrate any material, as long as its solvent is in the references library of the tool, already quantified. A general overview of the tool is presented in Figure 3.6.

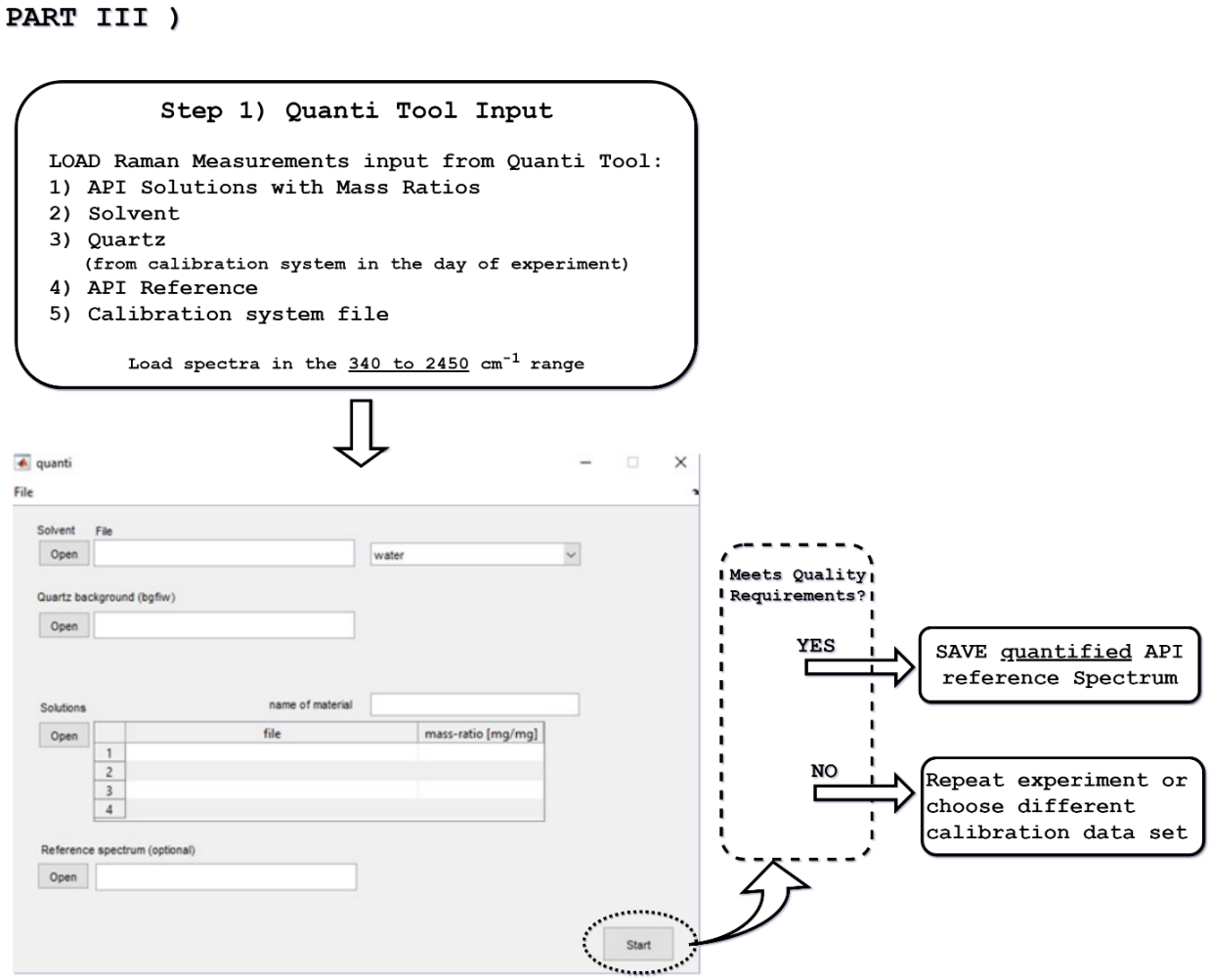

Figure 3.6 – Part III of the calibration methodology for a standard API calibration: Overview of Quanti tool.

The processing behind the Quanti tool to calibrate an API is explained in the chapter 3.3.2. Quanti tool.

In the end of the calibration, if all the solutions fit into a straight line with few deviations and the fit results of the solutions have a minimum amount of residuals, then the data set is suitable to be used in the API calibration. If these quality requirements are meet, click in “Save reference as” to save the quantified processed API reference spectrum.

This processed API spectrum file has all calibration constants, as well as all the information and measurements of the data set that was used for the experiment. After the quantified API reference spectrum is added to the library it can be used in two ways.

If the calibration was done for a standard API, the quantified spectrum will be used for the data analysis of *in vivo* measurements in skin. Therefore, from all the calibration steps the final quantified spectrum of the API is the only file needed to determine the amount of API in skin.

However, if the material was calibrated as a necessary intermediate step of adding a new solvent to the reference library, there is another Matlab tool to simplify this process, “Update Reference Index”. This tool automatically appends the new solvent calibrated to the library and saves the new library to be used for future API calibrations in the Quanti tool.

Quanti tool

The quanti tool most recent version is *Quanti20180226*. When the tool starts to run with all the inputs, there's a data process behind the software tool. An overview of this process is described in Figure 3.7.

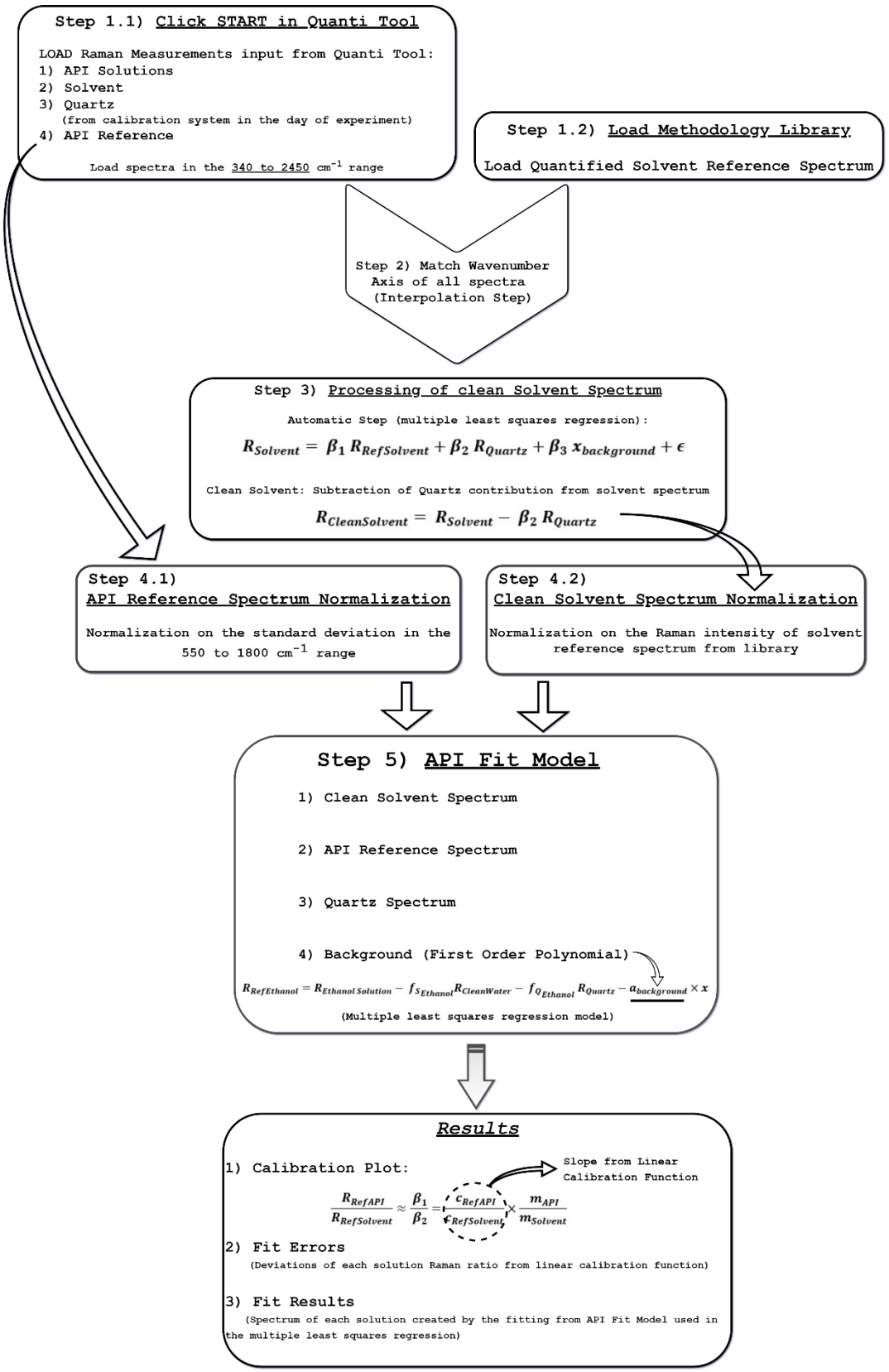

Figure 3.7 - Quanti Tool analysis: API general calibration method.

The Quanti tool was created to calibrate any API in fast, simple, reproducible and automatic way. Any user with no advanced programming skills or any vast knowledge on Raman spectroscopy can use it. This is a tool with the potential to be sold as a software add-on for clients of RiverD International B.V., but still needs to be upgraded since it's still considered to be complex and also needs further testing.

The calibration process behind the Quanti tool is very similar to ethanol calibration, however this general API calibration is processed automatically with a few approximations.

The main difference is that there's no processing of API reference spectrum besides the normalization step, since it's part of the input chosen by the user in the Quanti tool.

The second main difference is the automatic step of clean solvent processing. The solvent spectrum from the day of the experiment still needs to be processed by removing its quartz contribution.

This step uses the multiple least squares regression to estimate the quartz contribution in the solvent spectrum. The fit coefficient is an estimation of a scale factor needed to subtract the quartz from the solvent measurement, resulting in the clean solvent used in the API fit model. This clean solvent spectrum is then normalized on the standard deviation of the solvent reference spectrum.

This automatic approach introduces a bigger error deriving from the uncertainty of quartz quantification in the spectrum. However, this extra error compared to clean solvent spectrum in the ethanol calibrations is negligible for a common API calibration.

For a new solvent calibration, the user should consider if the calibration process should be done manually in Matlab to decrease the propagation error of the chain of the calibration constants.

After the calibration of the data set the *quanti* tool will display the results in different figures:

a. Calibration curve with mass ratios of each solution of the data set - x-axis - and the ratio of the fit coefficients between API and solvent in the model - y-axis. The calibration curve will display the slope constant of $c_{API}/c_{solvent}$ and the determination coefficient of the linear regression;
b. Deviations errors of each point calculated from the calibration line;
c. Average of each solution measured;
d. Normalized API reference spectrum;
e. Fit results of each solution, with original solution, processed solution created from the multiple least squares fit and the residuals of this processed solution.

The command window of Matlab also shows results, such as: original API reference spectrum file; fit coefficients of material and solvent; Raman ratios and mass ratios for each point of the calibration line; calibration constants and quantification factor to be used in SkinTools for measurements in skin.

If the calibration results meet the quality requirements, the API reference spectrum is saved as a quantified processed spectrum, which can be used in SkinTools for *in vivo* skin measurements.

3.3.3. Multiple least squares fit method

The multiple least squares regression fit method, MLSM, is used to determine the scale factors – fit-coefficients β - of each component of the API model, X, that reproduce each API solution spectrum, y.

For each component chosen in the fit model there is a fit coefficient that relates it to an API solution spectrum and the larger the amount of intensity from a component in the API solution spectrum, the higher will be its fit coefficient.

An overview of this method will have a multiple regression fit of the columns of matrix X to vector y, in other words, an unrestricted multiple least squares regression fit with an optional polynomial. Therefore, fit-coefficients can be positive and negative. Since y has to be a vector, it's represented by the average of frames collected in a Raman experiment, leading to just one spectrum.

The order N of the polynomial can be chosen as an input in the model. For $N = 1$, for example, y will be fitted by an extra offset and slope. If N is not specified, y will be fitted by the columns of X only.

The MLSM model with *k* predictor variables x_1, x_2, x_3,…, x_k and a response y, can be written as in equation 3.8.

$$y = \beta_0 + \beta_1 x_1 + \beta_2 x_2 + \beta_3 x_3 + \cdots + \beta_k x_k + \epsilon \tag{3.8}$$

With this compact notation, the MLSM model can be written in the form of equation 3.9.

$$y = \beta\, X + \epsilon \tag{3.9}$$

Where,

$$y = \begin{bmatrix} y_1 \\ y_2 \\ \vdots \\ y_k \end{bmatrix} \quad , \qquad X = \begin{bmatrix} 1 & x_{11} & x_{12} & \dots & x_{1k} \\ 1 & x_{21} & x_{22} & \dots & x_{2k} \\ \vdots & \vdots & \vdots & \ddots & \vdots \\ 1 & x_{n1} & x_{n2} & \cdots & x_{nk} \end{bmatrix} \tag{3.10}$$

$$\beta = \begin{bmatrix} \beta_0 \\ \beta_1 \\ \vdots \\ \beta_k \end{bmatrix} \quad , \qquad \epsilon = \begin{bmatrix} \epsilon_1 \\ \epsilon_2 \\ \vdots \\ \epsilon_n \end{bmatrix} \tag{3.11}$$

The residual terms of the model, designated as ϵ, is considered to be the residuals of the fitting that allows the evaluation of the remaining model parameters.

To adapt this MLSM model to an API fit model in the method studied in this thesis, the vector y represents an $API\ Solution_{spectrum}$, which is the vector *y* that can be characterized by equation 3.12.

$$API\ Solution_{spectrum} = \beta_1\, API_{spectrum} + \beta_2\, Solvent_{spectrum} + \beta_3\, Quartz_{spectrum} + \beta_4\, x_{background} + \beta_0 + \epsilon \tag{3.12}$$

In linear algebra terms, the least-squares parameters that estimates β are the vectors that minimize the residuals of the fitting, equation 3.13.

$$\sum_{i=1}^{n} \epsilon_i^2 = \epsilon'\epsilon = (y - \beta\, X)'(y - \beta\, X) \tag{3.13}$$

If the y vector and X matrix are fixed, the minimization sum of squared residuals only depends on the estimation of β parameters.

A perfect fitting between y vector and X matrix, will achieve a null sum of squared residuals. Therefore, equation 3.14 will represent the predicted $\hat{y}$ vector, which will be the API fit result spectrum.

$$\hat{y} = \hat{\beta}\, X \tag{3.14}$$

Here $\hat{y}$ vector is the projection of the n-dimensional data vector y onto the hyperplane spanned by X. The $\hat{y}$ vector is the predicted values in the regression model that all lie on the regression hyper-plane, represented in Figure 3.8.

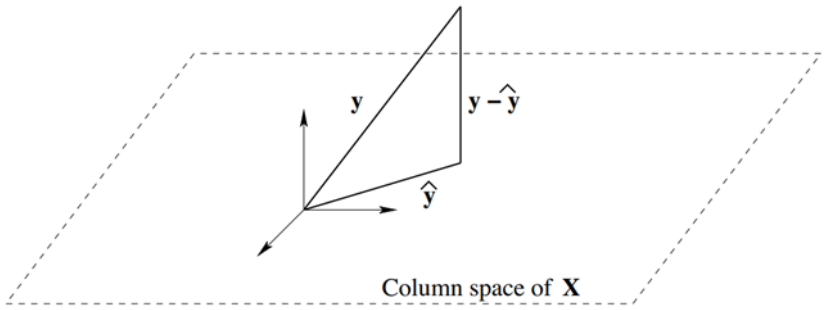

Figure 3.8 - $\hat{y}$ vector is the projection of the n-dimensional data vector y onto the hyperplane spanned by X

The residuals can be represented as $y - \hat{y}$ and are orthogonal to the columns of X, therefore Orthogonal Decomposition Theorem can be used (equation 3.15).

$$X'(y - \hat{\beta}\, X) = 0 \leftrightarrow$$

$$X'y - X'\hat{\beta}\, X = 0 \leftrightarrow$$

$$X'y = X'\hat{\beta}\, X \tag{3.15}$$

Thus, the least-squares estimator of vector $\hat{\beta}$ is given by equation 3.16.

$$\hat{\beta} = (X'\, X)^{-1}\, X'y \tag{3.16}$$

A representation of the MLSM method in the calibration results will be represented by equation 3.17.

$$API\ Solution_{spectrum} = Fit_{spectrum} + Residuals = \hat{y} + (y - \hat{y}) \tag{3.17}$$

3.3.4. Propagation Error Method

Two different definitions are necessary to explain the propagation of an error – there's two different types of error: absolute error and relative error.

An absolute error is estimated in a measured value of x and it's designated as $\pm\, \delta_x$. The value δ_x has the same units as x and is called the absolute error in x. On the other hand, the relative error of a value x derives from the ratio of the absolute error δ_x and the measured value of x, $\frac{\delta_x}{x}$. The relative error is usually represented as a percentage.

There are two different rules to calculate the propagation of an error of a certain value, and it depends on the mathematical operation that estimates the value. The estimation of an error based on the sum rule is given in equation 3.18 and 3.19, which states if there's a sum or subtraction of two different variables x and y, each with associated absolute errors δ_x and δ_y, respectively, the error is determined by the sum of the absolute errors.

$$\delta(x + y) = \delta_x + \delta_y \tag{3.18}$$

$$\delta(x - y) = \delta_x + \delta_y \tag{3.19}$$

The second rule, is only for multiplying or dividing two different variables x and y, each with associated absolute errors δ_x and δ_y, respectively, where the ultimate relative error derives from the sum of each fractional error, as given by equation 3.20 and 3.21.

$$\frac{\delta(xy)}{xy} = \frac{\delta_x}{x} + \frac{\delta_y}{y} \tag{3.20}$$

$$\frac{\delta(x/y)}{x/y} = \frac{\delta_x}{x} + \frac{\delta_y}{y} \tag{3.21}$$

The error of a given value with different sources of uncertainties can be resolved with the propagation of the error method of those given uncertainties. This approach can easily be calculated using differential calculus, associating the differential with the error of a quantity. Equation 3.22 represents f as a continuous function of two variables x, y.

$$f(t) = x(t)y(t) \tag{3.22}$$

If f has continuous partial derivatives $\partial f/\partial x, \partial f/\partial y$ and if x, y are differentiable functions $x = x(t), y = y(t)$ of a variable t, then the total derivative of f with respect to t is given by equation 3.23, following the chain rule for functions of functions to calculate the total derivative.

$$\frac{df}{dt} = \frac{dt}{dt}\frac{\partial f}{\partial t} + \frac{dx}{dt}\frac{\partial f}{\partial x} + \frac{dy}{dt}\frac{\partial f}{\partial y} \tag{3.23}$$

For a total derivative calculation there's a similarity between total differentials and total derivatives. The total derivative of f can be obtained by dividing the total differential by dt, equation 3.24.

$$df = dx\frac{\partial f}{\partial x} + dy\frac{\partial f}{\partial y} \tag{3.24}$$

Therefore, the total differential of the function f results in equation 3.25.

$$df = y\,dx + x\,dy \tag{3.25}$$

Finally dividing by $f = xy$, obtains equation 3.26.

$$\frac{df}{f} = \frac{y\,dx + x\,dy}{x\,y} = \frac{dx}{x} + \frac{dy}{y} \tag{3.26}$$

In the end, this differential equation 3.38 is the same formula as the rule for products above in equation 3.20 and 3.21, but with the error replaced by the differential of each variable, since the derivate definition in differential calculus is associated with the rate of change of one quantity with respect to another.

The propagation error method is used in this thesis to estimate an error of each calibration constant to quantify an API in skin. The first step of a calibration involves determining the calibration constant of $c_{API}/c_{solvent}$ that derives from the linear regression given by equation 1.5. Thus, one of the associated errors will be the experimental mass ratios of each solution prepared.

The error of the balance used is $0{,}1\ mg$, which will be the absolute error of the API and solution mass, the error mass of the solvent will be determined by equation 3.27.

$$\delta_{m_{solvent}} = \delta(m_{solution} - m_{API}) = \delta_{m_{solution}} + \delta_{m_{API}} = 0{,}2\ mg \tag{3.27}$$

Therefore, the absolute error of mass ration for each solution i is given by equation 3.28, and this will be the absolute error of x axis in the linear regression.

$$\delta_{x_i} = \delta_{mass\ ratio_i} = mass\ ratio_i \times \left(\frac{\delta_{m_{API}}}{m_{API}} + \frac{\delta_{m_{solvent}}}{m_{solvent}}\right) \tag{3.28}$$

To estimate the real quantification error of a calibration constant $c_{API}/c_{solvent}$, a validation analysis was implemented in the method. This validation uses an independent data set, therefore the validation model will have a relative error related to the uncertainty of quantification of mass ratios of these independent new API solutions.

For BSA and ethanol calibration, there're independent validation data sets that were used to determine which fit model of calibration studied best predicts the quantification of those data sets. However, those were the only calibrations that were studied with a validation model.

As a result the best calibration fit model that contains the API and solvent reference spectra will have the least amount of relative error between the real mass ratio and the predicted, and this relative error will be associated to one of the errors of the calibration constant $c_{API}/c_{solvent}$.

The error of the *Quantification Validation* per solution *i* is given by equation 3.29, which derives from the difference observed between the predicted mass ratio using the calibration constant estimated and the real experimental mass ratio of the solution in the validation data set.

$$\frac{\delta_{Quantification\ Validation_i}}{Quantification\ Validation_i} = \frac{\left(Mass\ Ratio_{i_{Predicted}} - Mass\ Ratio_{i_{Experimental}}\right)}{Mass\ Ratio_{i_{Experimental}}} \tag{3.29}$$

During the data analysis, lower concentration solutions show a higher relative error. API solutions closer in API concentration to the API solution that was used to extract the API reference spectrum will have a lower relative error in the quantification.

However, lower concentration solutions don't affect the calibration linear function as much as higher concentration solutions. Therefore, summing the relative error of each solution to get the final error of quantification will presume that each solution has the same weight in the calibration, which it's not accurate. Thus, this error was estimated by the average of all the solutions, equation 3.30.

$$\frac{\delta_{Quantification\ Validation_{data\ set}}}{Quantification\ Validation_{data\ set}} = \frac{\sum\left(mass\ ratio_{i_{Predicted}} - mass\ ratio_{i_{Experimental}}\right)}{\sum mass\ ratio_{i_{Experimental}}} \tag{3.30}$$

Besides the relative error of quantification of the validation data set and an error of experimental mass ratios that were used to estimate the calibration constant in the first place, there's still a third error to be considered which is the error of experimental mass ratios of the validation data set. The relative error of mass ratios of calibration and validation data set will have the same premise, equation 3.31.

$$\frac{\delta_{mass\ ratio_{data\ set}}}{mass\ ratio_{data\ set}} = \frac{\sum\left(\delta_{mass\ ratio_i}\right)}{\sum mass\ ratio_i} \tag{3.31}$$

An overview of the propagation error is represented in equation 3.32, for each relative error that affects the calibration constant.

$$\left(\frac{\delta_{c_{API}/c_{solvent}}}{c_{API}/c_{solvent}}\right) = \frac{\delta_{Quantification\ Validation_{data\ set}}}{Quantification\ Validation_{data\ set}} + \left(\frac{\delta_{mass\ ratio_{data\ set}}}{mass\ ratio_{data\ set}}\right)_{Calibration} + \left(\frac{\delta_{mass\ ratio_{data\ set}}}{mass\ ratio_{data\ set}}\right)_{Validation} \tag{3.32}$$

On the other hand, the error of $c_{API}/c_{keratin}$ must be determinated by the propagation of the errors of the different calibration constants in between the API and keratin, equation 3.33.

$$\frac{\delta\left(\frac{c_{API}}{c_{keratin}}\right)}{\frac{c_{API}}{c_{keratin}}} = \frac{\delta\left(\frac{c_{API}}{c_{solvent}}\right)}{\frac{c_{API}}{c_{solvent}}} + \frac{\delta\left(\frac{c_{solvent}}{c_{water}}\right)}{\frac{c_{solvent}}{c_{water}}} + \frac{\delta\left(\frac{c_{water}}{c_{BSA}}\right)}{\frac{c_{water}}{c_{BSA}}} + \frac{\delta\left(\frac{c_{BSA}}{c_{keratin}}\right)}{\frac{c_{BSA}}{c_{keratin}}} \tag{3.33}$$

Although, in theory, any API can be quantified in skin as long as that API can be linked to the calibration constant of keratin that includes a chain of different calibration constants, it's advised that a quantification of a new API should be done with the least number of constants possible to reduce the final error of that API quantification constant.

Consequently, the calibration of an API with the least amount of error will be one where the API is dissolved in water, only in the case that the API is insoluble in water, other solvent should be chosen.

3.4. Experimental Data Sets

Table 3-2 resumes all the experiments that were done for this thesis, with all the conditions applied to each data set, with a quality requirement evaluation to determine if the data set can be used for the calibration of the material. Note that an API calibration in this thesis might not use all the different mass ratios available in an experimental data set, since choosing which API solutions should be part of the calibration data set is a quality analysis optimization.

Table 3-2 – Experimental API data sets that were used in this thesis with all the conditions of measurements used

Date	Material	Solvent	Mass Ratios	Used for Quantified reference	Exposure Time (s)	Number of Frames	Depth above window
2017.10.11	BSA; Ethanol	Water	1,010%; 5,268%/ 5,283%; 11,198%		5	60	30
2017.10.13	Ethanol	Water	0,503%; 1,010%; 2,041%; 3,093%; 4,167%; 5,263%		5	120	30
2017.10.16	BSA	Water	1,042%; 2,078%; 3,101%; 5,172%		5	120	30
2017.10.19	Ethanol	Water	0,517%; 1,040%; 2,102%; 3,189%; 4,295%; 5,423%; 8,363%; 11,486%; 18,243%		5	120	30
2017.10.26	BSA	Water	0,099%; 0,101%; 0,103%; 0,105%		5	120	30
2017.10.27	Salicylic Acid	Ethanol	0,575%; 1,008%; 2,041%; 3,100%; 5,253%		5	120	30
2017.10.27	Ethanol	Water	0,505%; 1,013%; 2,050%; 3,103%; 4,182%; 5,279%; 8,153%; 11,170%; 14,324%		5	120	30
2017.10.30 to 2017.11.02	BSA	Water	1,012%; 3,089%; 5,256%; 7,515%; 11,124%; 26,510%; 42,674%		5	120	30
2017.10.31 to 2017.11.01	Salicylic Acid	Ethanol	0,503%; 1,013%; 2,042%; 3,093%; 5,264%; 11,109%; 24,973%; 42,857%		5	120	30
2017.11.08	BSA	Water	1,011%; 3,094%; 5,148%; 7,541%	x	5	200	30
2017.11.09	Salicylic Acid	Water/Ethanol	25,009%; 25,064%		5	100	30
2017.11.10	Ethanol	Water	0,500%; 1,004%; 2,022%; 4,145%; 5,289%; 853,552%; 392,135%; 228,549%; 98,794%; 24,190%	x	5	100	30
2017.11.10	Salicylic Acid	Water	Doesn't dissolve		5	100	30
2017.11.13	Methyl salicylate	Ethanol	1,001%; 2,021%; 5,210%; 10,994%	x	5	100	30

2017.12.04	MCT Oil	Ethanol	1,000%; 4,954%; 10,026%; 19,945%; 27,731%	x	5	100	30
2017.12.05	Acetone	Water	0,999%; 2,997%; 4,998%; 9,865%; 14,938%; 19,833%	x	5	200	30
2017.12.05	Ubiquinol	Acetone	0,490%; 0,980%; 2,944%; 4,822%; 4,487%	x	5	200	30
2017.12.06	4-Methylsalicylic Acid	Ethanol	1,010%; 2,039%; 5,261%; 11,119%	x	5	100	30
2017.12.06	5-Methylsalicylic Acid	Ethanol	1,010%; 2,043%; 5,261%; 11,102%	x	5	100	30
2017.12.07	3-Methylsalicylic Acid	Ethanol	1,010%; 2,034%; 5,257%; 11,104%	x	5	100	30
2017.12.07	Ibuprofen	Ethanol	1,000%; 1,996%; 4,986%; 10,004%; 19,336%; 26,288%; 38,341%	x	5	100	30
2017.12.07	Lidocaine	Ethanol	1,001%; 1,979%; 4,926%; 9,751%	x	5	100	30
2017.12.07	Salicylic Acid	Ethanol	0,988%; 1,955%; 4,929%; 9,865%; 19,734%; 29,355%; 39,539%; 49,244%	x	5	100	30
2017.12.08	Chemical UV filter I	MCT Oil	2,406%; 4,916%	x	5	100	30
2017.12.08	Hydrocortisone	Ethanol	0,984%; 1,977%; 2,968%; 2,967%; 9,877%	x	5	100	30
2017.12.08	Oleic Acid	Ethanol	0,990%; 1,980%; 4,945%; 9,845%	x	5	100	30
2017.12.08	Chemical UV filter II	Ethanol	1,959%; 4,924%; 9,787%	x	5	100	30
2017.12.08	Propylene Glycol	Water	1,000%; 2,996%; 4,991%; 9,987%; 14,941%; 18,244%	x	5	100	30
2017.12.08	Retinol	Ethanol	0,985%; 1,984%; 4,889%	x	5	100	30
2017.12.08	Testosterone	Ethanol	0,990%; 1,973%; 4,926%; 9,892%	x	5	100	30
2017.12.13	β-carotene	Ethanol	0,0028%; 0,0045%	x	5	50	30
2018.01.16	Caffeine	Water	0,500%; 1,001%; 1,999%	x	5	100	30
2018.01.25	BSA	Water	0,998%; 3,005%; 5,004%; 6,986%; 7,520%		5	100	30 / 60
2018.01.25	Ethanol	Water	0,997%; 2,990%; 4,979%; 7,470%		5	100	30 / 60
2018.02.13	Glycerol	Water	0,998%; 2,843%; 4,996%	x	5	100	30
2018.02.13	2-Pyrrolidone-5-carboxylic acid	Water	0,995%; 2,986%; 4,989%	x	5	100	30

Chapter 4

Results and Discussion

The following chapter will present the results obtained using the data sets previously introduced to optimize protocol and calibration methodology of new APIs. It will comprise different types of data, pre-processing techniques and various data analysis tools.

To calibrate an API there's a need to dissolve it in a solvent of choice of the user, thus the most relevant APIs (BSA, ethanol, acetone, caffeine, salicylic acid (SA), ubiquinol and a chemical UV filter) in this thesis are categorized by its solvent in this chapter (water, ethanol, acetone, MCT oil). The rest of APIs calibrated are summarize in the end of the chapter, as well as *in vivo* skin measurements of four skin products with ibuprofen, oleic acid, SA and caffeine as APIs.

4.1. APIs in Water

4.1.1. Bovine Serum Albumin

Measurements and Protocol Optimization

Several data sets of BSA in water were collected, in specific the data set from 2017.10.30 to 2017.11.02 was able to give enough information to optimize and finalize the protocol of BSA solutions preparation and Raman conditions measurements for BSA in water calibration.

In a Raman measurement, all frames collected should have the same spectral shape and intensity for the measurement to have quality enough to be consider for calibration, as it's presented in Figure 4.1.

Higher BSA concentration solutions have higher variation of backgrounds between frames, Figure 4.1. Higher amounts of protein in solution cause more fluorescence, that interferes with the Raman experiment, since BSA has an intrinsic fluorescence due to aromatic amino-acid residues present. [26] These difference in backgrounds between frames doesn't affect the quality of spectra for calibration, since it can be easily removed in the calibration analysis.

However, spectral shape and intensity between different peaks in the spectrum must be consistent between frames. This kind of observation results in bad quality spectra not suitable for calibration and it was observed in different data sets that there are specific ranges of concentrations of BSA solutions that are more likely to result in outlier measurements.

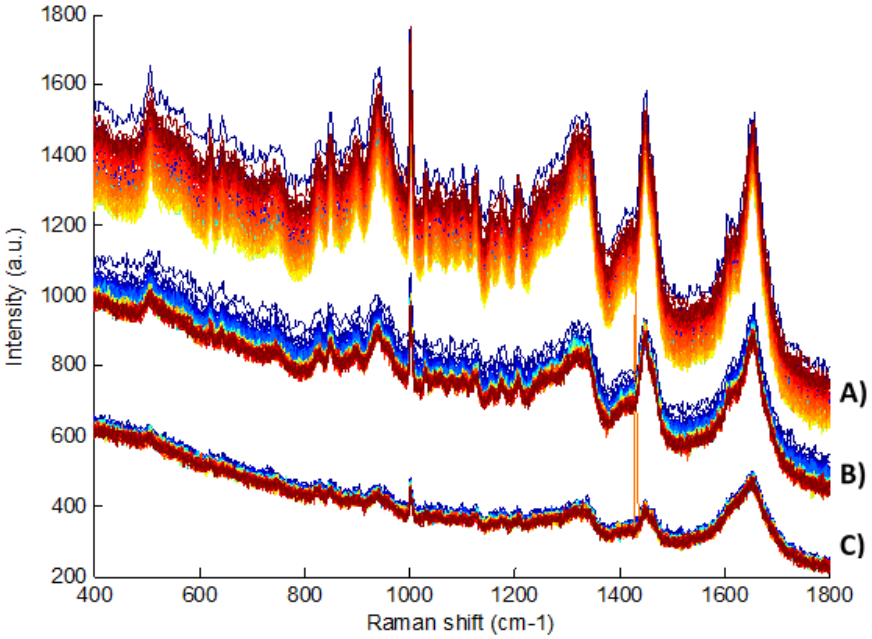

Figure 4.1 - BSA in Water solutions Measurements – 120 frames per spectrum. A) 20% BSA in Water Solution; B) 10% BSA in Water Solution; C) 4% BSA in Water Solution.

Data sets collected include solutions up to 30% of BSA/water mass ratio, outlier measurements are more common in mass ratio lower than 7,5% of BSA in solutions. A comnon outlier measurement observed throughout different data sets is shown in Figure 4.2. It's considered an outlier because the spectrum has different intensities between frames collected in a range of Raman shift between 770 to 1500 cm^{-1}. This variation isn't consistent with the rest of spectrum, thus different backgrounds between frames isn't a premise for the problem observed.

Only for mass ratio lower than 7,5% of BSA in solutions, a few particles in suspension with a filamentous shape were visible during the preparation of these BSA solutions, as well as foam in these solutions.

This could explain the outlier example in Figure 4.2, probably suggesting that these solutions weren't entirely homogenous. Two hypotheses were formulated to explain this type of outliers: the crystal of BSA was not well dissolved or the protein denatured.

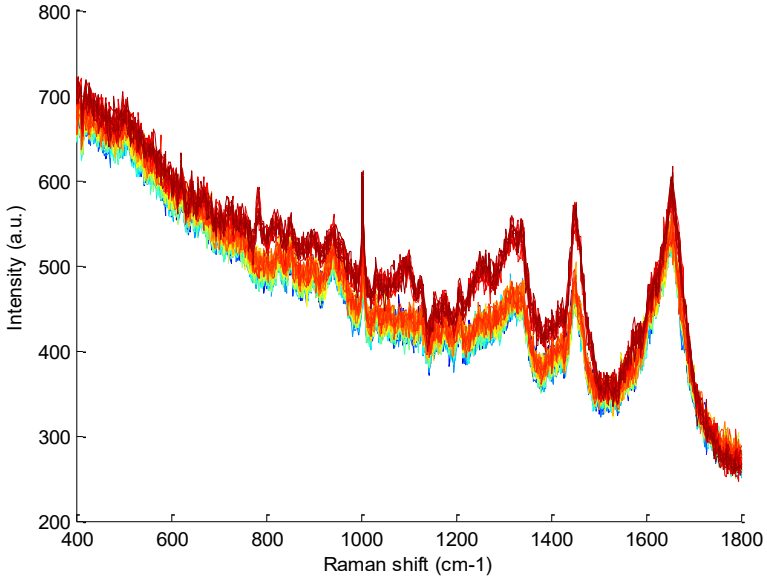

Figure 4.2 – Example of an outlier Raman measurement: 5% BSA in water solution measurement with 120 frames and 5 seconds exposure time.

Foaming is a common occurrence in the preparation of protein solutions and substantial damage is known to occur to protein molecules in this environment. Protein foams are usually stabilized by the protein molecules themselves, because they're amphiphilic molecules. [27]

Protein adsorption can reduce surface tension, since proteins undergo a change in its conformation by unfolding to let their hydrophobic regions become in contact with gaseous phase. These authors concluded that the main mechanism of protein damage is foaming through surface denaturation. [28]

Since protein denaturation in foam can be directly correlated with the interfacial exposure area, BSA as a protein which forms rigid films at the gas–liquid interface has an exposure area that can be estimated from the initial bubble size. For the BSA solutions investigated by these authors, it was found that about 10% of the molecules adsorbed and desorbed were denatured. [27], [28]

There are also spectroscopic studies of the conformational properties of foamed BSA that show that most of the protein damage is caused in the protein tertiary structure. These studies also concluded that structural changes were for the most part reversible in solutions. [27], [28]

Other studies stated that conformational changes during denaturation can occur in the BSA secondary structure, due to amide III feature that results from coupling of the C-N stretch to the N-H bend. [29]

In the protocol, BSA has to be for 24 hours in a rolling motion to dissolve, increasing the solubility and the exposure area of gas–liquid interface. Because of this step, the particles in suspension and foam can't be completely avoided in BSA solutions with a mass ratio lower than 7,5% of BSA in water.

BSA crystal doesn't have the same shape or size as the filamentous particles in solution. Moreover, in theory, higher BSA concentration solutions should be more susceptible to low solubility, however the same type of outliers weren't observed in these BSA solutions.

It was observed that there's an increase in viscosity as BSA concentration increase, which reduces the turbulence in the fluid and the interfacial exposure area, resulting in less denaturation of the protein and less outlier measurements. However, higher BSA concentration solutions have too much spectral changes compared to BSA reference spectrum to be considered to be part of calibration data set.

It was concluded that solubility wasn't the source of the problem for outliers. The best hypothesis would be that part of the protein aggregates after denaturation forming the filamentous particles seen. Thus, protocol was optimized to include BSA solutions lower than 7,5% BSA/water in mass ratio, with a sedimentation step to avoid collection of any particles in suspension in the BSA solutions.

The data set used for calibration of BSA was measured on 08/11/2017 and to test the final protocol, the 1% BSA in water solution was measured in two different ways, presented in Figure 4.3.

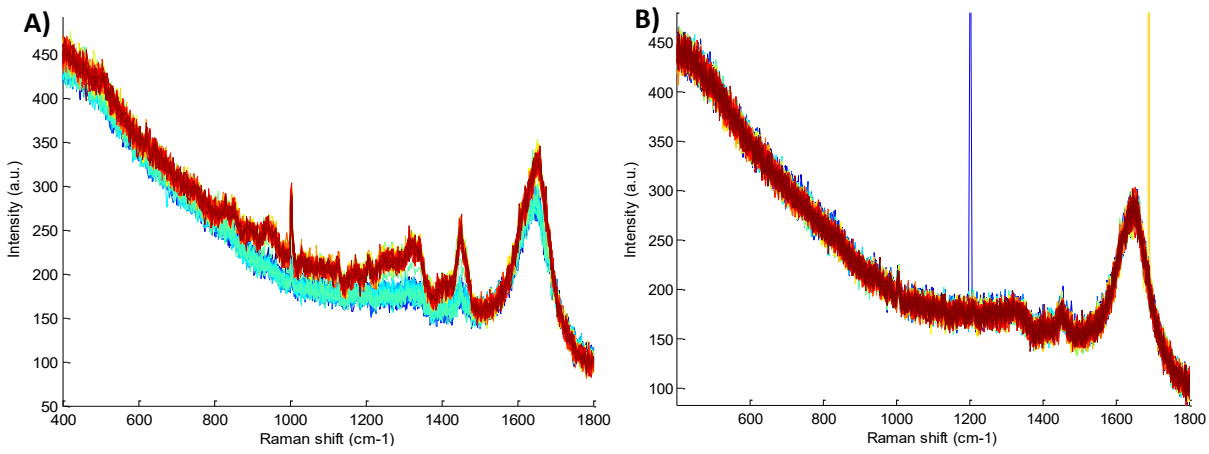

Figure 4.3 - 1% BSA in Water Solution; A) Solution was measured right after 24h of dissolution; B) Solution with 20 minutes of sedimentation.

The first Raman measurement was done without the sedimentation step and the second with 20 minutes of sedimentation. This extra step resulted in a better quality Raman measurement. All new measurements of other solutions resulted in almost no outliers, thus the protocol was validated.

The amount BSA denaturation in literature wasn't used in this thesis, it's assume that this denaturation it's negligible and the mass ratio of the solution is the same. Also, the BSA calibration function doesn't show deviations, which suggests that the mass ratios estimated are in fact close to reality.

The data set used for calibration has four different mass ratio solutions, presented in Figure 4.4.

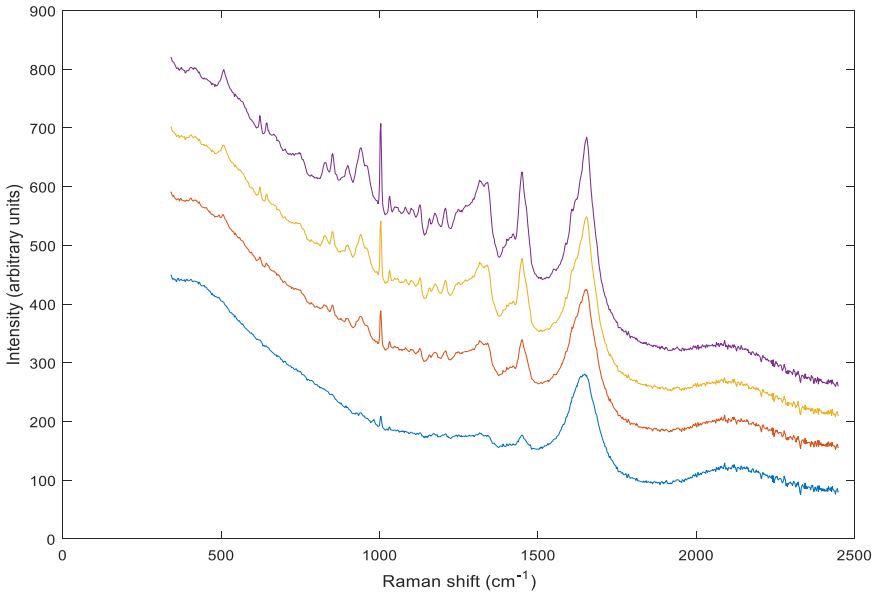

Figure 4.4 – Calibration data set BSA solutions. Mass Ratio of solutions: 1,01%; 3,09%; 5,15%; 7,54%.

The 25/01/2018 data set of BSA in water solutions was used as a validation model. All measurements for the four solutions that were used to predict its mass ratio are presented in Figure 4.5.

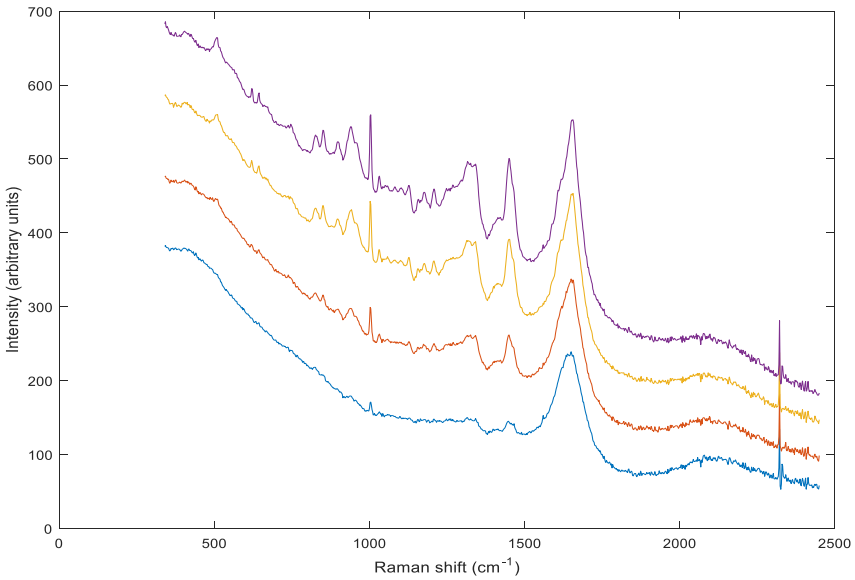

Figure 4.5 – Raman measurements of four solutions of the validation data set of BSA in water calibration.

All API solutions have quartz contribution in the spectra, and there is a need to subtract it during the processing of the final API reference spectrum. Therefore, there was a need to study the amount of quartz present and see if it is possible to automatically quantify its contribution.

Depths at 30 and 60 microns were measured without any solution present on the window – air measurement, presented in Figure 4.6.

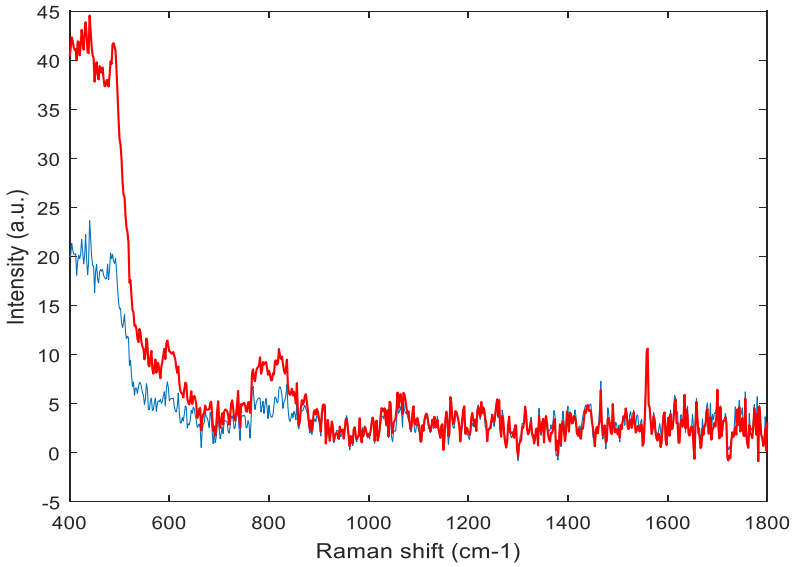

Figure 4.6 – Raman measurements in air at 60 microns in depth – blue – and 30 microns in depth – red, above window.

For one solution of 5% BSA/water mass ratio in the validation set, the same two depths were measured, presented in Figure 4.7.

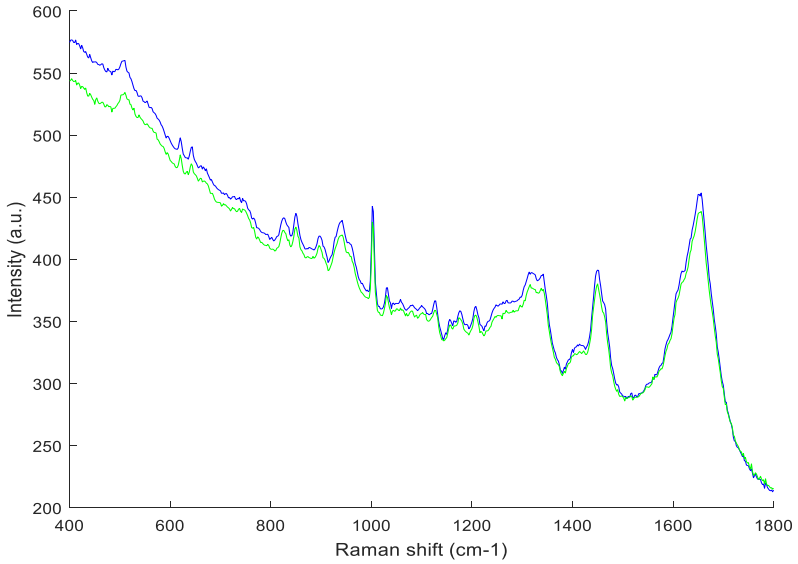

Figure 4.7 - Raman measurement of 5% BSA in water solution at two different depths: 30 and 60 microns above window.

The measurements in air and in a solution, at two different depths, didn't allow a correct quantification of quartz contribution in the spectra, in the 400 to 530 cm^{-1} range. The difference in intensity in this range between different depths in air in solution doesn't correlate to a real contribution of quartz.

All four spectra, from air and 5% BSA in water solution Raman measurements in Figure 4.6 and 4.7, have some amount of noise and a pattern that can't be identified. This pattern is probably overlapping the quartz range, not allowing a direct quantification of quartz intensity in those depths.

In summary, although it's useful to have an automatic approach to quantify quartz in the calibration, the quartz subtraction still requires a subjective approach of manual subtraction by the user.

Calibration

BSA and water calibration involves a fit model with different chosen references, such as: BSA, water, quartz and background. BSA and water references spectra are the only ones in the model that are processed from raw Raman measurements, as it was described in chapter 3.3.2.

Reference water spectrum was processed by subtracting a scaled quartz spectrum from the water measured in the day of the experiment, with a chosen scaling factor $f_{Q_{CleanWater}}$, as described in equation 3.2 and the result is presented in Figure 4.8.

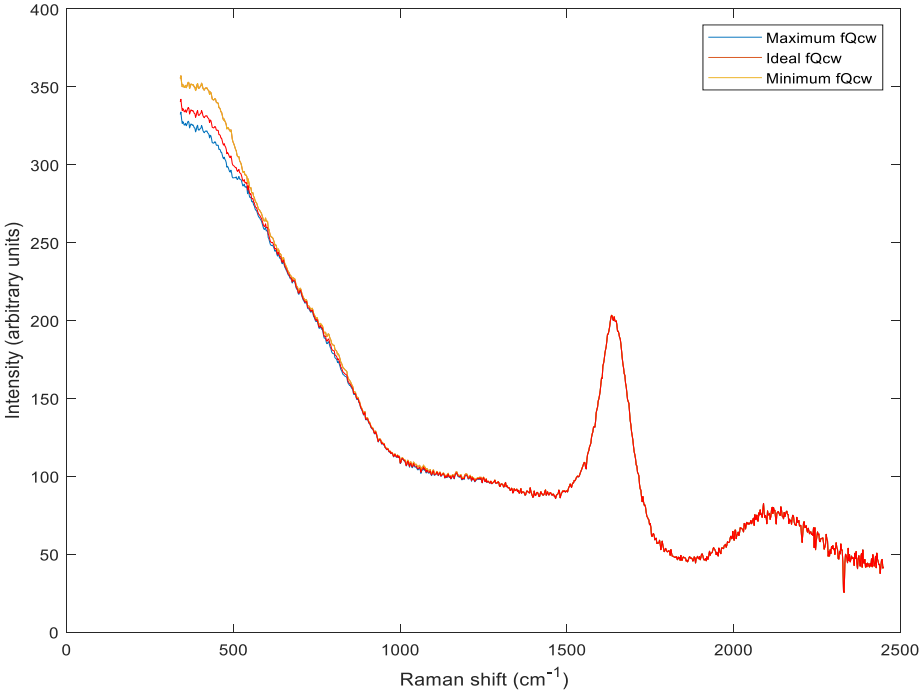

Figure 4.8 – Water Raman spectrum measured in day of calibration with three different quartz spectrum subtraction.

The range of scaling factors chosen are described in Table 4-1. The maximum value of factor of $f_{Q_{CleanWater}}$ will be when a negative peak at 496 cm^{-1} starts to appear, as it's seen in Figure 4.8. The ideal factor of $f_{Q_{CleanWater}}$ is the one that smooths out this negative peak. The minimum factor of $f_{Q_{CleanWater}}$ chosen is the case of a negligible quartz contribution. The final reference water spectrum should be clean of quartz contribution in the spectrum.

Table 4-1 : Values chosen by the user for scaling factor of quartz with relative error of variation, based on the peak at 496 cm^{-1}. Standard deviation of clean water spectrum with respective its relative error. Relative Error of minimum and maximum values are compared to ideal.

	Minimum	**Ideal**	**Maximum**
$f_{Q_{CleanWater}}$	0,0000	0,0200	0,0309
Standard Deviation of Clean Water Spectrum	57,073	56,295	55,876
Relative Error of Standard Deviation	1,38%		-0,75%

The relative error of the standard deviation of the water reference spectrum – after quartz subtraction – will be the most representative feature of how the quartz subtraction affects the reference in the fit model. The subtraction of quartz induces a change in the reference spectrum of +1,38% or -0,75%.

Processing the BSA reference spectrum requires the raw Raman measurement of BSA solution, with a mass ratio of 7,54% BSA/water.

There are three necessary steps to process this BSA solution spectrum: removing water present, removing quartz contribution and, finally, removing any background present in the spectrum.

From the previous study of quartz in Measurements and Protocol Optimization, it was concluded that its quantification can't be estimated automatically. Moreover, it's amount is almost negligible compared to overall spectrum. Therefore, processing BSA reference spectrum involves analysing first a final BSA spectrum where there was no subtraction of quartz, just water and background.

The subtraction of water from BSA solution spectrum includes choosing a scale factor $f_{S_{BSA}}$, explained in equation 3.3. There are none core bands of water that can guide the user to how much of the water should be subtracted, therefore the user can use a water combination band around 2100 cm^{-1}.

The minimum scale factor $f_{S_{BSA}}$ chosen leads to a spectrum with a small band present, but it's almost negligible. The maximum scale factor $f_{S_{BSA}}$ has a small negative band present. And the ideal factor $f_{S_{BSA}}$ has a smooth line with no band present in that range of the spectrum. The process to obtain the BSA reference spectrum, for the three possible factors $f_{S_{BSA}}$ are presented in Figure 4.9.

An additional background is detected in the 1800 to 2450 cm^{-1} range of the spectrum. Thus, a slope was extrapolated in this range of the spectrum enabling a subtraction of a first order polynomial to remove the background. Any additional background was considered to be part of the BSA spectrum.

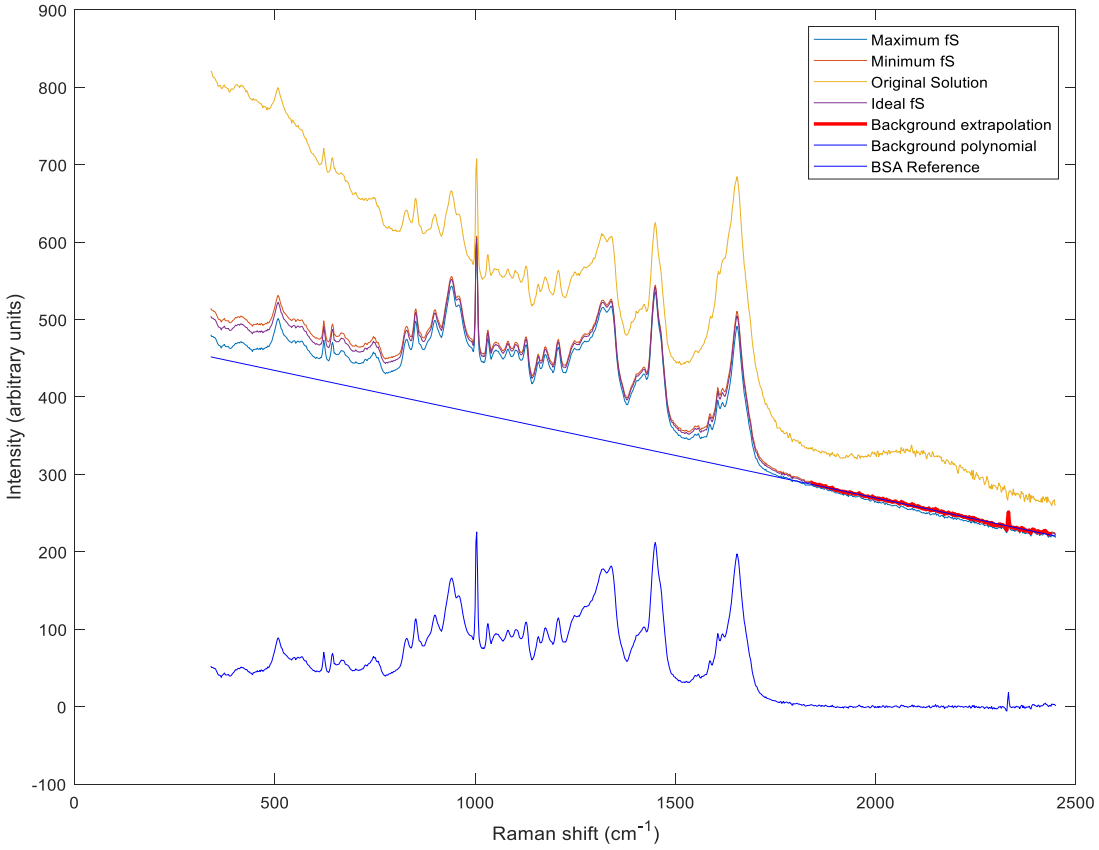

Figure 4.9 – 7,5% BSA in water solution measurement with subtraction of three different scale factors $f_{S_{BSA}}$, and, subsequently, a polynomial subtraction extracted from 1800 cm^{-1} to 2450 cm^{-1} range in the spectrum.

The range of scaling factors $f_{S_{BSA}}$ chosen are presented in the Table 4-2.

The relative error of the BSA reference spectrum standard deviation – after background subtraction – will be the most representative feature of reference water subtraction. The subtraction of reference water spectrum from the BSA solution spectrum will affect the BSA reference in the fit model with a relative error of +1,72% or -0,52%.

Table 4-2 Values chosen by the user of scaling factor $f_{S_{BSA}}$ to subtract the reference water from BSA solution spectrum with relative error of variation. Standard deviation of BSA reference spectrum with respective its relative error. Relative Error of minimum and maximum values are compared to ideal.

	Minimum	Ideal	Maximum
$f_{S_{BSA}}$	0,90	0,93	1,00
Relative Error of $f_{S_{BSA}}$	1,08%		7,53%
Standard Deviation of BSA Spectrum	44,232	44,464	45,230
Relative Error of std BSA Spectrum	-0,52%		1,72%

To further optimize the BSA reference spectrum in the fit model of calibration, there's a subtraction of a scaled quartz spectrum in the processing analysis (before removing the background), described in equation 3.3.

Quartz scale factor $f_{Q_{BSA}}$ takes into account that the range 350-484 cm^{-1} should be constant. If there is an accentuated decline in the spectrum might be due an excessive or not enough subtraction of quartz. Also, the range 485-616 cm^{-1} should be slightly above than the range 350-484 cm^{-1}, considering RiverD's library of older BSA references and literature. [29] This processing is presented in Figure 4.10.

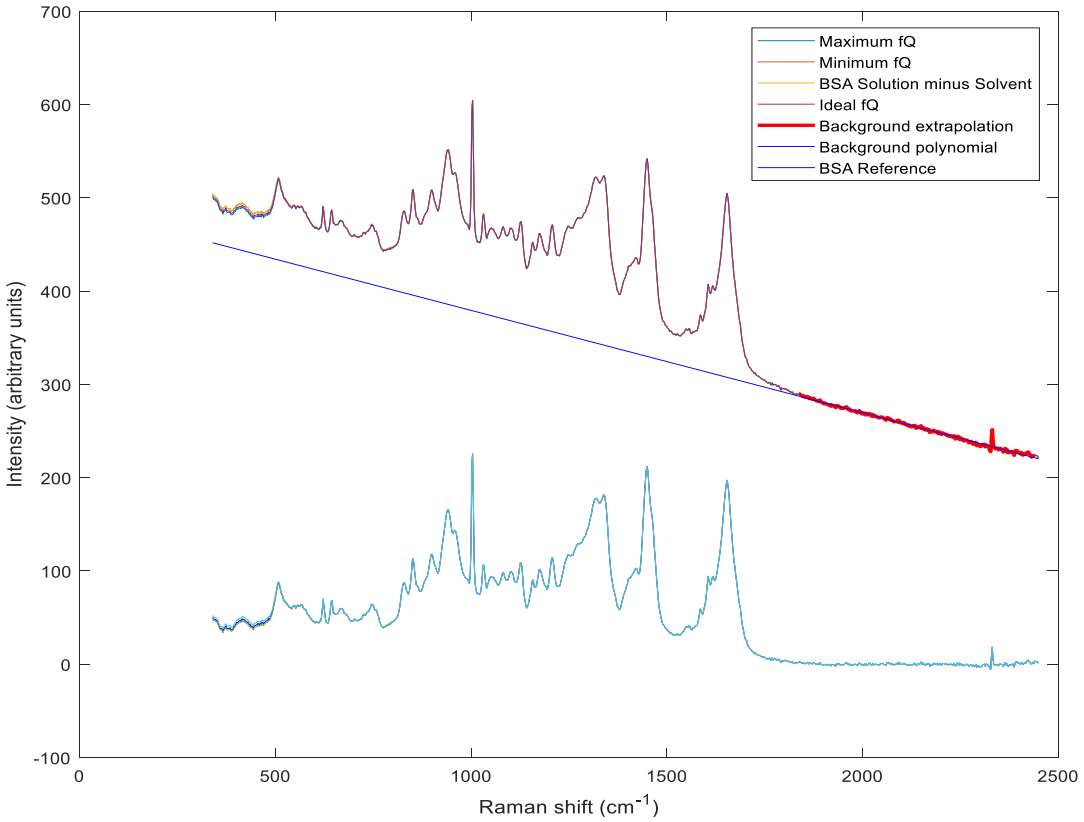

Figure 4.10 - 7,5% BSA in water solution spectrum minus reference water and a subtraction of three diferent quartz scaling factors. A polynomial subtraction was extracted from 1800-2450 cm^{-1} range in the spectrum.

Since the reference water spectrum might have a positive or negative contribution of quartz, the BSA spectrum after its subtraction will have more or less quartz than the BSA solution spectrum. So, the quartz factor $f_{Q_{BSA}}$ in equation 3.3 might not be the real representation of the actual quartz present.

This quartz factor can work as a correction factor of the error introduce in the subtraction of a water spectrum with an uncertainty of quartz contribution. Moreover, comparing the scale factors $f_{Q_{CleanWater}}$ and $f_{Q_{BSA}}$, there's a significant difference between the two, even though both spectra were measured at the same depth. Thus, both factors are independent and validates the premise that quartz can't be quantified with precision as a function of depth.

The range of scaling factors $f_{Q_{BSA}}$ that were chosen in the process are presented in the Table 4-3.

Table 4-3: Values chosen for scaling factor of quartz to obtain BSA reference spectrum with relative error of its variation. Standard deviation of BSA reference spectrum with respective relative error. Relative Errors are compared to ideal factor.

	Minimum	Ideal	Maximum
$f_{Q_{BSA}}$	0	0,002	0,005
Relative Error of $f_{Q_{BSA}}$	100,00%		150,00%
Standard Deviation of BSA Spectrum	44,4638	44,5018	44,5274
Relative Error of std BSA Spectrum	-0,09%		0,06%

The subtraction of quartz from the BSA solution minus reference water spectrum will affect the reference BSA in the fit model with a relative error of +0,06% or -0,09%. The results show a very limited range of how much it's possible to subtract quartz considering the requirements for this step.

After all the individual subtraction, there's a normalization on the standard deviation range of spectrum range 550 to 1800 cm^{-1}, the ideal BSA reference spectrum is presented in Figure 4.11.

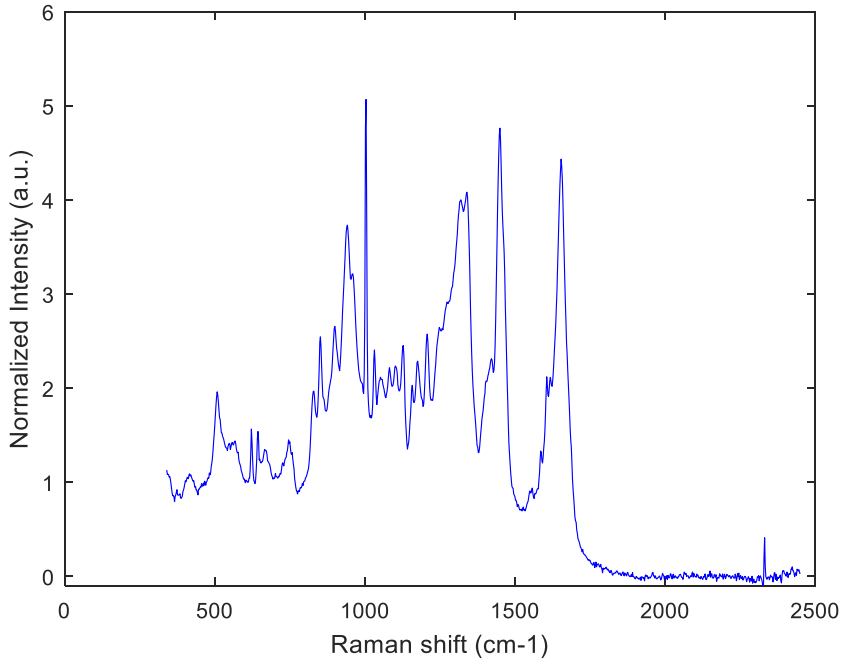

Figure 4.11 - Ideal BSA reference spectrum after all the individual subtraction of the main components of 7,5% BSA solution and normalization on the standard deviation spectrum range of 550 to 1800 cm^{-1}.

After processing both water and BSA references spectra with ideal scale factors for water and quartz subtraction, the calibration analysis can be done. The results of the fit coefficients for BSA and water references spectra of the fitting result to each solution of the data set are presented in Table 4-4.

Table 4-4: Fit coefficients of BSA and clean water relating the scaling between BSA solutions to BSA and clean water references spectra in the fit model chosen for BSA in water calibration.

	BSA Fit Coefficients	Water Fit Coefficients
Solution 1	6,039	57,969
Solution 2	18,656	56,029
Solution 3	30,389	54,085
Solution 4	44,502	52,355

The ratio of the fit coefficients will be then used on a linear regression to estimate the slope of the calibration constant, $c_{BSA}/c_{Water} = 11{,}256$. Figure 4.12 presents the linear function with all the fit errors of this regression, as it was outlined in Figure 3.3.

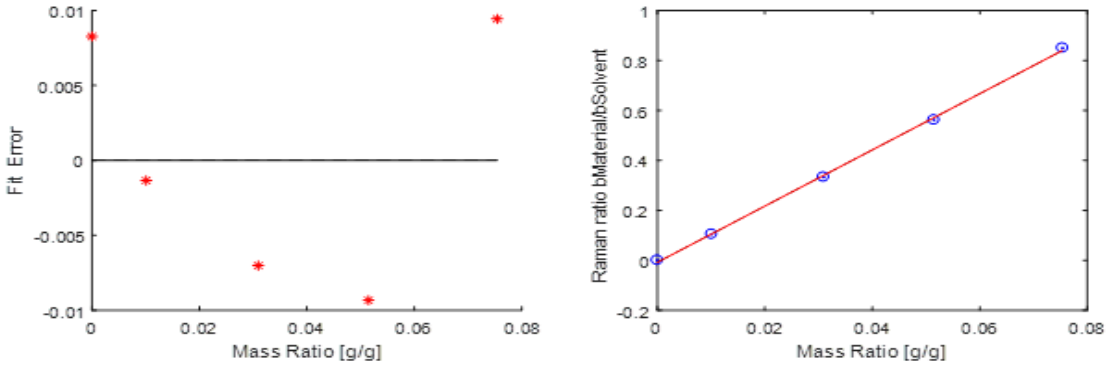

Figure 4.12 – Calibration linear function of Raman ratio between fit coefficients of BSA and water to mass ratio of each solution (slope of linear function = 11,256 with $R^2 = 0{,}999$); Fit Error of each solution point in the calibration to the calibration line with the Euclidean Norm of all solutions ($N = 2{,}958 \times 10^3$).

An optimal calibration has a fitting spectrum of all raw measurements solutions with the least amount of residuals. The results of the fitting of BSA solutions are represented in Figure 4.13.

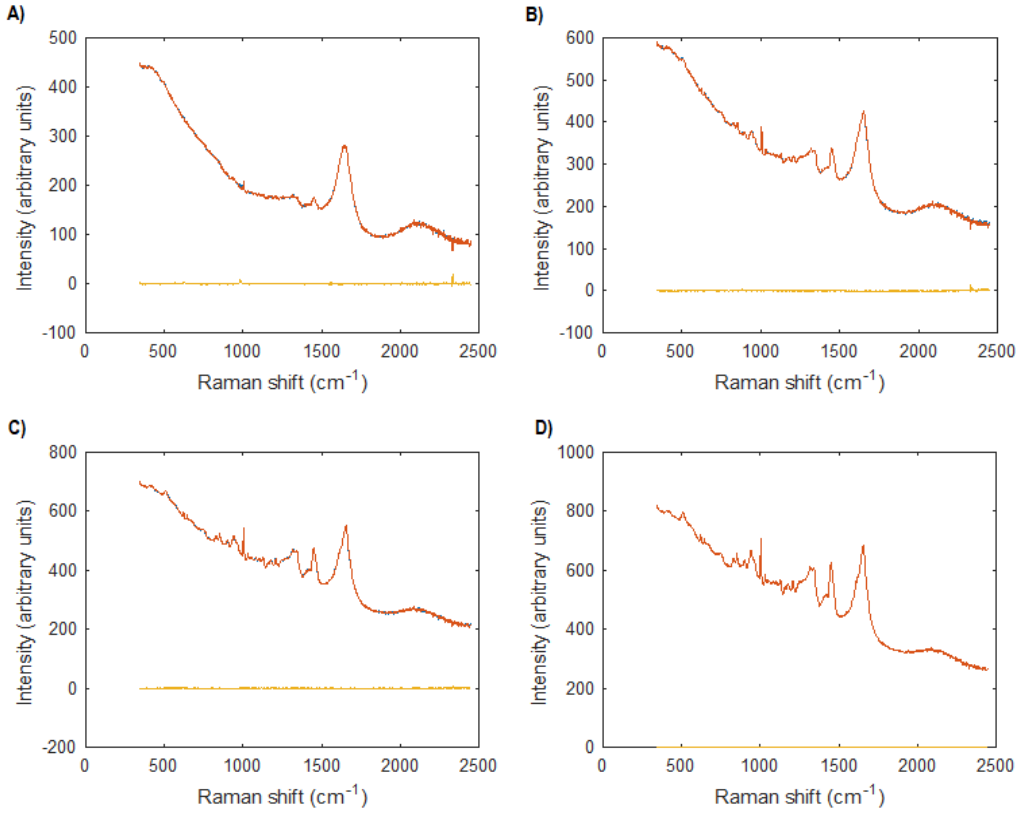

Figure 4.13 – Fitting Results of each solution based on the fit model chosen for BSA in water calibration. Mass Ratios of each solution: A) 1,01%; B) 3,09%; C) 5,15%; D) 7,54%.

Since there are three factors ($f_{Q_{CleanWater}}$, $f_{S_{BSA}}$and $f_{Q_{BSA}}$) that can be chosen by the user, in total there are 27 options for fit model that include the ideal and extremes cases for each scale factor.

These 27 combinations will include any in between model that can be formulated by a user, therefore evaluating all these possible outcomes will lead to all the different calibration constants. The two extremes cases that can obtain the highest variation of the constant are described in Table 4-5.

Table 4-5: The two extremes cases of possible scaling factors chosen are Model A and B, leading to the maximum and minimum of calibration constant $c_{RefBSA}/c_{RefWater}$. Any other possible fit model for BSA in water calibration is between the range of calibration constants estimated by these two models.

	Model A - Highest $c_{RefBSA}/c_{RefWater}$	Model B - Lowest $c_{RefBSA}/c_{RefWater}$
$c_{RefBSA}/c_{RefWater}$	12,119	10,378
$f_{Q_{CleanWater}}$	0,000	0,031
$f_{S_{BSA}}$	0,850	1,020
$f_{Q_{BSA}}$	0,005	-0,005

In total, three different models were studied (Model A, B and an Ideal Model). These models derive from the combination of different processing of references spectra represented in Figure 4.14.

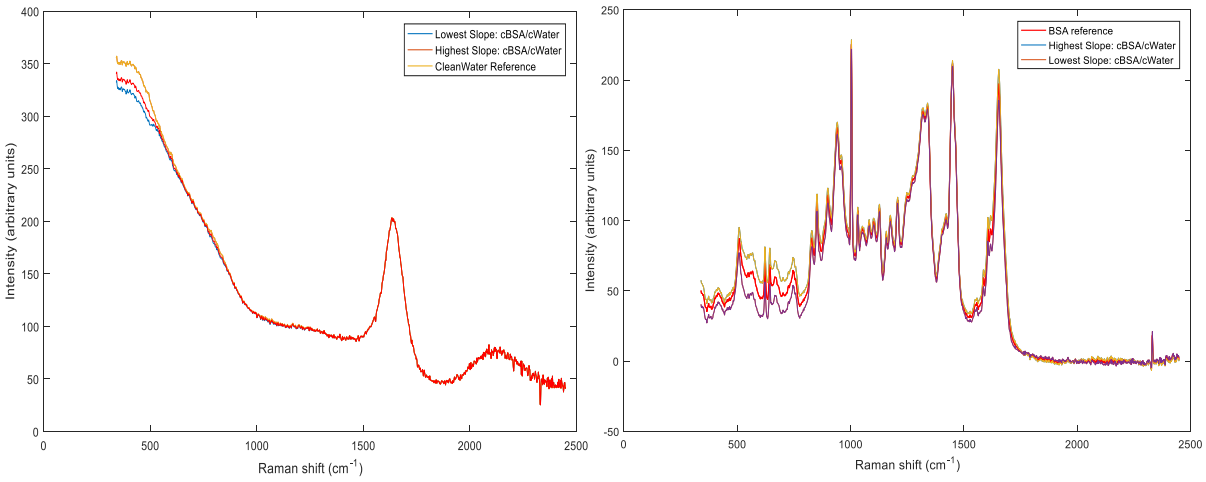

Figure 4.14 - BSA reference spectra and Clean Water reference spectra of three different fit models in the BSA in water calibration: Ideal Model; Model A and Model B. These represent all the possible outcomes of subjective choice of fit model in the calibration.

As a remark, the calibration constant fluctuates $\pm \approx 8{,}0\%$, due to the subjective approach of the user choosing the fit model, but this variation doesn't represent the relative error of the constant.

For each solution there's a steady contribution of BSA and water, in theory the fit coefficients for each one of them should not change if a reference spectrum in the fit model doesn't change either. Also, if the fit coefficients are just a scale factor of the reference spectrum, the relative error obtained to process the reference will be, in theory, the same as the relative error of the correspondent fit coefficient, because of the normalization step implemented.

However, it was observed that this isn't as straight forward as it was expected in theory. A faulty BSA and water references will make the multiple least squares fit minimize the residuals by compensating the incorrection in the reference spectrum by changing other fit coefficients. Therefore, there are two sources of variation of the slope, one by relative error of the standard deviation of the spectrum and another by dependency of its fit coefficient to other references spectra in the fit model.

Subsequently, a different calibration constant is directly link to a different reference spectrum in the fit model. The combination of the fit model chosen by the user and the calibration constant estimated by it will probably predict an accurate quantification of BSA. Thus, the quantification of new solutions might be, approximately, the same between two different fit models / calibration constants.

The variation of the calibration constant $\pm \approx 8{,}0\%$ doesn't have any meaning to conclude if a fit model in the calibration is precise and accurate. The error of quantification of new solutions or the material in skin is the real error of calibration constant estimated, therefore a validation step was necessary. Also, to conclude if in fact the Ideal model chosen is the most precise one.

Calibration Validation

The validation data set was used to test the accuracy of a calibration model formulated by the user. Three different calibration models were tested, the references spectra and the respective calibration constant should be able to preview the mass ratios of independent solutions, validation data set.

The validation method has the same mathematical approach as the calibration, in which there's a fit model created to fit the solutions of validation data set. In theory, the BSA and clean water reference spectrum from the calibration are the same in the validation fit model, the quartz spectrum is from the date of the validation experiment and a different slope is extrapolated to fit the background.

BSA reference spectrum can be use directly in the fit model, however the water reference spectrum can't. Since it leads to a very high error of quantification deriving from poor fit results, due to noise and artefacts in the solutions spectra that are not being considered in the fit model. Thus, the fit model used a water spectrum from the day of the validation experiment, with a subtraction of quartz and a scaling to the reference water used in the BSA in water calibration.

This normalization of the clean water spectrum in the validation fit model to the reference clean water used in the calibration relates the two water references, enabling the validation results to be ultimately link to the water reference spectrum from the calibration model.

Four solutions were used to test the quantification given by the calibration constant of BSA in water, the representation of the prediction model versus the experimental model of mass ratios is given by Figure 4.15, with the fit errors of each predicted mass ratio to its experimental value.

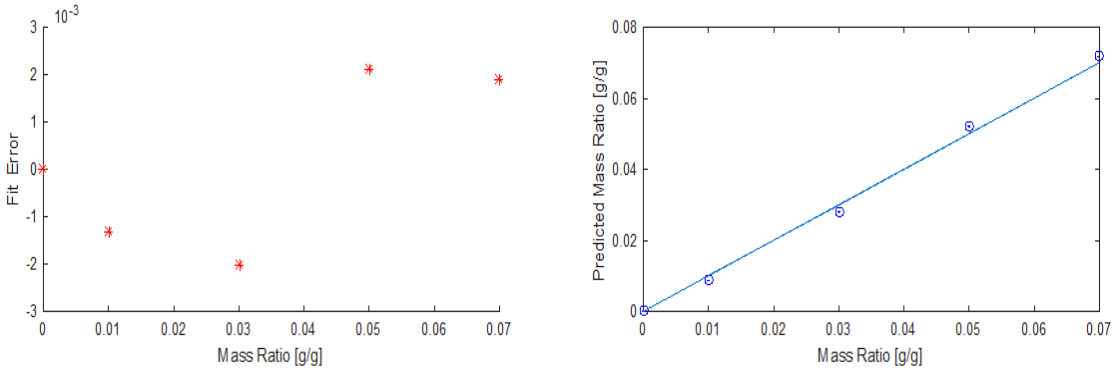

Figure 4.15 - Representation of the prediction model versus the experimental model of mass ratios from each solution of the validation data set of BSA in water ($R^2 = 0{,}996$); with the fit errors of each predicted mass ratio to its experimental value ($Eucledean\ Norm = 0{,}139 \times 10^3$).

The relative error of calibration constant was determined as it was explained in chapter 3.3.2, for each fit model studied in the calibration, its relative error is represented in Table 4-7.

Table 4-6: Relative error of quantification of the validation data set of BSA and water, with four different solutions, for each fit model of calibration: Ideal model, Model A and Model B.

	Ideal Model	**Model A**	**Model B**
$\frac{\delta_{Quantification\ Validation_{data\ set}}}{Quantification\ Validation_{data\ set}}$	4,60 %	4,98 %	4,74 %

The ideal fit model chosen has the least amount of relative error compared to Model A and B. It's expected since Model A and B are the two extreme models derive from a combination of possible incorrect subtraction of solvent and quartz from the references spectra in the fit model.

Even though these models are the worst possible outcome of the fit model, the difference in relative error compared to the Ideal Model is almost negligible. Validating the premise that this analysis and processing techniques result in accurate and precise results, which are reproducible regardless of the

subjectivity implied by the user. To evaluate how well the fit model of validation fits new solutions, the fitting result of the predicted solutions is given by Figure 4.16.

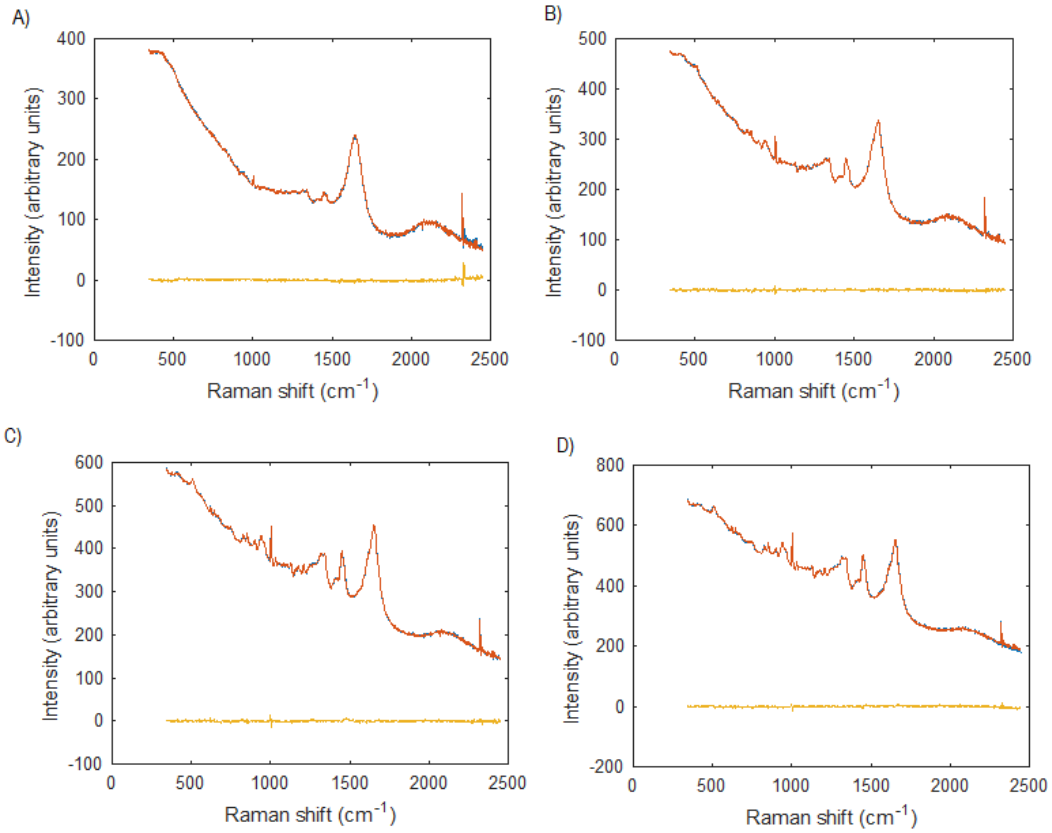

Figure 4.16 - Fitting result of the predicted solutions from validation data set of BSA in water, with mass ratios: A) 0,998%; B) 3,005%; C) 5,004%; D) 6,986%.

The relative error of 4,60% might not be the minimum value possible, since there's an infinite number of combinations possible to formulate a calibration fit model. New combinations will possibly lead to the same order of values as the relative errors obtained by the three that were studied. Thus, final error for BSA in water calibration is 4,80%, estimated by Table 4-8.

Table 4-7: Relative error of calibration constant of BSA to water, linked to each references spectra processed in the calibration.

Relative Error of $c_{RefBSA}/c_{RefWater}$	
$\frac{\delta_{Quantification\ Validation_{data\ set}}}{Quantification\ Validation_{data\ set}}$	$\pm$ 4,60 %
$\left(\frac{\delta_{mass\ ratio_{data\ set}}}{mass\ ratio_{data\ set}}\right)_{Calibration}$	$\pm$ 0,06 %
$\left(\frac{\delta_{mass\ ratio_{data\ set}}}{mass\ ratio_{data\ set}}\right)_{Validation}$	$\pm$ 0,14 %
$\frac{\delta_{c_{RefBSA}/c_{RefWater}}}{c_{RefBSA}/c_{RefWater}}$	$\pm$ **4,80** %

All new materials calibrated in this thesis, except for ethanol, will have the same relative error of the calibration constant as an approximation in this method, since new APIs don't have a validation step to determine its relative error.

Water Quantification Factor

The quantification factor estimated here will be the starting point of this calibration method, every API calibrated after this step will be link to this quantification factor, since it's the only one linked to keratin, described by equation 4.1. This quantification factor is the constant that's going to be used in SkinTools to quantify an API in skin in units of $mg_{API}/g_{keratin}$.

$$Quantification\ Factor_{water} = \left(\frac{c_{RefWater}}{c_{RefKeratin}}\right)^{-1} = \frac{c_{RefKeratin}}{c_{RefWater}} \tag{4.1}$$

This quantification factor of water derives from a chain of constants linking water to BSA, and BSA to keratin. Since the method introduces the approximation of BSA to keratin due to its spectral similar features, the Raman ratio of intensities between BSA and keratin is scale factor that scales the intensity of BSA spectrum to the reference spectrum of keratin. This ratio of intensities will be equal to the calibration constant between the two, since it's assume that the mass ratio / density between the BSA and keratin is equal to one, described by equation 4.2, thus $\boldsymbol{c_{RefBSA}/c_{RefKeratin}} = 3{,}4169 \times 10^{-5}$.

$$\frac{R_{RefBSA}}{R_{RefKeratin}} = \frac{c_{RefBSA}}{c_{RefKeratin}} \times \frac{m_{RefBSA}}{m_{RefKeratin}} \cong \frac{c_{RefBSA}}{c_{RefKeratin}} \tag{4.2}$$

The last step indicates the estimation of the calibration constant of water to keratin, described by equation 4.6. The relative error of the calibration constant of the reference water to reference keratin, derives from sum of each relative error of the constants in equation 4.3.

$$\frac{c_{RefWater}}{c_{RefKeratin}} = \frac{c_{RefWater}}{c_{RefBSA}} \times \frac{c_{RefBSA}}{c_{RefKeratin}} \tag{4.3}$$

Note that the relative error of an inverse function is the same as the function. Therefore, the quantification factor error only depends on the BSA in water calibration and the BSA and keratin approximation with relative error of 15%, the final error of 19,80% is determined by Table 4-9. [5]

Table 4-8: Calibration constant of water to keratin and quantification factor of water. Relative error of both values estimated.

Relative Error of Water Quantification Factor	
$\boldsymbol{c_{RefWater}/c_{RefKeratin}}$	$3{,}036 \times 10^{4}$
$\boldsymbol{Quantification\ Factor_{water}}$	$3{,}294 \times 10^{-5}$
$\dfrac{\boldsymbol{\delta(c_{RefKeratin}/c_{RefWater})}}{\boldsymbol{c_{RefKeratin}/c_{RefWater}}}$	$\boldsymbol{\pm 19{,}80\%}$

4.1.2. Ethanol

Measurements

Different experimental data sets of ethanol in water solutions were collected to achieve the best possible quality calibration of the new solvent, Raman measurements are represented in Figure 4.17.

Ethanol is a material highly soluble in water, different solutions were prepared from 0,5% up to 80% in mass fraction. The challenge in the ethanol calibration was choosing the right range of concentration for an accurate calibration. The observation made BSA in water calibration that higher concentration solutions didn't allow a precise calibration of the material was also confirmed with ethanol in water.

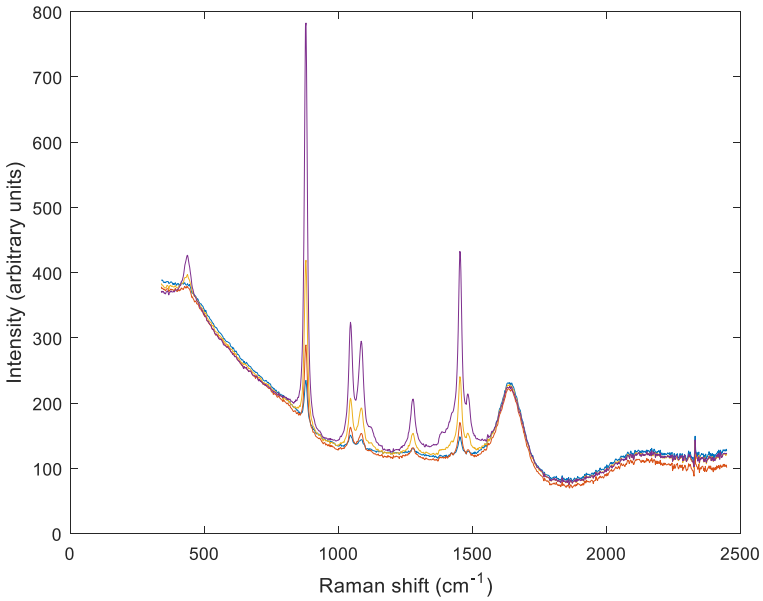

Figure 4.17 – Calibration data set of ethanol and water solutions with mass ratio: 0,50%; 1,00%; 2,02%; 5,29%. Raman measurements with average of 100 frames and 5 seconds exposure time, at 30 microns above window.

The highest concentration solution in the data set should've an equal Raman intensity contribution between ethanol and water, for the same reason discussed in the BSA calibration. It was observed that ethanol in water measurements have significant spectral changes as the concentration of ethanol in solutions increases. Therefore, the range of concentrations in the calibration data set has to be limited to have the best possible fitting results between the ethanol reference spectrum and these solutions.

The strong intermolecular hydrogen-bonding ability of pure water, makes water clusters quite complex structures that are dominated by the hydrogen-bonding with distinctive properties in both experimental and theoretical studies. Moreover, the presence of an ion in an aqueous solution might influence the local water structure, creating a structured network of hydrogen bonds in solution. [30] Hydrogen bonds between binary systems of alcohol-water have been studied and it's known that these can cause peak shifts between different solutions in Raman spectra.

Ethanol and water are polar molecules, therefore there is a hydrogen-bonding network of water that can be reinforced by an increase of ethanol molecules, especially due to the presence of the hydroxyl group in ethanol. In addition, the ethyl group in ethanol is hydrophobic and it's small enough to exist in the cage of hydrogen-bonding network structure. The energy shift of vibration due to the hydrogen bonds depends on the constitution ratio in the alcohol-water solution. [24] [25]

The increase of ions in solution will interfere with the structure and behaviour of water molecules, causing changes in the equilibrium of hydrogen bonds in the first and second solvation shells of ions as well as in bulk water and the properties such as the ionic radius and the strength of the ion–water interaction play a central role in this phenomenon. The vibrational modes are analysed with respect to the coordination of both donor and acceptor molecules participating in the hydrogen bond. [30]

Raman spectroscopy can study inter- and intra-molecular vibrational modes of different molecules. It can also obtain information of molecular vibration and rotation to understand not only the water structure but also the interaction between water molecules and other materials. Therefore, Raman shifts depend upon structural change or phase transition at the specific conditions in a solution. [25]

Figure 4.18 represents Raman measurements of ethanol in water solutions with mass fractions from 2,0% up to 70,0%. There is a graduation shift observed in the main ethanol peaks in the fingerprint region, which includes all the peaks related to CH_2, the wagging mode at 1450 cm^{-1} and the deformation wagging mode at 1279 cm^{-1}. The weak mode at 1470 cm^{-1} belongs to the symmetric

deformation mode. The peak at 1095 cm^{-1} is due to the CO stretching mode. The two peaks at 884 and 1053 cm^{-1} correspond to the skeletal CCO stretching and deformation modes, respectively. [25]

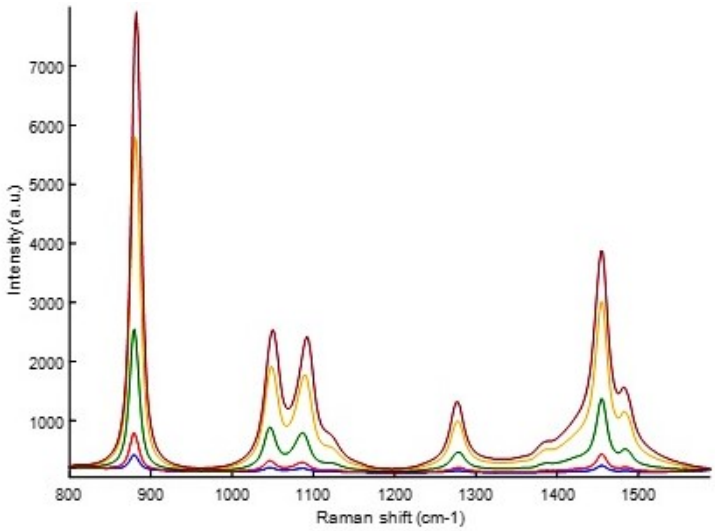

Figure 4.18 – Set of ethanol-water solutions with mass fraction: 2,02%; 5,29%; 19,59%; 49,99% and 69,98%. Measurements in the fingerprint region with average of 100 frames and 5 seconds exposure time, at 30 microns above window.

Figure 4.19 represents Raman measurements of ethanol in water solutions with mass fraction from 2,0% up to 70,0%. There is a graduation shift observed in the set in the main ethanol peaks in the high wavenumber region. The Raman shift peaks at 2929 and 2974 cm^{-1} are attributed to symmetric and asymmetric CH_3 stretching mode, respectively, while the CH_2 stretching mode is in 2880 cm^{-1}. The three peaks at 3286, 3434 and 3615 cm^{-1} appear in the spectra. The peak at 3286 is attributed to symmetric OH stretching vibrational mode. The assignment of the peak at 3434 cm^{-1} is still controversial. The shoulder peak at 3615 cm^{-1} results from free OH vibrational mode.[25] [24]

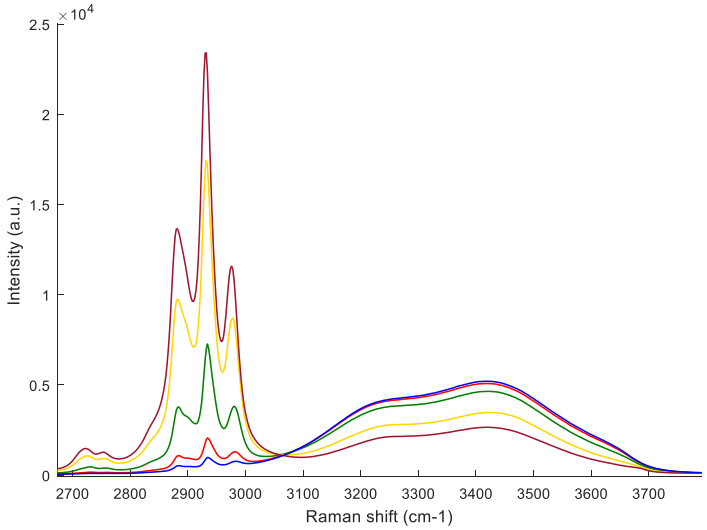

Figure 4.19 – Set of ethanol-water solutions with mass fraction: 2,02%; 5,29%; 19,59%; 49,99% and 69,98%. Measurements in the wavenumber region with average of 100 frames and 5 seconds exposure time, at 30 microns above window.

Ethanol strengthens the hydrogen bonds of water resulting in Raman shifts in spectra. The increase of ethanol concentration in a mixture can cause an increase in this interaction and a change in the equilibrium of the solution. The literature suggests that an ethanol-water structure generates a phase transition at a certain range of molar ratio of the solution that can be visible in a Raman spectra. [25]

Ethanol calibration in this thesis also confirmed that even when the ethanol mass in a solution is low and the difference of mass ratio between solutions is small, a few shifts can occur in the spectra. However, up to 7,5% in mass ratio these shifts can be negligible in an ethanol calibration and the calibration has a linearity behaviour.

The 25/01/2018 validation data set of ethanol has four Raman measurements presented in Figure 4.20.

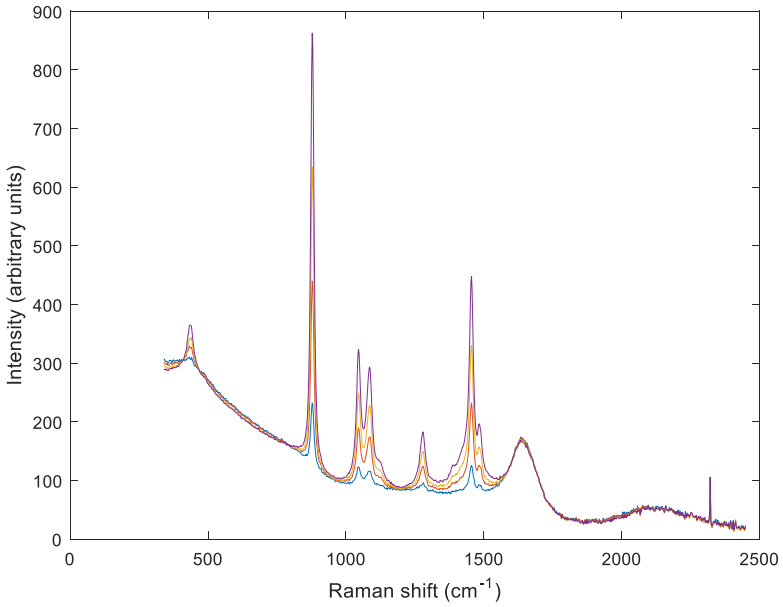

Figure 4.20 - Validation data set of ethanol and water solutions with mass ratio: 1,00 %; 2,99%; 4,98%; 7,47%. Raman measurements with average of 100 frames and 5 seconds exposure time, at 30 microns above window.

Calibration

Ethanol calibration was outlined in chapter 3.3.2. The first step is obtaining a clean water spectrum by choosing the scaling factor $f_{Q_{CleanWater}}$, the values evaluated are presented in Table 4-9. The three resulting spectra are presented in Figure 4.21.

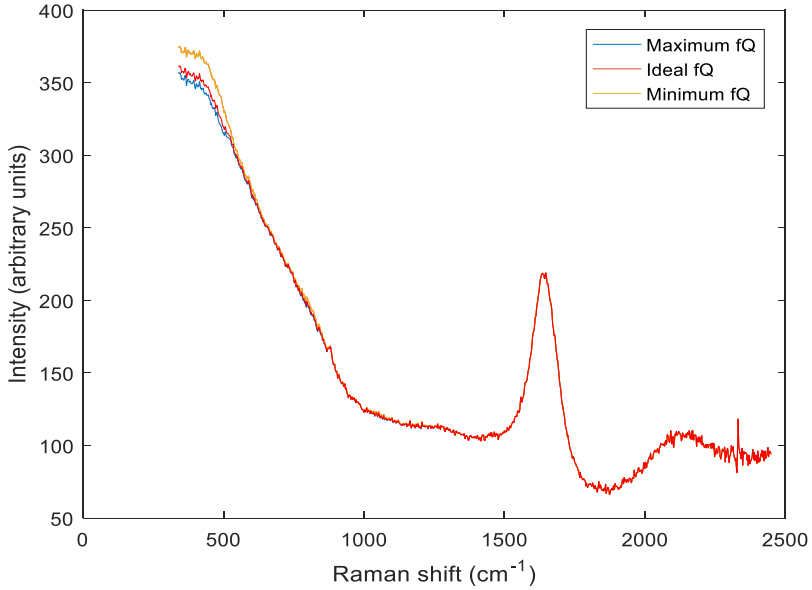

Figure 4.21 - Clean water spectrum of ethanol and water fit model of calibration after three different subtractions of quartz from average raw water measurement: minimum; ideal and maximum.

Table 4-9: Scaling Factors for quartz subtraction from water measurement, with factor deviation from ideal subtraction. Standard deviation of each clean water spectrum, with relative error of each compared to ideal.

	Minimum	Ideal	Maximum
$f_{Q_{CleanWater}}$	0,00	0,02	0,027
Standard Deviation of clean water spectrum	56,722	56,047	55,812
Relative Error of std clean water spectrum	1,21%		-0,42%

The subtraction of quartz from the water spectrum will affect the clean water spectrum in the fit model with a relative error of +1,21% or -0,42%.

This ideal water spectrum used in the fit model of ethanol calibration derives from the raw water measurement of the day of ethanol calibration experiment – without quartz. However, this water must be related to the water reference spectrum in the library (from BSA calibration). If not, this ethanol calibration can't be traceable to keratin.

In theory, the link between ethanol in keratin needs the calibration constant $c_{RefWater}/c_{Water}$, described in equation 4.4, since the water spectrum from the experiment isn't going to be stored and doesn't have any significant meaning in the quantification method.

$$\frac{c_{RefEthanol}}{c_{RefKeratin}} = \frac{c_{RefEthanol}}{c_{water}} \times \frac{c_{water}}{c_{RefWater}} \times \frac{c_{RefWater}}{c_{RefKeratin}} \tag{4.4}$$

The intermediate step of traceability links the water spectrum to the water reference spectrum in the library, enabling future repetitions of ethanol calibration to be reproducible.

Thus, it was implemented a different normalization step. The clean water spectrum processed has a normalization based on the standard deviation of the reference water spectrum from the library. That is, the multiple least squares fit method is used to determine the scale factor between the two spectra to match the two Raman intensity. The scale factor is the ratio between the Raman intensity of both spectra, which is approximately equal to its calibration constant, described in equation 4.5.

$$\frac{R_{RefWater}}{R_{Water}} = \frac{c_{RefWater}}{c_{Water}} \times \frac{\rho_{RefWater}}{\rho_{Water}} \cong \frac{c_{RefWater}}{c_{Water}} \tag{4.5}$$

With this normalization step, the result of calibration gives directly the calibration constant of ethanol to the reference water spectrum in the library.

Ethanol reference spectrum was extracted from 5,29% in mass ratio ethanol-water solution. Table 4-10 represents the range of scale factors of $f_{S_{Ethanol}}$ possible to subtract water from the ethanol solution. The table presents the two extremes cases that the user can subtract water and one that's considered the ideal subtraction, the final spectra after subtraction is presented in Figure 4.22.

Table 4-10: Values chosen for scaling factor of clean water with relative error of variation. Standard deviation of ethanol reference spectrum with respective its relative error. Relative Error of minimum and maximum values are compared to ideal.

	Minimum	Ideal	Maximum
$f_{S_{Ethanol}}$	0,93	0,95	1,00
Relative Error of $f_{S_{Ethanol}}$	2,11%		5,26%
Standard Deviation of ethanol Spectrum	67,746	67,892	68,381
Relative Error of std of ethanol Spectrum	-0,21%		0,72%

The subtraction of clean water spectrum from the ethanol solution spectrum will affect the ethanol reference spectrum in the fit model with a relative error of +0,72% or -0,21%.

The water peak at 1640 cm^{-1} determines the amount of water that should be subtracted from the spectrum. After this subtraction, there's still a background present in the spectrum in the 750 to 2050cm^{-1} range of the spectrum. This range should be approximately zero in Raman intensity. Thus, a slope was extrapolated in this range of the spectrum to use in a first order polynomial. This polynomial is then subtracted in the spectrum removing the background from the Raman experiment.

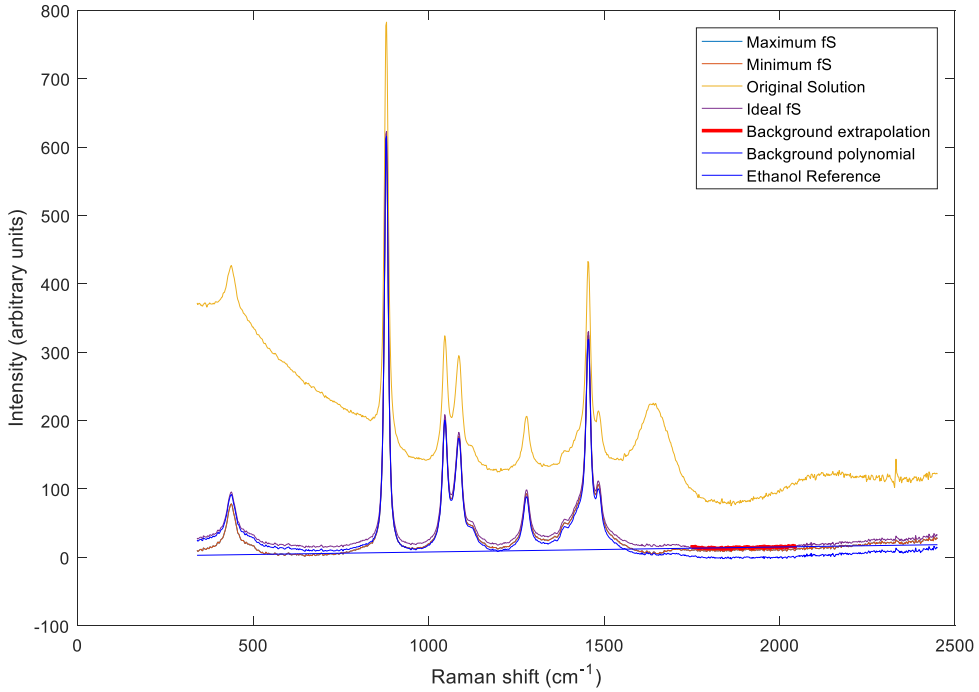

Figure 4.22 – 5,3% ethanol in water solution measurement with the result of subtraction of three different water scale factors, and, subsequently, a polynomial subtraction extracted from 1750-2050 cm^{-1} range in the spectrum.

Finally, there's still a need to study quartz subtraction to optimize this ethanol reference spectrum, since it was concluded that the water subtraction doesn't result in the best reference. Note that quartz subtraction must be done before background subtraction.

The quartz peak at 490 cm^{-1} can guide the user to how much quartz be subtracted from the spectrum. Like in the BSA calibration, this quartz factor used for scaling might not be the real representation of the actual quartz present. The range of possible values of $f_{Q_{Ethanol}}$ are presented in Table 4-11.

Table 4-11: Values chosen for scaling factor of quartz to obtain BSA reference spectrum with relative error of its variation. Standard deviation of BSA reference spectrum with respective relative error. Relative Errors are compared to ideal factor.

	Minimum	**Ideal**	**Maximum**
$f_{Q_{Ethanol}}$	0,000	0,028	0,032
Relative Error of $f_{Q_{Ethanol}}$	100,00%		14,29%
Standard Deviation of ethanol spectrum	67,8919	68,0032	68,0209
Relative Error of std of ethanol spectrum	-0,16%		0,03%

The subtraction of quartz from the ethanol solution minus water spectrum will affect the reference ethanol in the fit model with a relative error of +0,03% or -0,16%, presented in Figure 4.23.

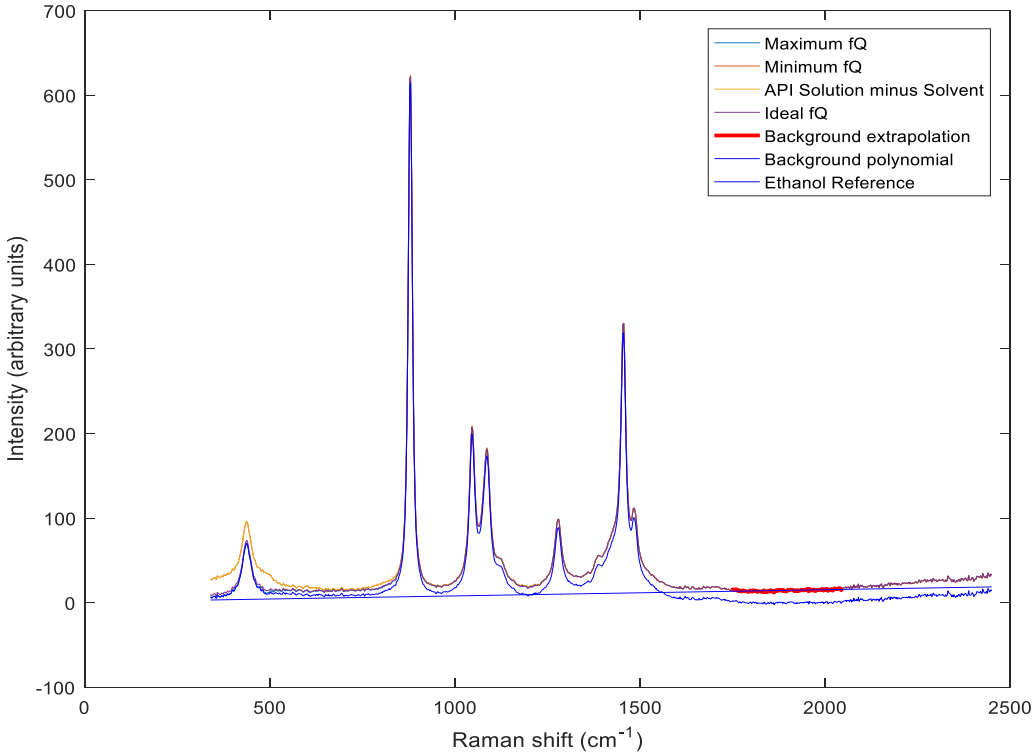

Figure 4.23 – 5,3% ethanol in water solution measurement with the result of subtraction of three different quartz scale factors, and, subsequently, a polynomial subtraction extracted from 1750-2050 cm^{-1} range in the spectrum.

The ideal ethanol reference spectrum presented in Figure 4.24 was normalized on the standard deviation of the 550 to 1800 cm^{-1} range of the spectrum and it's going to be used in the calibration fit model.

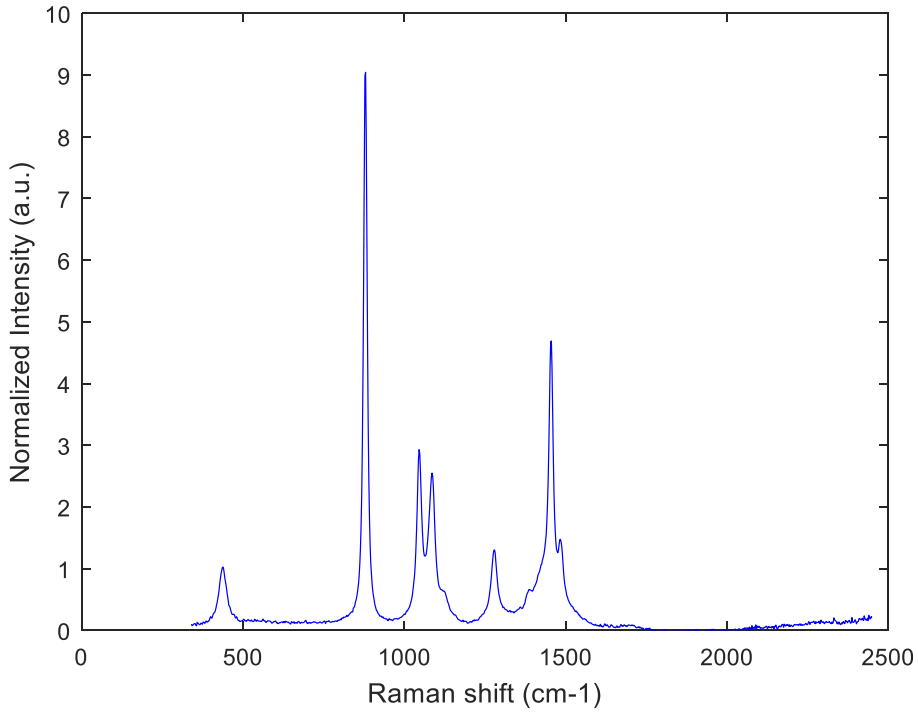

Figure 4.24 - Ideal ethanol reference spectrum after all the individual subtraction of the main components of 5,3% ethanol in water solution and normalization on the standard deviation spectrum range of 550 to 1800cm^{-1}.

The multiple least squares fit method gives the results of the fit coefficients for ethanol and water, Table 4-12, which will be then used on a linear regression to determine the calibration constant.

Table 4-12: Fit coefficients of ethanol and clean water relating the scaling between ethanol solutions to ethanol and clean water references spectra in the fit model chosen for ethanol in water calibration.

	Ethanol Fit Coefficients	Water Fit Coefficients
Solution 1	6,563	58,316
Solution 2	13,134	56,031
Solution 3	27,194	56,439
Solution 4	68,003	53,244

The calibration results indicate that the calibration constant $c_{RefEthanol}/c_{RefWater} = 23{,}378$, slope estimated from results in Figure 4.25, which the linear regression fits with accuracy all the solutions.

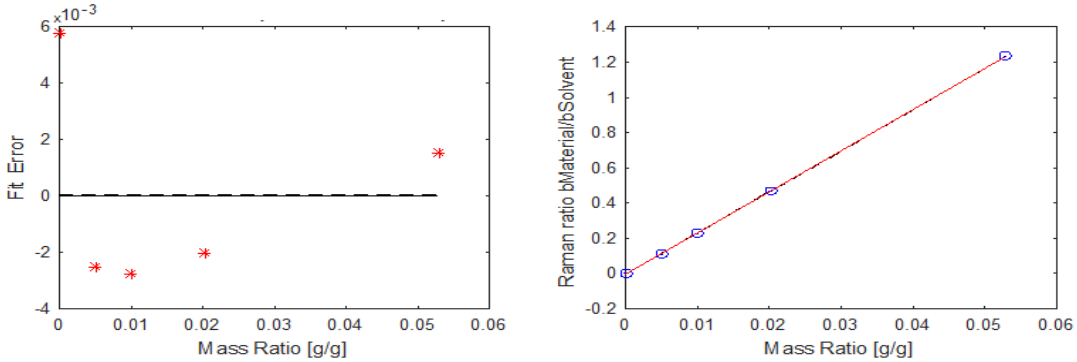

Figure 4.25 - Calibration linear function of Raman ratio between fit coefficients of ethanol and water to mass ratio of each solution (slope of linear function = 23,378 with $R^2 = 0{,}9998$); Fit Error of each solution point in the calibration to the calibration line with the Euclidean Norm of all solutions ($N = 0{,}582 \times 10^3$).

The results of the fitting of ethanol solutions spectra are presented in Figure 4.26.

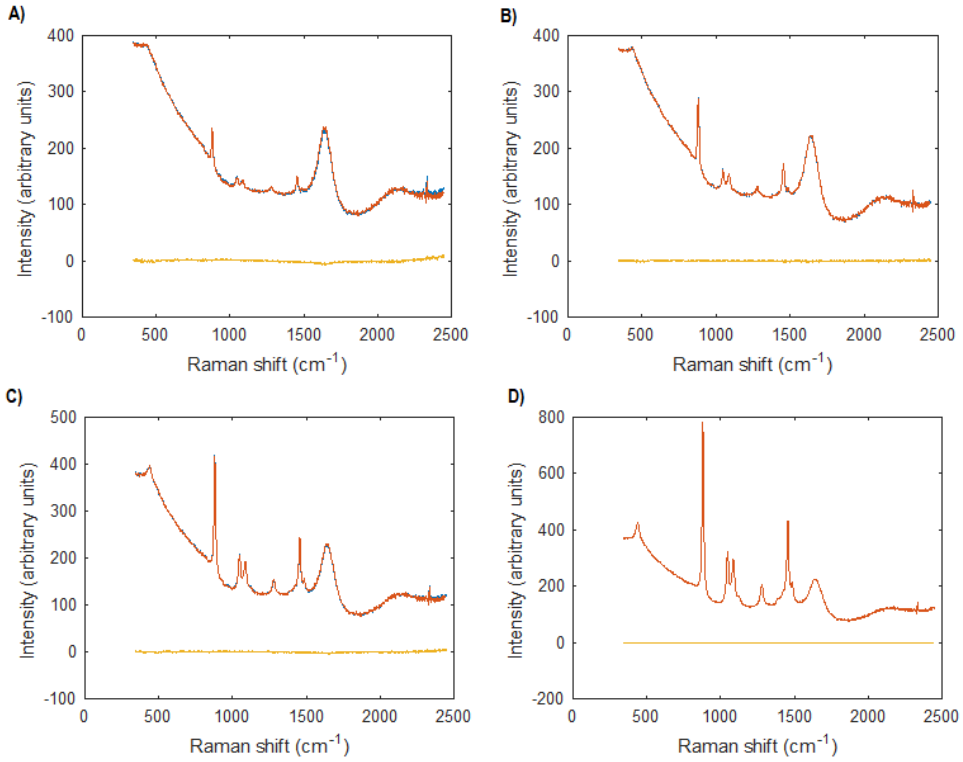

Figure 4.26 – Fitting Results of each solution based on the fit model chosen for BSA in water calibration. Mass Ratios of each solution: A) 0,50%; B) 1,00%; C) 2,02%; D) 5,29%.

In the end of the calibration, three different calibration models were formulated (Ideal Model, Model C and D), for the reasons it was discussed in the BSA calibration. The two extremes cases that result in the highest variation of the calibration constant are described in Table 4-13.

Table 4-13: The two extremes cases of possible scaling factors chosen are Model C and D, leading to the maximum and minimum of calibration constant $c_{RefEthanol}/c_{RefWater}$. Any other possible fit model for ethanol in water calibration is between the range of calibration constants estimated by these two models.

	Model C - Highest $\frac{c_{RefEthanol}}{c_{RefWater}}$	Model D - Lowest $\frac{c_{RefEthanol}}{c_{RefWater}}$
$c_{RefEthanol}/c_{RefWater}$	25,403	22,999
$f_{Q_{CleanWater}}$	0,027	0,000
$f_{S_{Ethanol}}$	0,910	0,990
$f_{Q_{Ethanol}}$	0,060	0,000

The three fit models are described by the combination of water and ethanol reference spectra, presented in Figure 4.27.

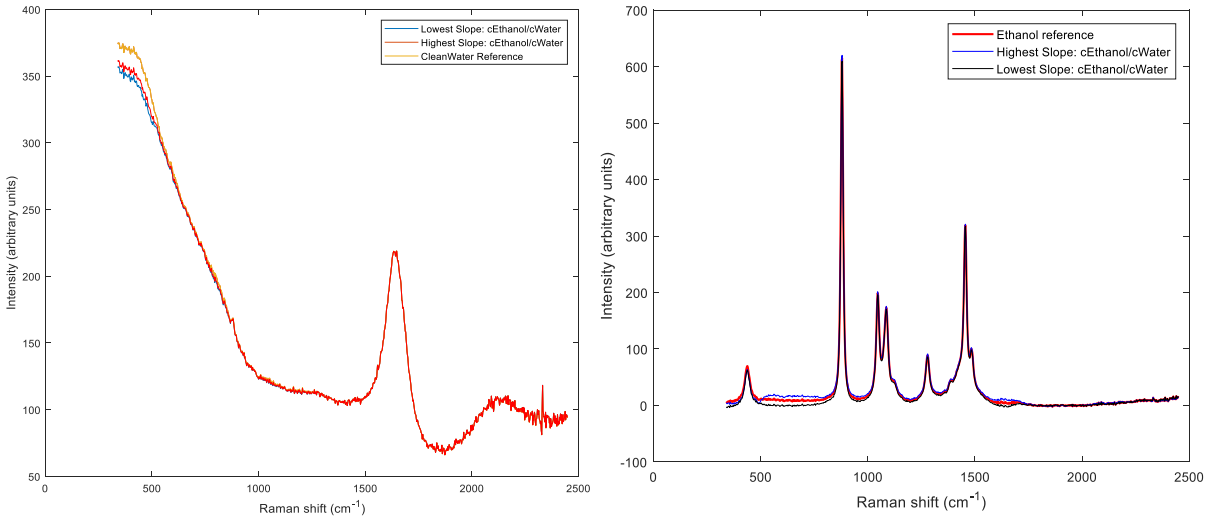

Figure 4.27 – Ethanol and clean water reference spectra of three different fit models in the ethanol in water calibration: Ideal Model; Model C and Model D.

Calibration Validation

As it was explained in the BSA in water calibration, the accuracy of the calibration constant and the fit model is studied by a validation model. Four solutions were used to test the quantification given by the calibration constant of ethanol in water, the representation of the prediction model versus the experimental model of mass ratios is given by Figure 4.28.

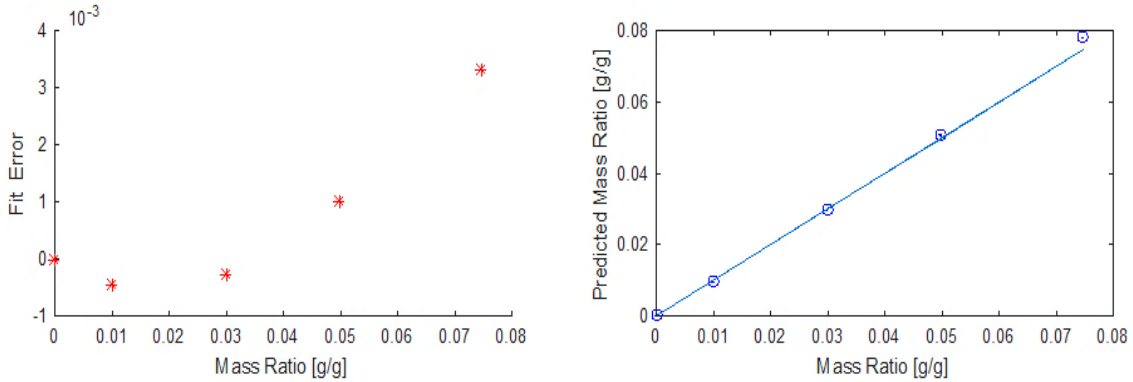

Figure 4.28 - Representation of the prediction model versus the experimental model of mass ratios from each solution of the validation data set of ethanol in water ($R^2 = 0{,}997$); with the fit errors of each predicted mass ratio to its experimental value ($Eucledean\ Norm = 0{,}124 \times 10^3$).

The relative error of calibration constant was determined as it was explained in chapter 3.3.4, the relative error of each fit model studied in the calibration is represented in Table 4-7.

Table 4-14: Relative error of quantification of the validation data set of ethanol in water, with four different solutions, for each fit model of calibration: Ideal model, Model C and Model D.

	Ideal Model	**Model C**	**Model D**
$\frac{\delta_{Quantification\ Validation_{data\ set}}}{Quantification\ Validation_{data\ set}}$	2,63 %	3,08 %	4,78 %

To evaluate how well the ideal fit model of validation fits new solutions, the fitting result of the predicted solutions spectra is presented in Figure 4.29.

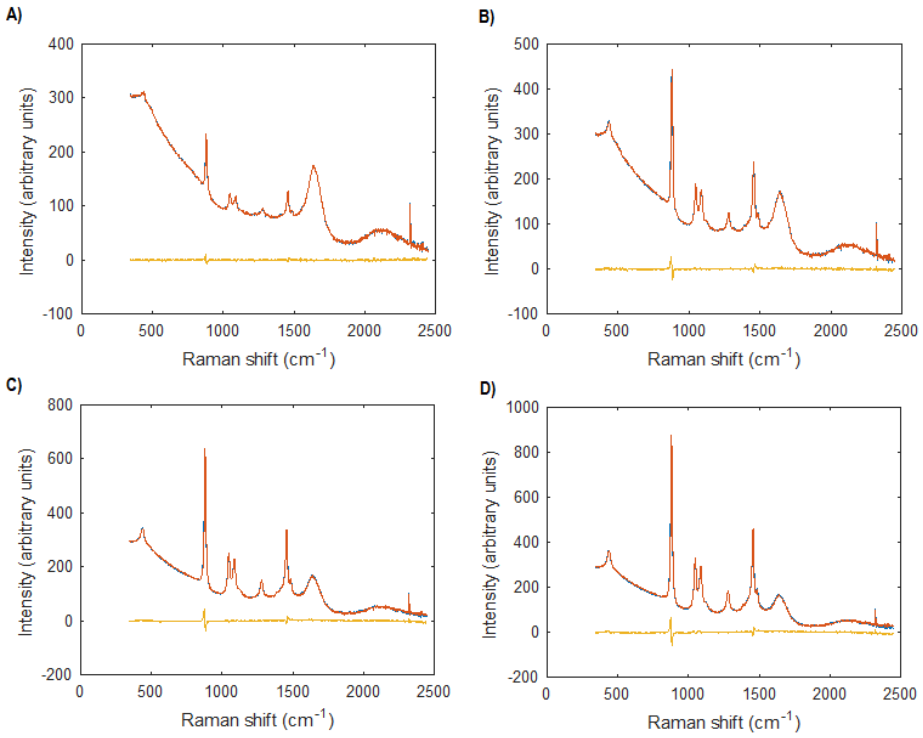

Figure 4.29 - Fitting result of the predicted solutions from validation data set of BSA in water, with mass ratios: A) 1,00 %; B)2,99%; C) 4,98%; D) 7,47%.

The ideal fit model chosen in the calibration has the least amount of relative error compared to Model C and D, which validates the same conclusion taken in the BSA validation. The optimization of the fit model chosen for calibration will improve the accuracy of the estimated calibration constant.

The final relative error is $\delta_{c_{API}/c_{solvent}}/c_{API}/c_{solvent} = \pm 2{,}74$ %. presented in Table 4-15.

Table 4-15 Relative error of calibration constant of ethanol to water.

Relative Error of $c_{RefBSA}/c_{RefWater}$	
$\frac{\delta_{Quantification\ Validation_{data\ set}}}{Quantification\ Validation_{data\ set}}$	$\pm$ 2,63 %
$\left(\frac{\delta_{mass\ ratio_{data\ set}}}{mass\ ratio_{data\ set}}\right)_{Calibration}$	$\pm$ 0,05 %
$\left(\frac{\delta_{mass\ ratio_{data\ set}}}{mass\ ratio_{data\ set}}\right)_{Validation}$	$\pm$ 0,06 %
$\frac{\delta_{c_{RefEthanol}/c_{RefWater}}}{c_{RefEthanol}/c_{RefWater}}$	$\pm$ **2,74** %

Ethanol Quantification Factor

The quantification factor estimated is described by equation 4.6. And the calibration constant $c_{RefEthanol}/c_{RefKeratin}$ must be related to keratin, described by equation 4.7.

$$Quantification\ Factor_{ethanol} = \left(\frac{c_{RefEthanol}}{c_{RefKeratin}}\right)^{-1} = \frac{c_{RefKeratin}}{c_{RefEthanol}} \quad (4.6)$$

$$\frac{c_{RefEthanol}}{c_{RefKeratin}} = \frac{c_{RefEthanol}}{c_{RefWater}} \times \frac{c_{RefWater}}{c_{RefKeratin}} \quad (4.7)$$

The relative error of the calibration constant derives from the sum relative errors of both constants define in equation 4.11. The relative error of the reference water to the water measured in the ethanol calibration experiment is considered null. Therefore, the quantification factor error only depends on the ethanol in water calibration and the water to keratin calibration constant, presented in Table 4-16.

Table 4-16 : Calibration constant of ethanol to keratin and quantification factor of ethanol, with respective relative errors.

Relative Error of Ethanol Quantification Factor	
$c_{RefEthanol}/c_{RefKeratin}$	$7{,}097 \times 10^{5}$
$Quantification\ Factor_{ethanol}$	$1{,}409 \times 10^{-6}$
$\frac{\delta(c_{RefKeratin}/c_{RefEthanol})}{c_{RefKeratin}/c_{RefEthanol}}$	$\pm 22{,}53\%$

4.1.3. Acetone

Measurements

Acetone was added as a solvent in the calibration methodology library, since there are a few APIs that are more soluble in acetone and it validates the premise that this method can be extended to different kinds of organic solvents. The calibration data set of acetone was measured on 05/12/2017, Raman measurements are presented in Figure 4.30.

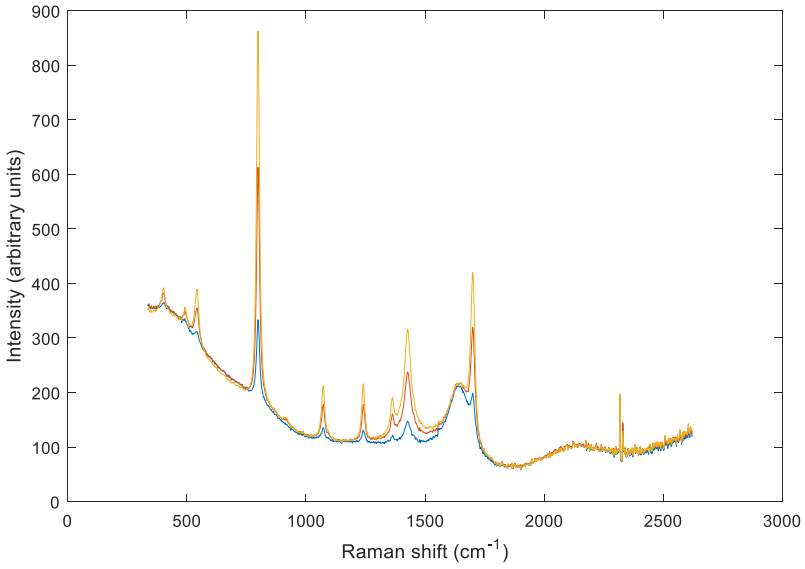

Figure 4.30 – Calibration data set of acetone and water solutions with mass ratio: 1,00%; 3,00%; 5,00%. Raman measurements with average of 200 frames and 5 seconds exposure time, at 30 microns above window.

To achieve this data set there was a study of the range of concentrations that should be used, since acetone in water solutions have the same type of behaviour as ethanol-water mixtures, studied in the chapter 4.1.2. Acetone in water is an aqueous solution dominate by a hydrogen-bonding network from the interaction of these two molecules. The nonlinear behaviour of the mole fraction dependence is associated with intramolecular vibration for several liquid mixtures.

The excess enthalpy variation of acetone-water solutions with the mole fractions of acetone is an indication of the structure-breaking role of acetone. The peak position shifts and the wavenumber change with the mole fractions indicates that the distribution of water molecules isn't homogeneous. At high acetone mole fractions, the peak position can describe the caging effect by acetone molecules, becoming increasingly rigid, since the interaction acetone-water is stronger than the interaction between acetone molecules. [30], [31]

At low mole fractions, the variation of the peak position suggests that the distance between the two oxygen of water and acetone atoms increases. Thus, the intramolecular vibration of water, which involves a stretching of the O-H, should shift to higher frequencies. [31]

The formation of hydrogen bonds between acetone and water at low mole fractions is counter-balanced by the breakdown of the water structure, with a subsequent net decrease in hydrogen bonding between water molecules. Thus, there's a different phase transitions dependent on the molar fraction, which the variation of the network interactions is visible in the spectra, since vibrational spectra are generally sensitive to intermolecular interactions. [30], [31]

Calibration

Acetone was calibrated with the general API calibration method, was determined as described in chapter 3.3.2. The acetone reference spectrum after normalization is presented Figure 4.31,.

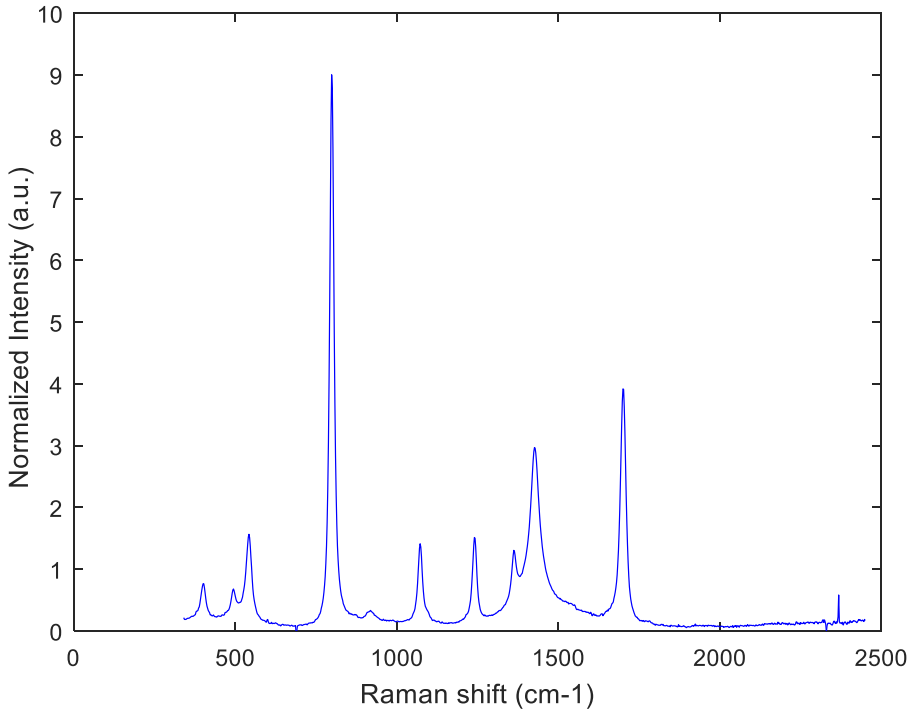

Figure 4.31 - Acetone reference spectrum after subtraction of water measurement from 5,00% acetone in water solution and normalization on the standard deviation spectrum range of 550 to 1800 cm^{-1}.

The calibration results indicate that the constant $c_{RefAcetone}/c_{RefWater} = 28{,}238$, Figure 4.32, which the linear regression fits all the solutions into one straight line with fit errors of the regression.

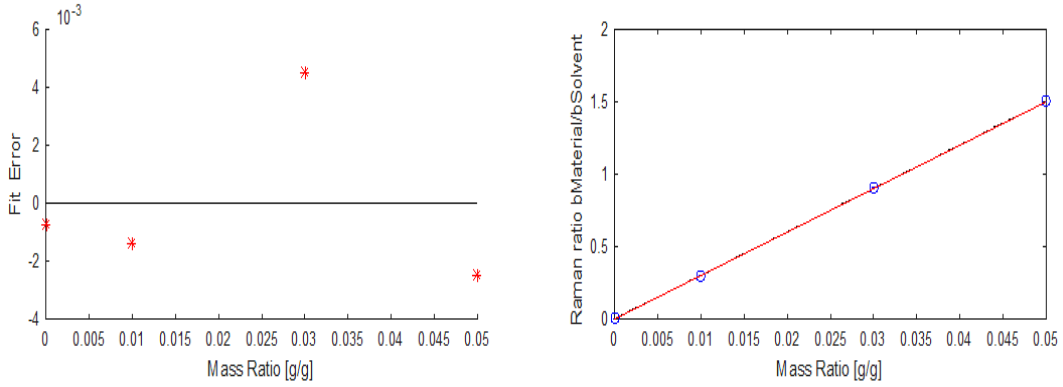

Figure 4.32 - Calibration linear function of Raman ratio between fit coefficients of acetone and water to mass ratio of each solution (slope of linear function = 28,238 with $R^2 = 1{,}000$); Fit Error of each solution point in the calibration to the calibration line with the Euclidean Norm of all solutions ($N = 0{,}290 \times 10^3$).

The results of the fitting of acetone in water solutions are presented in Figure 4.33.

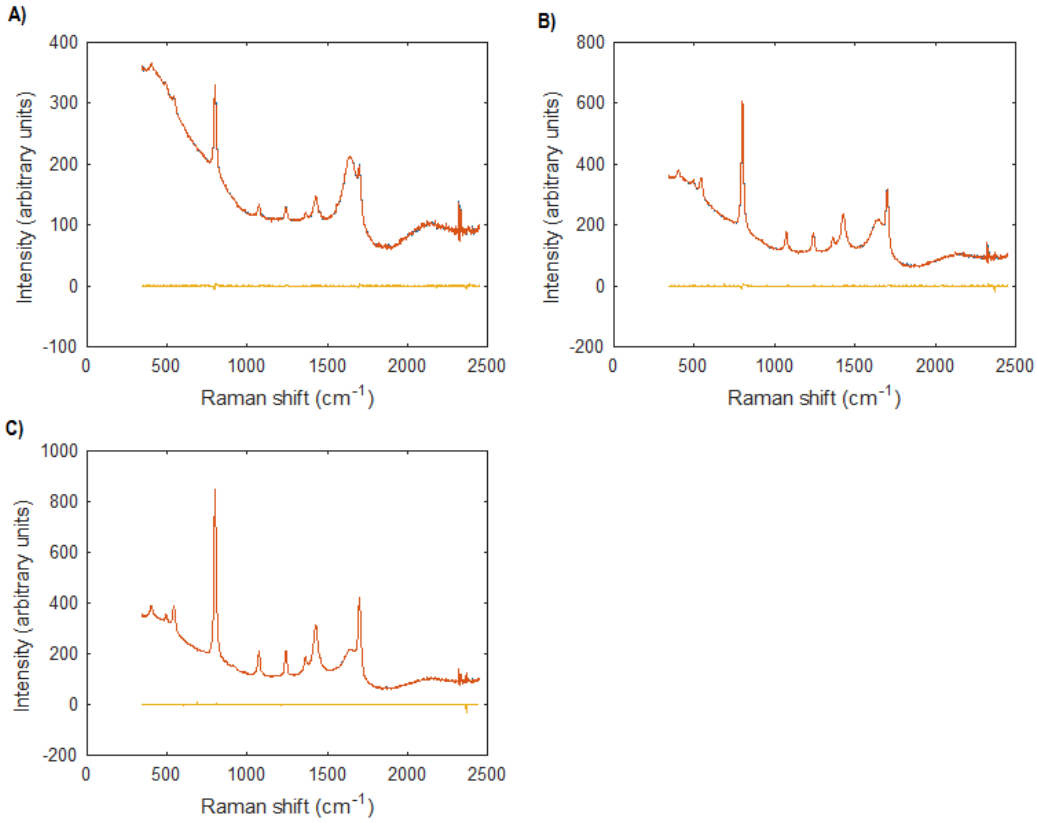

Figure 4.33 - Fitting Results of each solution based on the fit model chosen for acetone in water calibration. Mass Ratios of each solution: A) 1,00%; B) 3,00%; C) 5,00%.

Since there isn't a validation data set of acetone in water, the relative error of the constant $c_{RefAcetone}/c_{RefWater} = 4{,}80\%$, estimated from BSA calibration.

Acetone Quantification Factor

Acetone quantification factor enables the quantification of acetone to keratin in $mg_{acetone}/g_{keratin}$, which is the inverse of the constant $c_{RefAcetone}/c_{RefKeratin}$, described by equation 4.8.

$$\frac{c_{RefAcetone}}{c_{RefKeratin}} = \frac{c_{RefAcetone}}{c_{RefWater}} \times \frac{c_{RefWater}}{c_{RefKeratin}} \quad (4.8)$$

The relative error of the calibration constant of t$c_{RefKeratin}/c_{RefAcetone}$ derives from the sum relative errors of both constants define in equation 4.12, the results are presented in Table 4-17.

Table 4-17: Calibration constant of acetone to keratin and quantification factor of acetone, with respective relative errors.

Relative Error of Acetone Quantification Factor	
$c_{RefAcetone}/c_{RefKeratin}$	$8{,}572 \times 10^{5}$
$Quantification\ Factor_{Acetone}$	$1{,}167 \times 10^{-6}$
$\frac{\delta(c_{RefKeratin}/c_{RefAcetone})}{c_{RefKeratin}/c_{RefAcetone}}$	$\pm 24{,}59\%$

4.1.4. Caffeine

Measurements

The data set used for calibration of caffeine was measured on 16/01/2018 has three different solutions, the Raman spectra are presented in Figure 4.34.

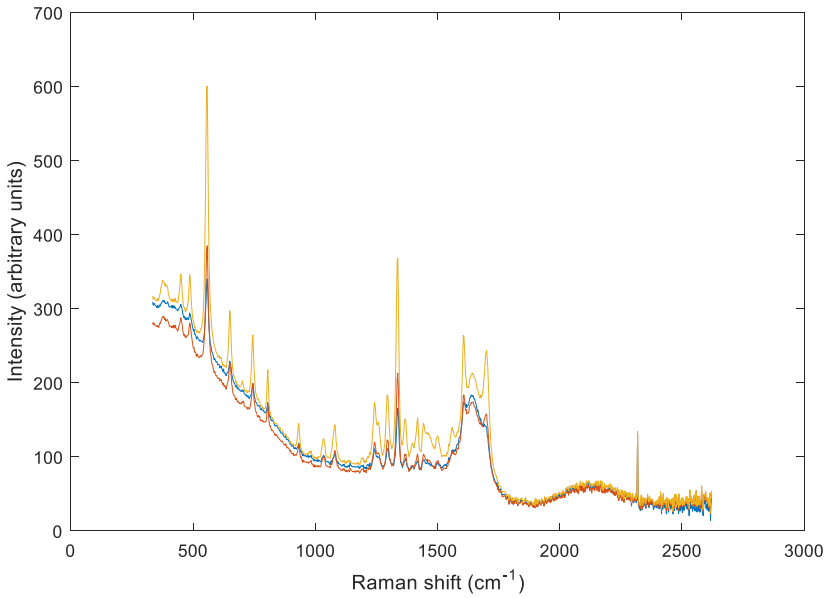

Figure 4.34 - Calibration data set of caffeine and water solutions with mass ratio: 0,50%; 1,00%; 2,00%. Raman measurements with average of 100 frames and 5 seconds exposure time, at 30 microns above window.

Calibration

Caffeine was calibrated with the general API calibration method, thus serves as an example for other APIs calibration dissolved in water, which uses the Quanti tool as an automatic approach. The normalized caffeine reference spectrum is presented in Figure 4.35, it was determined as described in chapter 3.3.2.

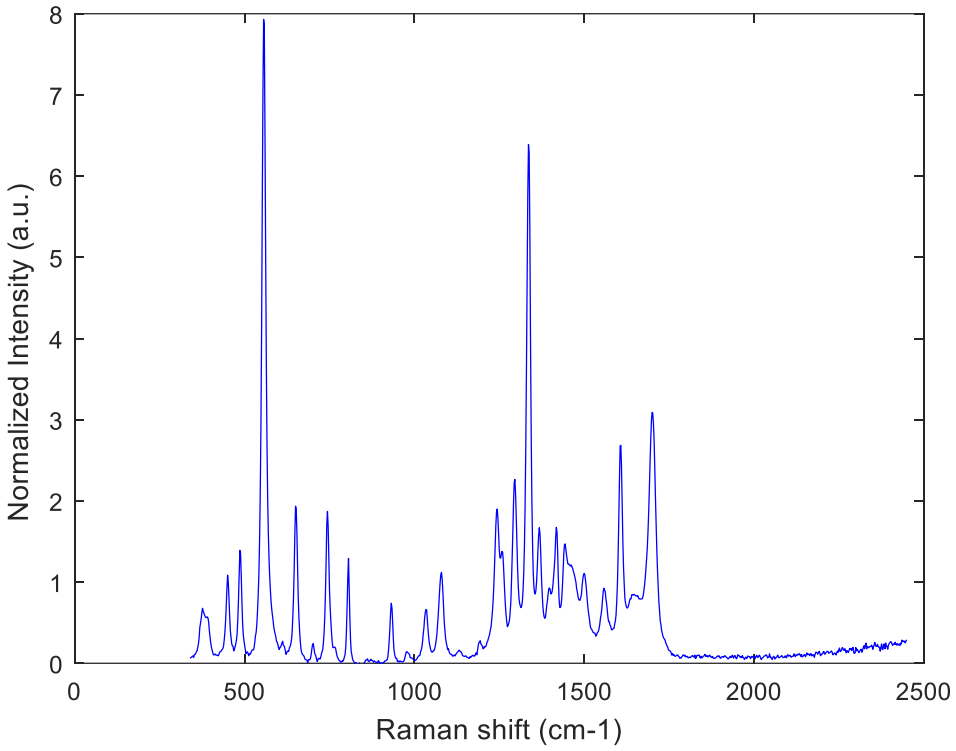

Figure 4.35 - Caffeine reference spectrum after subtraction of water measurement from 2,00% caffeine in water solution and normalization on the standard deviation spectrum range of 550 to 1800 cm^{-1}.

The calibration results indicate that the constant $c_{RefCaffeine}/c_{RefWater} = 46{,}020$, slope estimated in the results presented in Figure 4.36, which the linear regression fits all the solutions.

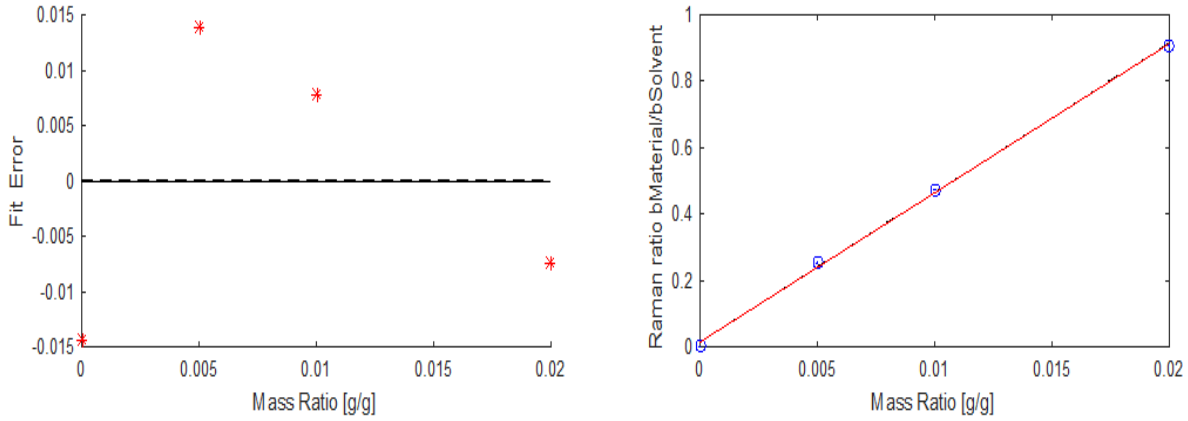

Figure 4.36 - Calibration linear function of Raman ratio between fit coefficients of caffeine and water to mass ratio of each solution (slope of linear function = 46,020 with $R^2 = 0{,}997$); Fit Error of each solution point in the calibration to the calibration line with the Euclidean Norm of all solutions ($N = 5{,}127 \times 10^3$).

The results of the fitting of caffeine in water solutions are represented in Figure 4.37

Since there isn't a validation data set of caffeine in water, the relative error of the constant $c_{RefAcetone}/c_{RefWater} = 4{,}80\%$, estimated from BSA calibration.

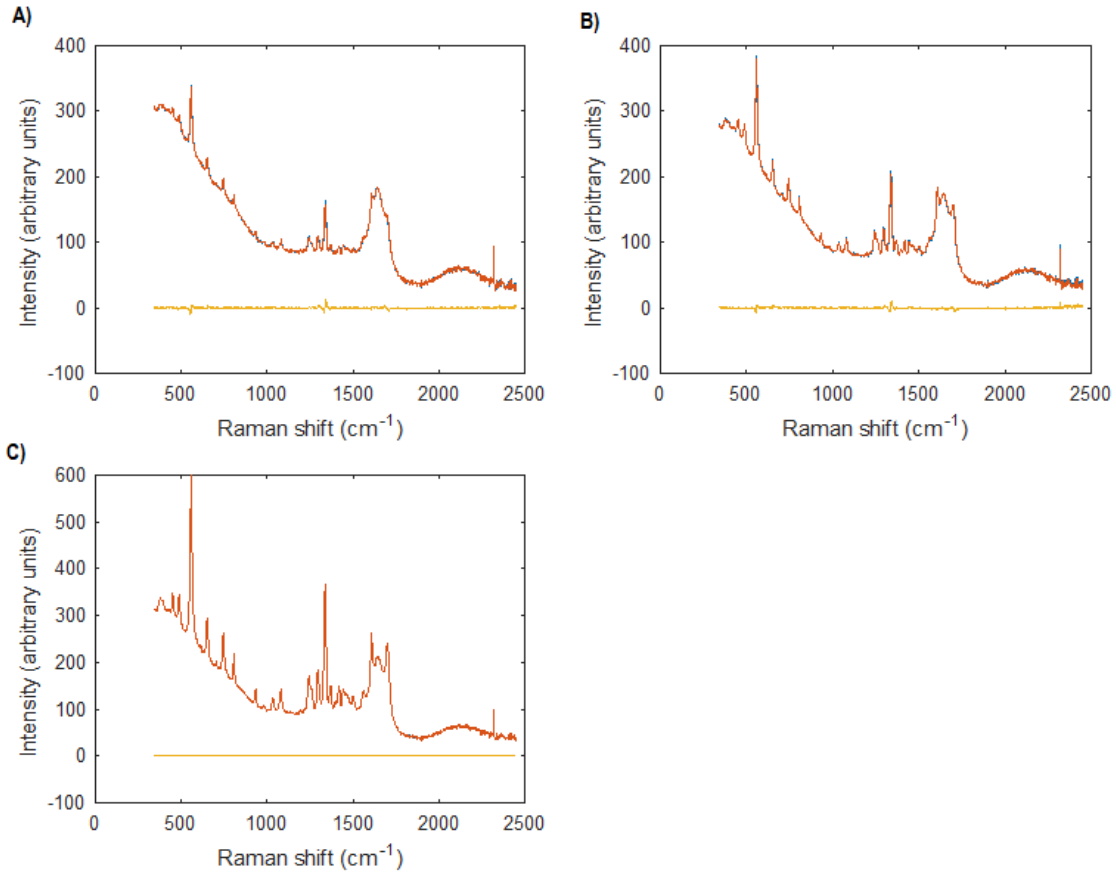

Figure 4.37 - Fitting Results of each solution based on the fit model chosen for caffeine in water calibration. Mass Ratios of each solution: A) 0,50%; B) 1,00%; C) 2,00%.

The calibration of caffeine in water didn't show any significant deviations of the three solutions in the linear calibration plot. Thus, this calibration data set resulted in a good quality calibration of the API.

Caffeine Quantification Factor

Caffeine quantification factor enables the quantification of caffeine to keratin in $mg_{caffeine}/g_{keratin}$, which is determined the same way the acetone quantification factor, as well as its relative error. The results are presented in Table 4-18.

Table 4-18: Calibration constant of caffeine to keratin and quantification factor of caffeine, with respective relative errors.

Relative Error of Caffeine Quantification Factor	
$c_{RefCaffeine}/c_{RefKeratin}$	$8{,}572 \times 10^{5}$
$\boldsymbol{Quantification\ Factor_{Caffeine}}$	$1{,}167 \times 10^{-6}$
$\frac{\delta(c_{RefKeratin}/c_{RefCaffeine})}{c_{RefKeratin}/c_{RefCaffeine}}$	$\pm\mathbf{24,59}\%$

4.2. APIs in Ethanol

Ethanol was the second solvent to be added to the library. There were a few previous studies with APIs calibrations in ethanol, thus this chapter serves as a validation and optimization study. Since this new calibration method has a few changes and new steps were implemented in the methodology, new APIs calibration in ethanol are considered more accurate and precise than previous ones.

API calibrations in ethanol might result in spectral changes in the API reference spectrum and in the fitting results of the API solutions spectra, due to molecular interactions between the API and the solvent in a solution. This must take into consideration in the data analysis and processing, if necessary other optimization steps should be included to achieve the best possible API calibration.

4.2.1. Salicylic Acid

Measurements

The data set used for calibration of salicylic acid, SA, was measured on 07/12/2017. The data set has four different solutions measurements, the Raman spectra are presented in Figure 4.38.

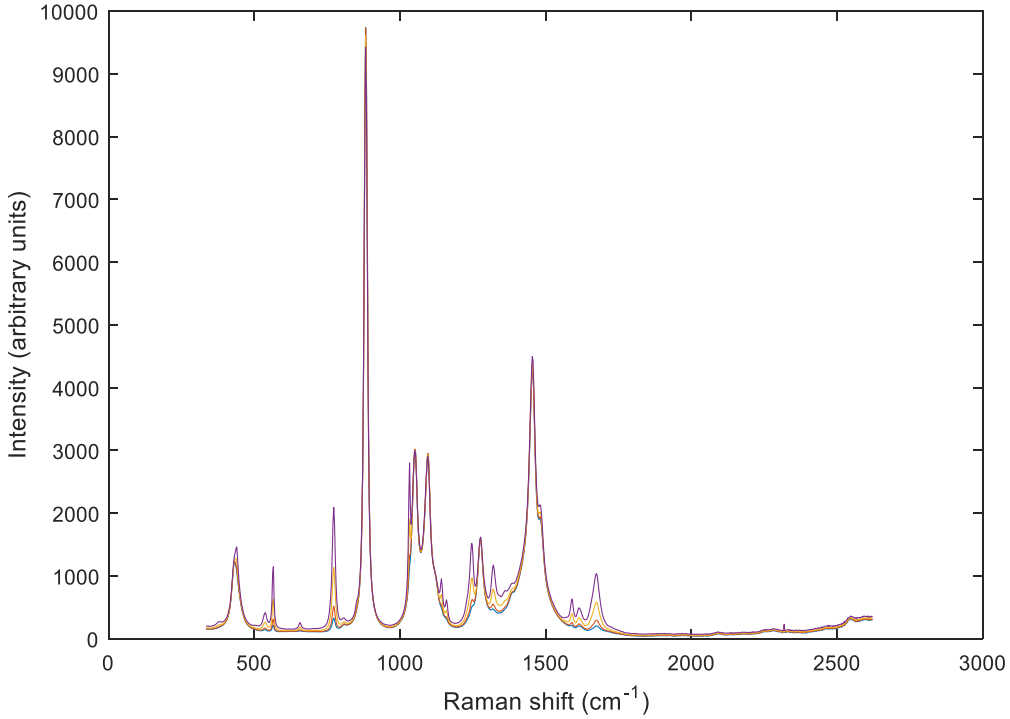

Figure 4.38 - Calibration data set of salicylic acid and ethanol solutions with mass ratio: 0,99%; 1,96%; 4,93%; 9,87%. Raman measurements with average of 100 frames and 5 seconds exposure time, at 30 microns above window.

Calibration

SA was calibrated with the general API calibration method, which uses the Quanti tool as an automatic approach. The SA reference spectrum was determined as described in chapter 3.3.2

The general solvent subtraction added a new artefact in the SA reference spectrum due to an ethanol shift in the Raman measurements between the pure ethanol and the SA solution, resulting in a default subtraction of the solvent. Therefore, there was a need of further processing the spectrum in Matlab, correcting the ethanol shifts in the range of 881 to 1095 cm^{-1}. A background can be also identified in the range 2150 to 2450 cm^{-1} that needed to be removed.

The SA reference spectrum result can be observed in Figure 4.39. Any other artefacts in the spectrum that might be present don't have as much Raman intensity contribution to the overall reference spectrum, thus its contribution is negligible.

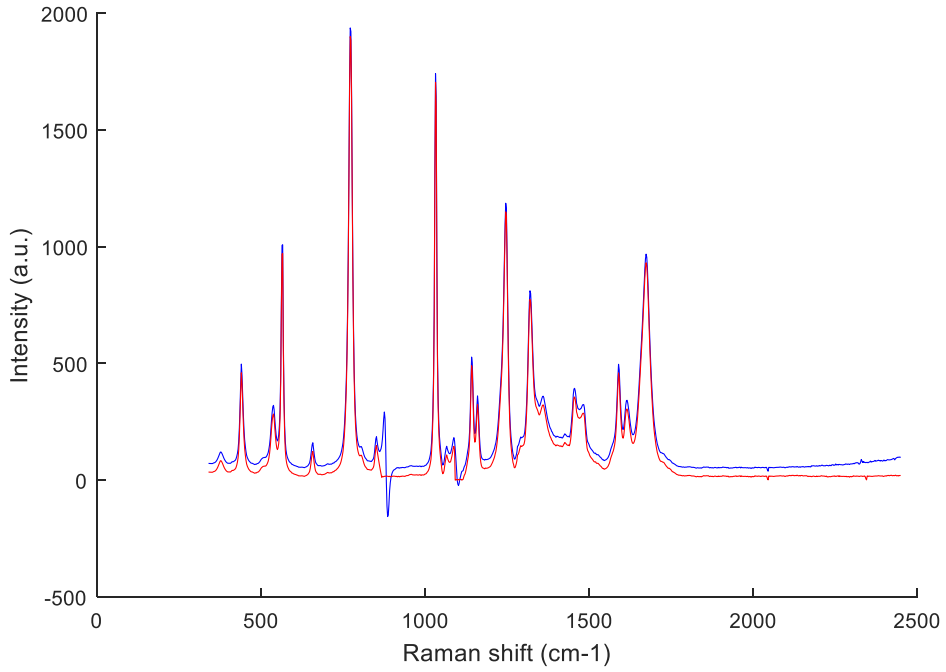

Figure 4.39 – SA spectrum after ethanol spectrum subtraction from 9,87% solution – blue – SA reference spectrum after further processing and before normalization on the standard deviation spectrum range of 550 to 1800 cm^{-1} - red.

The calibration results indicate that the calibration constant is $c_{RefSA}/c_{RefEthanol} = 2{,}631$, the slope was estimated with the results presented in Figure 4.40, which the linear regression fits all the solutions.

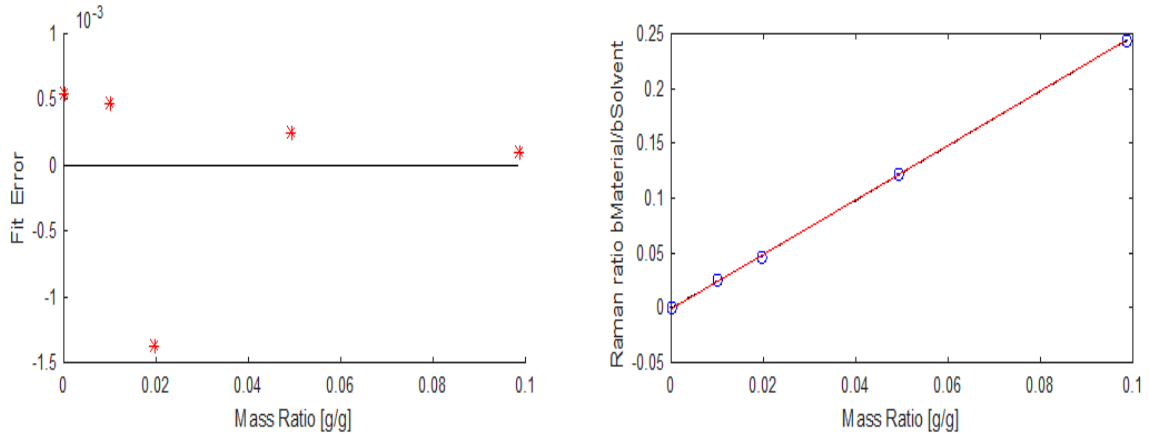

Figure 4.40 - Calibration linear function of Raman ratio between fit coefficients of salicylic acid and ethanol to mass ratio of each solution (slope of linear function = 2.631 with $R^2 = 1{,}000$); Fit Error of each solution point in the calibration to the calibration line with the Euclidean Norm of all solutions ($N = 0{,}025 \times 10^3$).

The results of the fitting of SA in ethanol solutions spectra are presented in Figure 4.41.

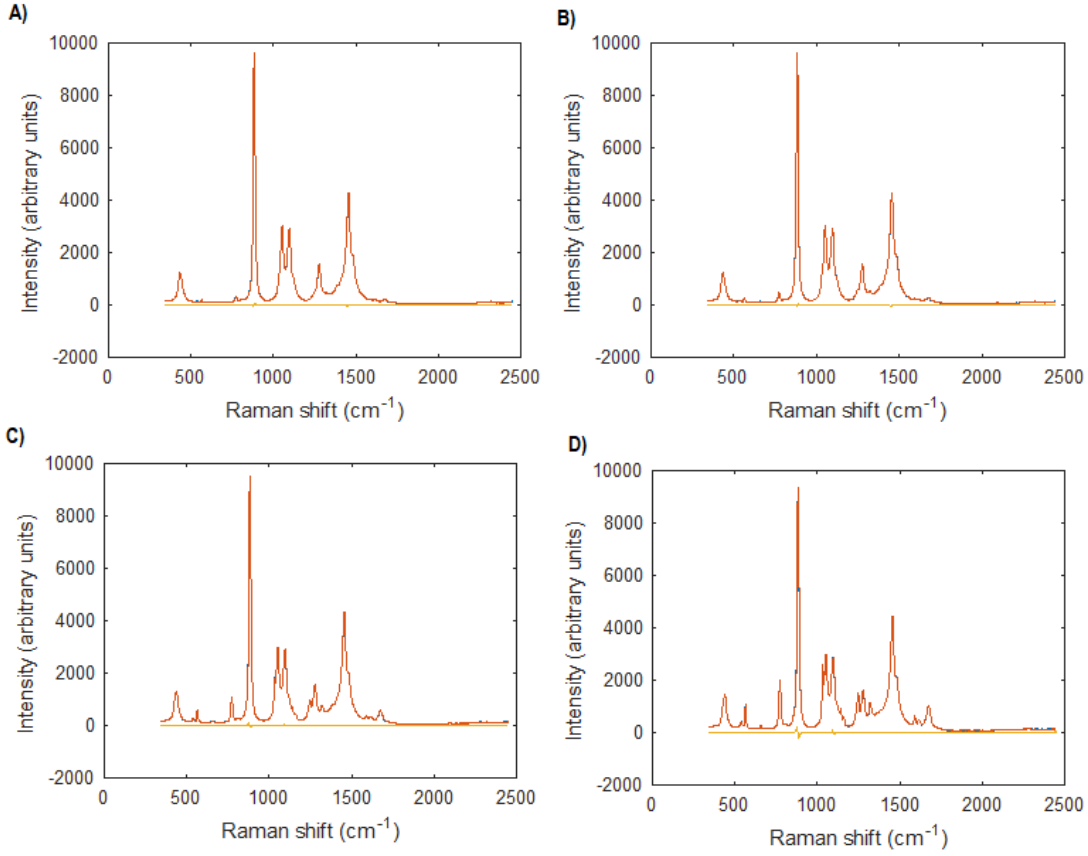

Figure 4.41 - Fitting Results of each solution based on the fit model chosen for SA calibration. Mass Ratios of each solution: A)0,99%; B) 1,96%; C) 4,93%; D) 9,87%.

The calibration of SA in ethanol didn't show any significant deviations of the four solutions in the linear calibration plot. Thus, this calibration data set resulted in a good quality calibration of the API. Since there isn't a validation step for salicylic acid in ethanol calibration, the relative error of the constant $c_{RefSA}/c_{RefEthanol} = 4{,}80\%$, estimated by the BSA calibration.

Salicylic Acid Quantification Factor

Salicylic acid quantification factor enables the quantification of salicylic acid to keratin in $mg_{SA}/g_{keratin}$, which is the inverse of the constant $c_{RefSA}/c_{RefKeratin}$, described by equation 4.9.

$$\frac{c_{RefSA}}{c_{RefKeratin}} = \frac{c_{RefSA}}{c_{RefEthanol}} \times \frac{c_{RefEthanol}}{c_{RefWater}} \times \frac{c_{RefWater}}{c_{RefKeratin}} \tag{4.9}$$

The relative error of the calibration constant of $c_{RefSA}/c_{RefKeratin}$ derives from the sum relative errors of the three constants define in equation 4.9, results are presented in Table 4-20.

Table 4-19: Calibration constant of SA to keratin and quantification factor of SA, with respective relative errors.

Relative Error of SA Quantification Factor	
$\boldsymbol{c_{RefSA}/c_{RefKeratin}}$	$1{,}867 \times 10^{6}$
$\boldsymbol{Quantification\ Factor_{SA}}$	$5{,}355 \times 10^{-7}$
$\frac{\boldsymbol{\delta(c_{RefKeratin}/c_{RefSA})}}{\boldsymbol{c_{RefKeratin}/c_{RefSA}}}$	$\boldsymbol{\pm 27{,}33\%}$

4.3. APIs in Acetone

Acetone was the third solvent to be added to the library of this methodology. After the acetone calibration was completed, one API – ubiquinol - was dissolved in it to validate the premise that the quantification method can also have other solvents besides ethanol and water.

Those two solvents were the only two tested before this thesis. Since ethanol already introduce the hypothesis that the method could work for other solvents besides water, acetone was used to validate this idea. The only known limitation of acetone is the same as ethanol, using another polar organic solvent might result in peak shifts in the calibration analysis.

4.3.1. Ubiquinol

Measurements

Ubiquinol was the only API in this thesis to be dissolve in acetone, its calibration serves as an example for future calibration of APIs in acetone, since it resulted in a good quality calibration of the data set chosen. This data set was measured on 05/12/2017 and it has four different solutions, the Raman spectra are presented in Figure 4.46.

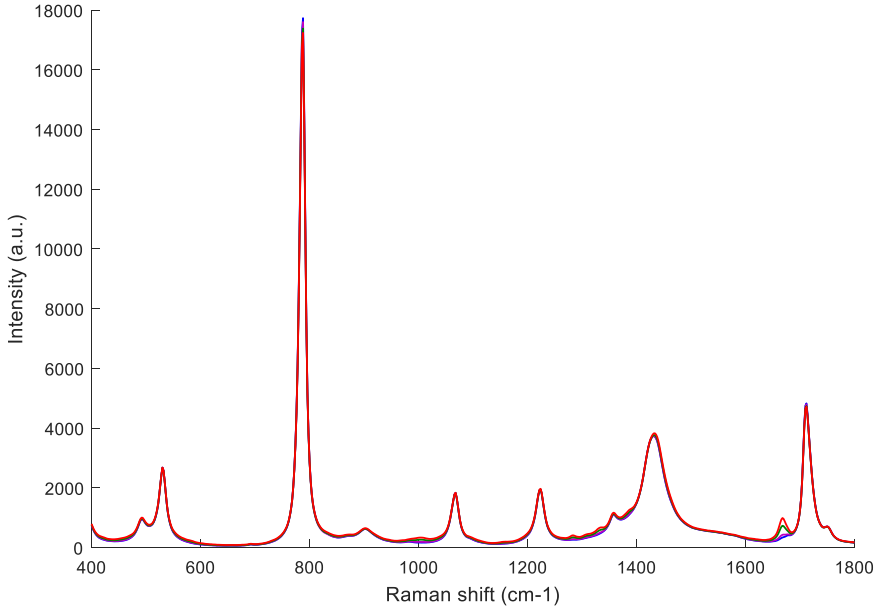

Figure 4.46 - Calibration data set of ubiquinol and acetone solutions with mass ratio: 0,49%; 0,98%; 2,94%; 4,82%. Raman measurements with average of 200 frames and 5 seconds exposure time, at 30 microns above window.

Calibration

Ubiquinol was calibrated with the general API calibration method and its reference spectrum was determined as described in chapter 3.3.2. The general solvent subtraction resulted in a good quality ubiquinol reference spectrum, the normalized spectrum is presented in Figure 4.47.

There wasn't any major shifts or background that needed to be removed. The standard subtraction resulted in a good quality ubiquinol reference spectrum. The only small shift in the difference spectrum didn't add any major artefacts to the spectrum, thus it was considered to be negligible to the overall spectrum.

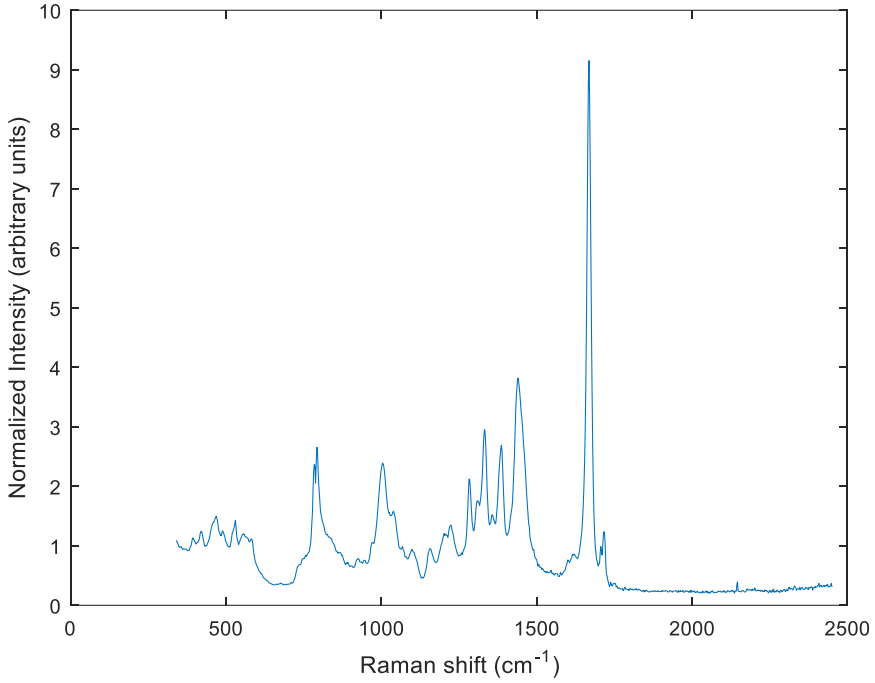

Figure 4.47 - Ubiquinol reference spectrum after subtraction of acetone measurement from 4,82% ubiquinol in acetone solution and normalization on the standard deviation spectrum range of 550 to 1800 cm^{-1}.

As it was predicted, using a polar solvent might result in molecular interaction in the dissolution of materials in this solvent, which can result in peak shifts visible in Raman spectra, as it was explained in chapter 4.1.

The calibration results indicate that the constant is $c_{RefUbiquinol}/c_{RefAcetone} = 2{,}070$, the slope is estimated with the results presented in Figure 4.48, which the linear regression fits all the solutions.

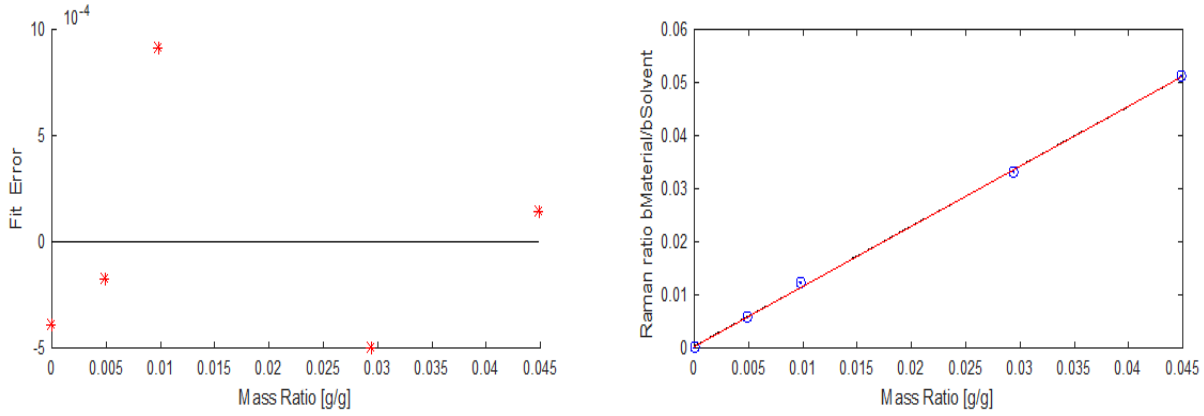

Figure 4.48 - Calibration linear function of Raman ratio between fit coefficients ubiquinol and acetone to mass ratio of each solution (slope of linear function = 2,070 with $R^2 = 0{,}999$; Fit Error of each solution point in the calibration to the calibration line with the Euclidean Norm of all solutions ($N = 0{,}013 \times 10^3$).

The results of the fitting of ubiquinol in acetone solutions spectra are presented in Figure 4.49.

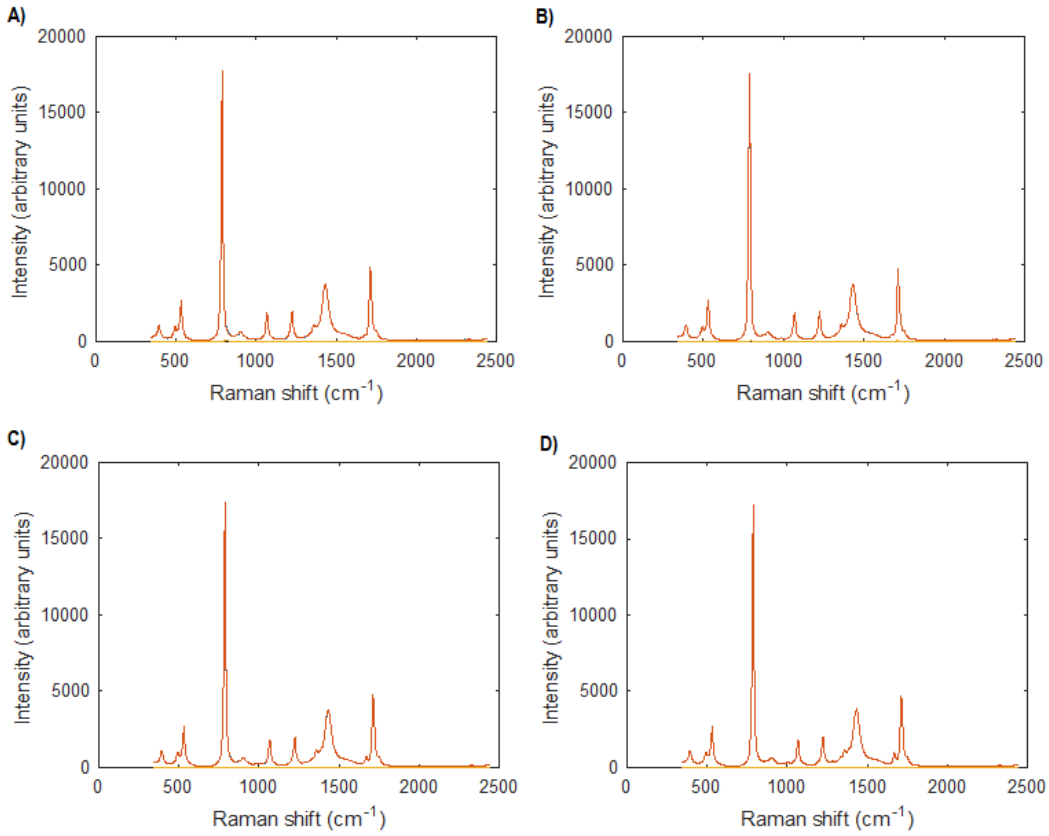

Figure 4.49 - Fitting Results of each solution based on the fit model chosen for ubiquinol calibration. Mass Ratios of each solution: A) 0,49%; B) 0,98%; C) 2,94%; D) 4,82%.

The calibration of ubiquinol in acetone didn't show any significant deviations of the four solutions in the linear calibration plot. Thus, this calibration data set resulted in a good quality calibration of the API. There isn't a validation step for ubiquinol calibration, the relative error of the constant is $c_{RefUbiquinol}/c_{RefAcetone} = 4{,}80\%$.

Ubiquinol Quantification Factor

Ubiquinol quantification factor enables the quantification of ubiquinol to keratin in $mg_{ubiquinol}/g_{keratin}$, which is the inverse of the constant $c_{RefUbiquinol}/c_{RefKeratin}$, as it was describe before, equation 4.14.

$$\frac{c_{RefUbiquinol}}{c_{RefKeratin}} = \frac{c_{RefUbiquinol}}{c_{RefAcetone}} \times \frac{c_{RefAcetone}}{c_{RefWater}} \times \frac{c_{RefWater}}{c_{RefKeratin}} \tag{4.11}$$

The relative error of the calibration constant of the reference ubiquinol to reference keratin, derives from the sum relative errors of both constants define in equation 4.14, Table 4-23.

Table 4-23: Calibration constant of ubiquinol to keratin and ubiquinol quantification factor, with respective relative errors.

Relative Error of Ubiquinol Quantification Factor	
$c_{RefUbiquinol}/c_{RefKeratin}$	$1{,}774 \times 10^{6}$
$\boldsymbol{Quantification\ Factor_{Ubiquinol}}$	$5{,}636 \times 10^{-7}$
$\frac{\delta\left(c_{RefKeratin}/c_{c_{RefUbiquinol}}\right)}{c_{RefKeratin}/c_{c_{RefUbiquinol}}}$	$\pm\mathbf{29{,}39}\%$

4.4. APIs in MCT Oil

Medium-chain triglycerides oil, MCT oil, was the fourth solvent to be added to the methodology in this thesis. After the MCT oil calibration was completed, one API – chemical UV filter I - was dissolved in it to validate the premise that the method can be universal to different kinds of solvents.

Not only the quantification method can be use with for an unlimited number of solvents, but also the method doesn't have to be exclusive to water and organic solvents, confirming its potential as a diverse and easy method to use and the potential to upgrade it.

4.4.1. Chemical UV filter I

Measurements

The chemical UV filter I was the only API in this thesis to be dissolve in MCT oil, its calibration serves as an example for future calibration of APIs in MCT oil, since it resulted in a good quality calibration of the data set chosen. This data set was measured on 08/12/2017 and it has two different solutions, the Raman spectra of these solutions is presented in Figure 4.50.

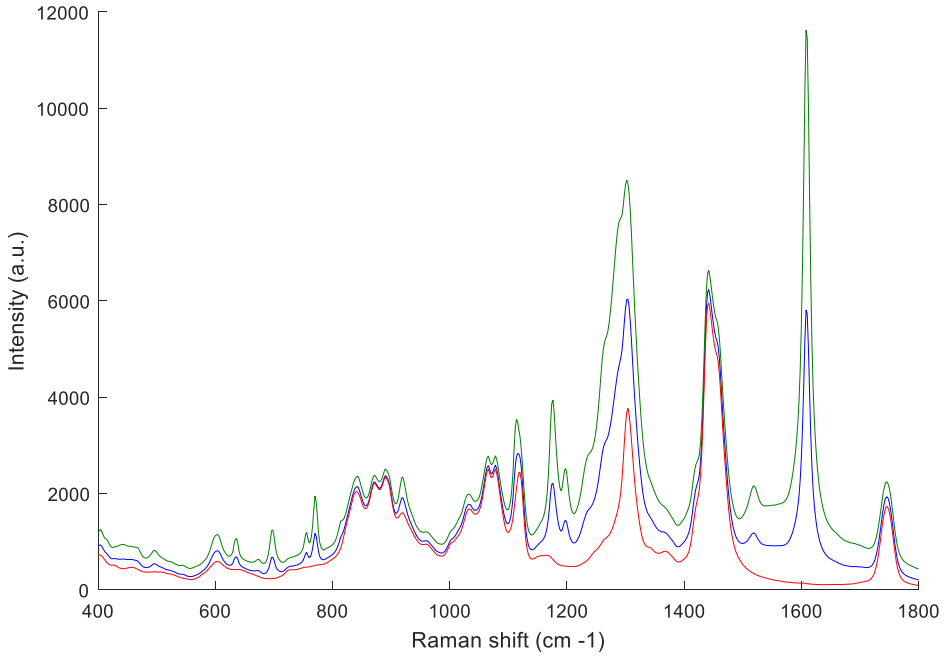

Figure 4.50 - Calibration data set of chemical UV filter I in MCT oil solutions with mass ratio: 2,41% - blue; 4,92% - green. Pure MCT oil measurement – red. Raman measurements with average of 100 frames and 5 seconds exposure time, at 30 microns above window.

Calibration

The chemical UV filter I was calibrated with the general API calibration method and its reference spectrum was determined as described in chapter 3.3.2.

The general solvent subtraction resulted in a good quality chemical UV filter I reference spectrum, the normalized spectrum is presented in Figure 4.51. There aren't any shifts or background in the spectrum, which means that oil can work as well as water in terms of enabling an easier extraction of API spectrum, compared to organic solvents that often need further processing due to peak shifts.

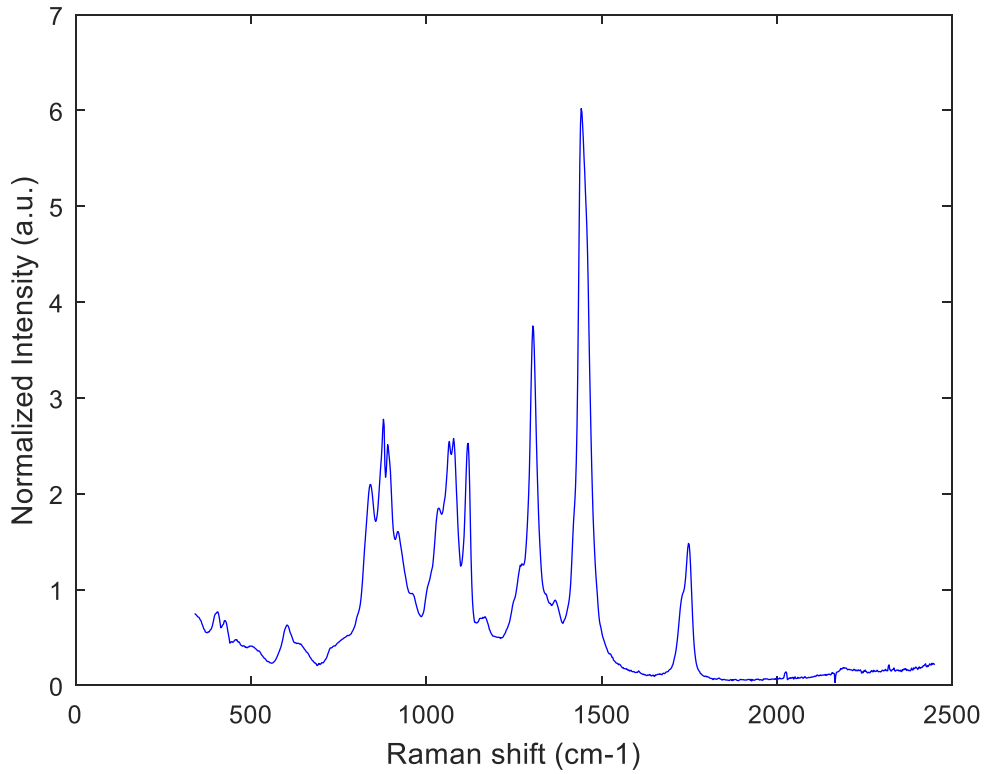

Figure 4.51 – Chemical UV filter I reference spectrum after subtraction of MCT oil measurement from 4,92% solution and normalization on the standard deviation spectrum range of 550 to 1800 cm^{-1}.

The calibration results indicate that the constant $c_{RefChemUV\ I}/c_{RefMCToil} = 28{,}151$, the slope was estimated with the results presented in Figure 4.52, which the linear regression fits all the solutions.

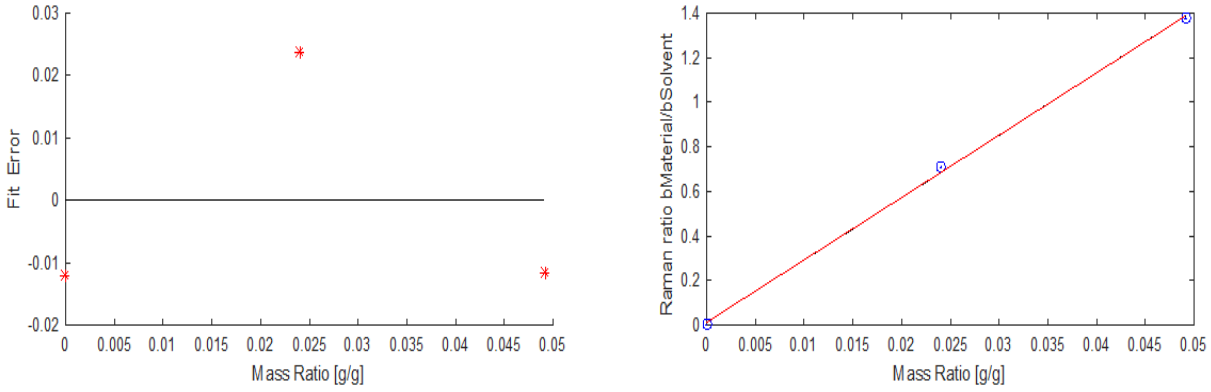

Figure 4.52 - Calibration linear function of Raman ratio between fit coefficients chemical UV filter I and MCT oil to mass ratio of each solution (slope of linear function = 28,151 with $R^2 = 0{,}999$; Fit Error of each solution point in the calibration to the calibration line with the Euclidean Norm of all solutions ($N = 8{,}436 \times 10^3$).

The results of the fitting of the chemical UV filter I in MCT oil solutions spectra are presented in Figure 4.53.

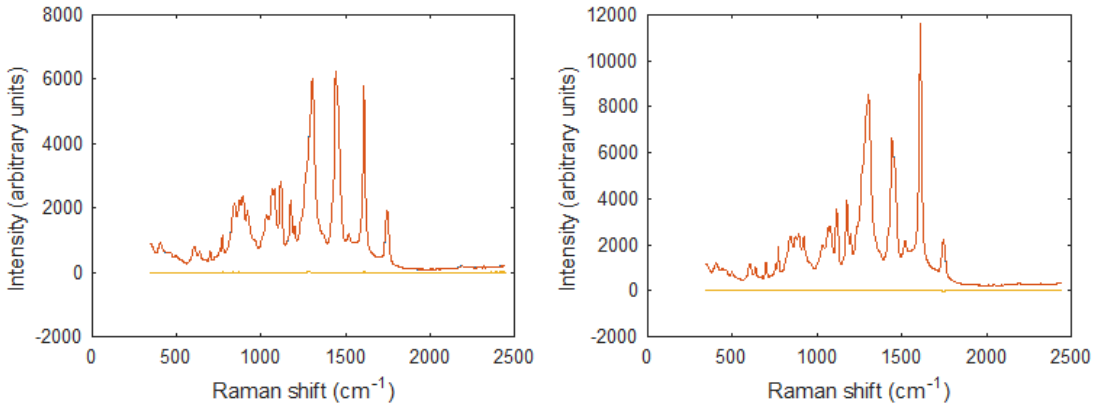

Figure 4.53 - Fitting Results of each solution based on the chemical UV filter I calibration fit model. Mass Ratios: A)2,41%; B) 4,92%.

The calibration of the chemical UV filter I in MCT oil didn't show any significant deviations of the two solutions in the linear calibration plot. Thus, this calibration data set resulted in a good quality calibration of the API. There isn't a validation step for the chemical UV filter I calibration, the relative error of the constant is $c_{RefChemUV\ I}/c_{RefMCTOil} = 4{,}80\%$.

Chemical UV filter I Quantification Factor

The chemical UV filter I quantification factor enables the quantification of the chemical UV filter I to keratin in units of $mg_{RefChemUV\ I}/g_{keratin}$, which is the inverse of the constant $c_{RefChemUV}/c_{RefKeratin}$, described by equation 4.14.

$$\frac{c_{RefChemUV\ I}}{c_{RefKeratin}} = \frac{c_{RefChemUV\ I}}{c_{RefMCToil}} \times \frac{c_{RefMCToil}}{c_{RefEthanol}} \times \frac{c_{RefEthanol}}{c_{RefWater}} \times \frac{c_{RefWater}}{c_{RefKeratin}} \quad (4.12)$$

The relative error of the calibration constant of $\mathbf{c}_{RefChemUV\ I}/c_{RefKeratin}$ derives from the sum relative errors of both constants define in equation 4.14,Table 4-23.

Table 4-25: Calibration constant of chemical UV filter I to keratin and the chemical UV filter I quantification factor, with respective relative errors.

Relative Error of the chemical UV filter I Quantification Factor	
$\boldsymbol{c_{RefChemUV\ I}/c_{RefKeratin}}$	$1{,}532 \times 10^{7}$
$\boldsymbol{Quantification\ Factor_{RefChemUV}}$	$6{,}529 \times 10^{-8}$
$\frac{\boldsymbol{\delta\left(c_{RefKeratin}/c_{c_{RefChemUV}}\right)}}{\boldsymbol{c_{RefKeratin}/c_{c_{RefChemUV}}}}$	$\boldsymbol{\pm 32,13\%}$

4.5. Other APIs

In total there were 6 solvents and 19 APIs calibrated in this thesis, a summary of all materials calibration is in the Appendix VI, with the respective API reference spectrum used for calibration of the materials that weren't referred in this chapter, presented in Appendix VI.

4.6. *In vivo* Skin Measurements

This chapter presents skin applications of the method optimized in this thesis. Four different experiments were studied to monitor *in vivo* delivery of different APIs into human skin. The results presented were able to validate the work done in this methodology.

The methodology shows that the APIs penetration and permeation into the skin can successfully be measured *in vivo* in more accurate and precise way in the SC, compared to previous studies.

The boundary between the SC and the viable epidermis (VE) is not well defined and can be difficult to determine, but the chemical differences between these two layers have been studied. The inner cells of the SC, which cover the viable cells of the epidermis, contain around 70% water, whereas the outer cells of the SC are hydrated at a much lower degree. Considering these variations in NMF and water content within the epidermis, the position of the boundary between the SC and the VE can be estimated. [1]

In this case, each measurement has 3 different locations in the volar forearm skin (4cmx4cm limited area) on the same subject, the SC thickness was determined by the average of all three with the boundaries of the standard deviation to the average. This gives the proportion of each compound above and below the SC depth.

Measurements were taken every 30 to 60 minutes for up to 3 hours. There're represented by the mean of compound proportion by averaging all the profiles taken within that time slot, considering any spatial variations on the skin. Profiles represented as baseline were taken at time zero without any product in skin, to detect the differences between a treated and non-treated skin.

4.6.1. Ibuprofen

The first product is a gel with an API of ibuprofen, present at 5% w/w, and levomenthol, present at 3% w/w. The gel is anti-inflammatory product that provides pain relief. Levomenthol wasn't calibrated in this work, therefore it can't be detected in skin. Moreover, this gel has propylene glycol – PG – and ethanol as ingredients, that can be detected in these measurements since they've been calibrated.

The fit model of skin measurements should include not only the API reference spectrum but also any other quantified reference spectra of high concentration ingredients, enabling the detection of different materials in the product that aren't the API itself for a more complete overview of *in vivo* skin measurements.

Profiles shown in this section show that the Raman signal intensity measured at the surface of the skin decreases with time and that both molecules go deeper into the skin with time. This type of concentration gradient in profiles is typically observed in systems in which the diffusion process involves a homogeneous sample. This is explained by Fick's Second Law of Diffusion and it's generally thought to be the dominate mechanism in skin penetration and permeation. [32]

In the case of ibuprofen gel, the 30 min measurement was considered an outlier for all profiles studied, which can be explained by the fact that ethanol is present at such high concentration in the gel that disrupts the SC layer. Moreover, it was observed after the first 30 minutes of gel application in skin that there was still a thin layer of product that didn't evaporate or penetrate. The amount of product present in skin might create some outlier measurements in the outermost layer of skin.

Figure 4.54 presents the NMF and Ibuprofen concentration profile. The NMF concentration can be affected while the product is being absorbed. At 60 and 120 min there's a noticeable change in the

highest amount of NMF present in the SC. The reason might be related to the 30 minutes outlier, since ethanol disrupts the SC and decreases the level of hydration in skin. However, since ethanol is also a very volatile compound, it's visible that this effect only affects the NMF temporarily and it's only present for a short amount of time in skin. After 180 minutes, NMF is restored to baseline values.

The depth profile of ibuprofen in Figure 4.54 illustrates that the ibuprofen concentration decreases with time and that the API has penetrated deeper and with a higher concentration into the skin. However, it was considered that the 180 minutes profile is an outlier, since it doesn't respect Fick's Second Law of Diffusion. After 180 minutes the concentration profile should be lower than the 60 minutes profile, as it is presented by the 120 minutes profile.

Although, the 120 minutes profile should have a lower concentration gradient, the outlier measurement might not be related to the quantification method. Each measurement isn't done in the same location in the arm, thus the reason might just be an uneven application of the gel.

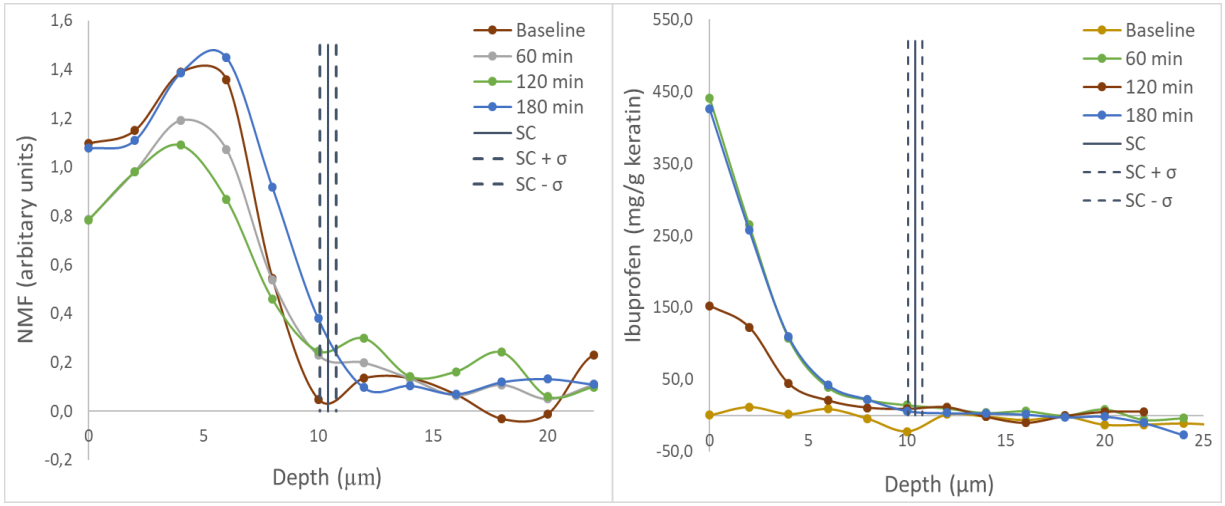

Figure 4.54 - Concentration profiles of NMF (arbitrary units) and ibuprofen (mg per g keratin) in the volar forearm over 3 hours. The thickness of SC was estimated to be 10,415 ± 0,36 µm.

The PG profiles in Figure 4.55 show a consistent concentration gradient, with respect to Fick's Second Law of Diffusion. PG Raman signal illustrates that the concentration decreases with time and that PG penetrates deeper and with a higher concentration into the skin.

Although, PG has a higher concentration than ibuprofen right after product application, PG has a higher permeation since it disperses out of the SC quicker than ibuprofen. Ibuprofen drops 67,8% in concentration between the first and last measurement, and PG drops 74,1% in the same conditions.

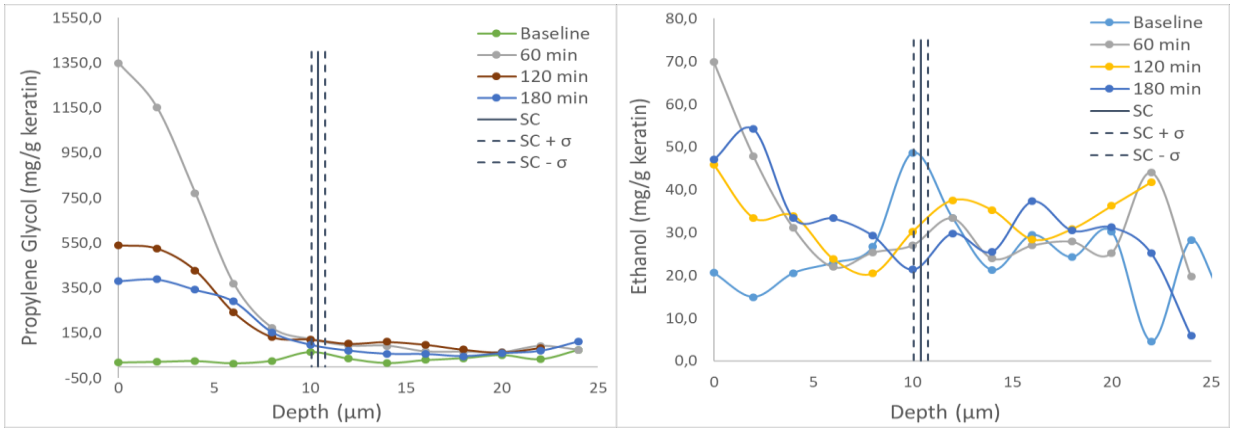

Figure 4.55 - Concentration profiles of PG (mg per g keratin) and ethanol (mg per g keratin) in the volar forearm over 3 hours. The thickness of SC was estimated to be 10,415 ± 0,36 µm.

On the other hand, ethanol profiles in Figure 4.55 don't follow the same type of permeation as the others. The amount of ethanol present in the SC is negligible compared to the baseline profile. The hypothesis state before that ethanol is so volatile that evaporates too quickly to be detected with a cohesive gradient concentration is validated in these ethanol profiles.

This hypothesis doesn't mean that before the 60 minutes measurement, there wasn't any permeation of ethanol. It was already proven that ethanol was at such high concentration in the SC that it might have disturbed every Raman measurement resulting in outliers measurements at 30 minutes.

4.6.2. Oleic Acid

The second product tested is a Marula oil with oleic acid and linoic acid, only oleic acid was calibrated and quantified for these measurements. Marula oil is a nutritive skin care oil, it's rich in anti-oxidants and amount of oleic acid present is around 67,2%. [33]

The NMF profile presented in Figure 4.56 doesn't show any major differences in time and with the application of the product. The 60 minutes measurement isn't consistent with the rest of the profiles, thus it can be considered an outlier profile.

Oleic acid profiles presented in Figure 4.56 show that this API can be detected in the SC with a high concentration after product application, which is expected from its high concentration in the oil itself. Oleic acid concentration in the profile decreases over time and the API penetrates deeper and with a higher concentration into the skin. Since the flux isn't studied in detail in this thesis, there isn't enough information to conclude that oleic acid doesn't permeate deeper into the VE.

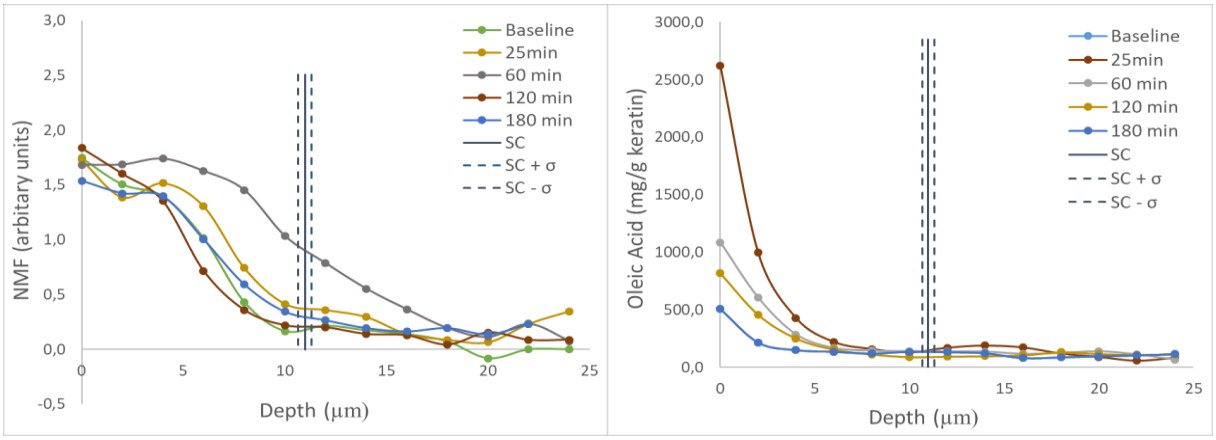

Figure 4.56 - Concentration profiles of NMF (arbitrary units) and oleic acid (mg per g keratin) in the volar forearm over 3 hours. The thickness of SC was estimated to be 11,424 ± 0,33 µm.

4.6.3. Salicylic Acid

The third product tested is an acne cream with 2% w/w salicylic acid (SA) as the API, with PG as a high concentration ingredient in the cream.

The NMF profile presented in Figure 4.57 doesn't show any significant differences in time and with the application of the product, except for the 25 minutes measurement that presents a very high NMF concentration in the SC. Ethanol is the second ingredient listed in the cream and as it was also confirmed in the ibuprofen gel, ethanol can disrupt the SC layer and high concentrations of alcohol in the skin product might lead to outlier Raman measurements.

In the case of PG profile presented in Figure 4.57, PG concentration in the profiles decrease over time and PG penetrates deeper and with a higher concentration into the skin. At 25 minutes measurement the same conclusions are taken, this measurement is an outlier.

After 60 minutes of product application, the PG profiles and gradient concentration are approximately the same. This conclusion doesn't mean that the flux is the same as well. Fick's law states that the flux is proportional to diffusion coefficient and to concentration, which in a steady state can be the same.

The skin isn't a homogenous material, since it's composition can change over time specially after the application of a product. In the case of the SA cream, NMF profile has already proven that the layer of SC in skin suffered a few changes in its composition between measurements. That is, the diffusion rate in skin isn't the same, therefore the flux can be different as well, even though the concentration gradient is approximately the same after 60 minutes of product application.

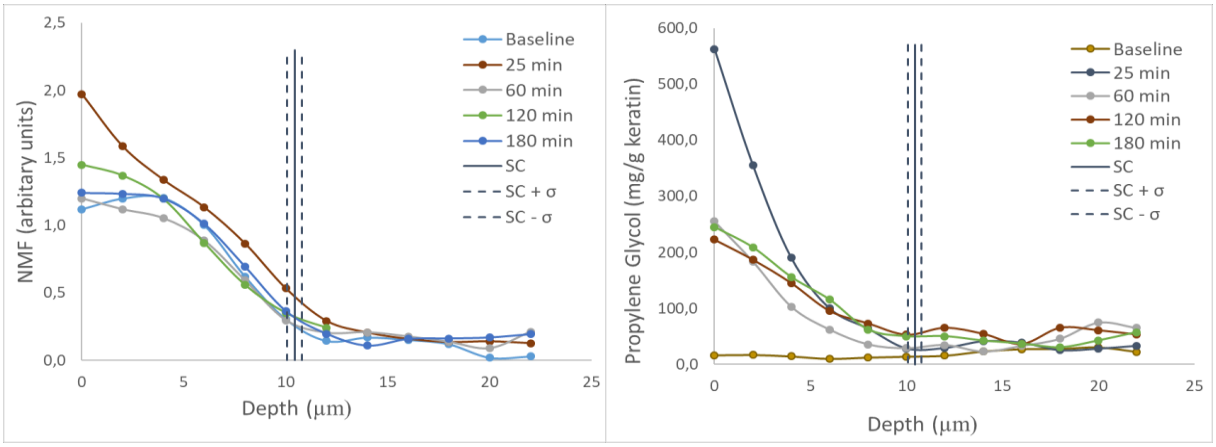

Figure 4.57 - Concentration profiles of NMF (arbitrary units) and PG (mg per g keratin) in the volar forearm over 3 hours. The thickness of SC was estimated to be 10,456 ± 0,36 µm.

The SA profiles presented in Figure 4.58 show a decrease in the concentration gradient over time and the API penetrates deeper and with a higher concentration into the skin. The API might permeate into the VE, since there's still a small difference in concentration when it gets to the SC limit. Since the flux wasn't studied in this chapter, this hypothesis cannot be confirmed.

The measurement at 25 minutes has the highest concentration gradient in the profile, because it's the first measurement after product application this profile can be expected. However, it might be also an outlier measurement as the NMF and PG profile, since the disruption of the SC by alcohol present might affect SA detection as well.

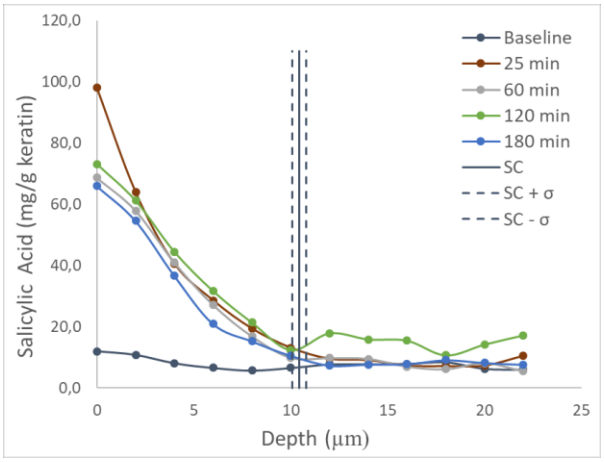

Figure 4.58 - Concentration profiles of salicylic acid (mg per g keratin) in the volar forearm over 3 hours. The thickness of SC was estimated to be 10,456 ± 0,36 µm.

4.6.4. Caffeine

The last product is a caffeine oil, present at 5% w/w, with glycerin (or glycerol) as an ingredient. Caffeine and glycerin were calibrated and quantified for these measurements.

The NMF and glycerin profiles are presented in Figure 4.59. NMF profiles show that there's a change in the NMF concentration with product absorption. The NMF present in the top layer drops to almost zero after product application and gradually increases to normal values. After 3 hours, NMF concentration is in healthy range of NMF values. [5] However, compared to baseline values and to the other three products NMF baseline, this amount of time isn't sufficient to restore the SC layer.

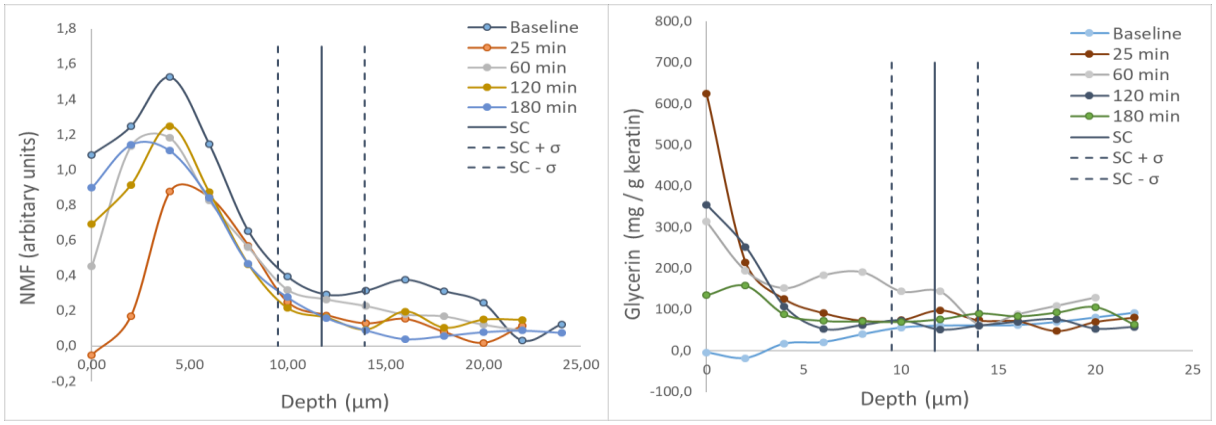

Figure 4.59 - NMF (A.U.) and glycerin (mg/$g_{keratin}$) profiles in the forearm. Thickness of SC is 11,742 ± 2,21 µm.

This oil application causes a higher decrease of NMF compared to the products in this thesis with high amount of alcohol. Even though there's several ingredients present in the oil (such as glycerin; propanediol and hyaluronic acid) that are known to increase hydration in skin. This oil is sold as an eye skin product which claims to promote the looks of puffiness, using caffeine to constrict small blood vessels. Other studies with caffeine in the eye show an increase in hydration, which isn't consistent with the results obtain here. [34]

Glycerin profiles presented in Figure 4.59 show a concentration gradient decrease over time in the SC. After 60 minutes of product application, glycerin penetrates deeper and with a higher concentration into the skin, going through the SC into the VE.

Caffeine profiles presented in Figure 4.60 show a decrease in the concentration gradient over time and the API penetrates deeper and with a higher concentration into the skin. Since the flux wasn't studied in this chapter, there isn't enough information to conclude if caffeine permeates into the VE.

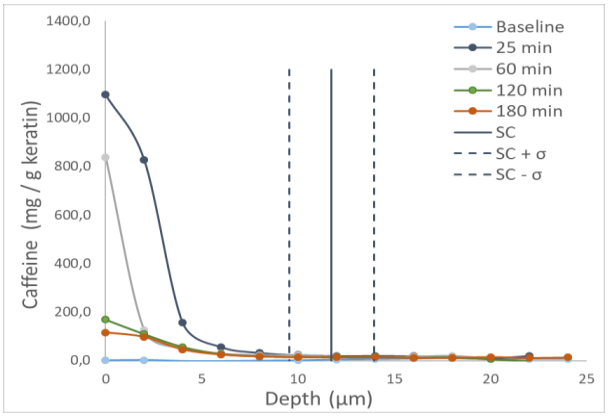

Figure 4.60 - Concentration profiles of caffeine (mg per g keratin) in the volar forearm over 3 hours. The thickness of SC was estimated to be 11,742 ± 2,21 µm.

Chapter 5

Conclusions

5.1. Summary Conclusions

The work developed in this thesis was able to optimize a methodology that enables to quantitively determine the penetration and permeation through skin of compounds that are topically applied. The optimization done was able to achieve an easy to apply method that provides more reliable quantitative results with respect to skin applications, compared to previous studies.

The experimental work developed was completed by different experiments study and data analysis in Matlab, but first a general protocol of solutions preparation for every API calibration was developed, as well as standard Raman conditions were established, to achieve good quality data sets for a viable calibration for every material calibrated in this thesis.

The calibration methodology in this thesis uses the multiple least squares fit method, which uses a personalized fit model for the API that it's being calibrated with four different components: API reference spectrum, clean solvent reference spectrum, quartz spectrum from system calibration and a polynomial fitting for background in the Raman experiment.

The components in the fit model are used to be fitted to the spectra of a series of calibration solutions and this fitting determines the accuracy of the calibration. Therefore, the calibration is highly dependent on the references chosen for this calibration fit model. The main limitation in this method is the subjectivity implied in the fit model created for all API calibrations, since both API and clean solvent reference spectra are processed by the user in the calibration analysis.

Processing those references implies the subtraction of quartz and solvent that is an uncertainty by itself. The user can have guided requirements to optimize the subtraction, but since the real contribution can't be quantified, a perfect subtraction will always have different interpretations depending on the user and the calibration data set chosen. This uncertainty of error was minimized by the type of data analysis and processing done throughout the calibration.

Firstly, manually processing the API reference and inputting its spectrum in the *Quanti* tool minimized the error of having a semi-automatic approach that was previously implemented in the tool, since the previous approach didn't result in a consistent and good quality output.

Secondly, the normalization on standard deviation of the API reference spectrum on the range 550 to 1800 cm^{-1} was crucial to have a robust method with reproducible results. Different types of normalization were also studied and the use of standard deviation yielded the best results.

Moreover, the range of the spectrum that it's used for the standard deviation affects the estimated calibration constant. A study of the range of Raman shift that should be used in the normalization concluded that the 400 to 550 cm^{-1} range is the most sensitive to quartz and water subtraction, resulting in higher variation of the standard deviation of the API reference spectrum. Consequently, this variation will result in a higher variation of the fit coefficients (since they're just scale factors of Raman spectra) and in a higher variation of the calibration constant. Thus, this range of the spectrum was taken out of the normalization, leaving only the 550 to 1800 cm^{-1} range.

The clean solvent spectrum is always normalized on the intensity of the solvent reference spectrum in the library, thus it has indirectly the same type of normalization as the API. All solvents in the library are treated previous as a standard API calibration, therefore all are normalized on standard deviation on the range 550 to 1800 cm^{-1}. This step of solvent spectrum normalization is crucial to link the API calibration to the quantification of keratin in the SC.

After the mathematical optimization of the method was settled, a library of different solvents and APIs was created to validate this optimization and to update previous studies done in water and ethanol.

The first two materials calibrated were BSA and water, since BSA is the link chosen as an approximation to keratin, and it also enables water to be used as a first choice of solvent for new APIs calibration. This calibration was very detailed and personalized, since it's the starting point of the methodology. It was important to guarantee the minimum error of the calibration constant water to keratin, because every new calibrated API is ultimately link to this calibration constant.

The approximation used between BSA and keratin has an error of 15%, while the calibration constant of water to BSA has a relative error of 4,80%. This combination is the highest error of the method, which is the reason that BSA and water experiments were repeated several times to achieve the best quality data set and the optimization done in the method was personalized for this specific calibration.

Ethanol and water have the same type of personalized calibration as BSA, not only because the ethanol reference spectrum doesn't have a straight forward processing as well, but also because ethanol is the number one solvent of choice to dissolve new APIs in this thesis.

The minimization of the relative error of ethanol calibration constant will achieve a more precise and accurate calibration for new APIs. Ethanol calibration resulted in a relative error of 2,74% of the calibration constant of ethanol to water, which demonstrates again the accuracy of this method. These relative errors validate the premise that this analysis and processing techniques results in accurate and precise results, which are reproducible regardless of the subjectivity implied by the user.

An important conclusion was taken with the study of both validation models of BSA/water and ethanol calibration. A personalized fit model for every API calibration has the uncertainty of estimating different calibration constants due to the subjective interpretation of different users and different calibration data set used. This observation doesn't result in the assumption that the variation of the calibration constant is the relative error of the calibration. All calibration constants are linked to their own references spectra in the fit model, which mean that different fit models/calibration constants can result in, approximately, the same quantification of the API in skin.

The correct approach to determine relative errors of calibration constants is to test if the calibration fit model used to estimate the calibration constant is able to preview mass ratios of independent data. This validation study was only completed for BSA in water and ethanol in water calibration, for the reasons mentioned. Since, BSA in water achieve the highest error, it was assumed that every new API calibration has the same error, to estimate the worst-case scenario of a calibration.

All new materials were calibrated with the general API method, using the *Quanti* tool to achieve a simple and easy to apply method. This approach has the approximation that an API solution and solvent spectra have approximately the same amount of quartz, to enable an easier extraction of the

API reference spectrum. Moreover, the clean solvent spectrum is processed automatically using MLSM, which has a higher uncertainty than the manual processing, but it's considered to be negligible.

There's a limitation in this calibration method which is the range of mass ratios of the calibration data set that is viable to use. An API with low solubility can't be calibrated with this method, if the mass ratio is lower than 0,5%. Since the API Raman signal is too low to be considered as a viable calibration. Thus, other types of calibration can be used, but it probably resulted in a higher calibration error. This limitation of the method developed can have a great impact on skin applications, since there are a lot of skin products available in the pharmaceutical market with low solubility.

There are 6 solvents and 19 APIs calibrated in this thesis, a few observations were taken into consideration. Even though the API reference spectrum is processed by extracting the API Raman intensity from the highest concentration API solution, many of the APIs fitting results might still show spectral changes between the API solutions spectra and the API reference spectrum. Resulting in poor fitting of these solutions that can affect the calibration and the estimated constant.

The fact that API molecules interact with the solvent, which disturbs the equilibrium of the intermolecular forces present in the solution can justify this observation. Moreover, the increase in API concentration results in an increase in API molecules that will interact with the solvent, leading to an increase in spectral changes in the Raman spectra of solutions. Thus, choosing the correct range of concentrations is crucial to achieve a good quality calibration and to avoid non-linearity behaviour.

The calibration data sets studied in this thesis had a pattern, it was observed that 3 different solutions with mass ratios between 0,5% to 5% should enable a good quality API calibration, regardless of the solvent chosen. If the API calibration can include more solutions with higher mass ratios, with no spectral shifts in the fitting results, that will result in a better-quality calibration. However, this improvement was considered to be negligible for a standard API calibration.

Although, there were 6 solvents calibrated in this thesis, only four were used to calibrate new APIs: water; ethanol; acetone and MCT oil. These last two were able to validate the premise that the method is not restricted to water and ethanol as solvent choices. Other organic solvents and even oil can be considered as viable choices that result in good quality calibration as well.

5.2. Future Work

This thesis achieved an optimization of a method that can produce more reliable and reproducible results, nevertheless there are a few remarks in the methodology that should be studied further.

The first remark is related to the starting point of this method, which makes an approximation of BSA to keratin, to quantify an API in units of $mg/g_{keratin}$. This approximation with the calibration of BSA in water, as a starter error of 19,80% for any new API that is going to be calibrated.

Other approaches should be studied, this would mean that a different method should be developed with a different starting point. However, using the multiple least squares fit method is still a viable choice for calibrations, since the validation models studied only obtain a relative error of 4,60% and 2,74%. Therefore, the method itself is robust and is able to achieve accurate results.

Another suggestion to improve the overall methodology is to implement an automatic creation of a validation model during an API calibration, enabling a relative error to be estimated for each API. For example, the user should prepare one more solution and the second highest solution in the experimental data set should be taken out of the calibration and should be used to preview its mass ratio, the uncertainty in this value will be the relative error of this API calibration.

References

[1] P. D. a Pudney, M. Mélot, P. J. Caspers, A. Van Der Pol, and G. J. Puppels, "An in vivo confocal Raman study of the delivery of trans retinol to the skin.," *Appl. Spectrosc.*, vol. 61, no. 8, pp. 804–811, 2007.

[2] P. J. Caspers, G. W. Lucassen, R. Wolthuis, H. A. Bruining, and G. J. Puppels, "In vitro and in vivo Raman spectroscopy of human skin.," *Biospectroscopy*, vol. 4, no. 5 Suppl, pp. S31-9, 1998.

[3] A. Van Der Pol, W. M. Riggs, and P. J. Caspers, "In vivo Raman Confocal Microspectroscopy of Skin," *Pharm. Appl. Raman Spectrosc.*, pp. 193–221, 2007.

[4] P. J. Caspers, G. W. Lucassen, E. A. Carter, H. A. Bruining, and G. J. Puppels, "In vivo confocal raman microspectroscopy of the skin: Noninvasive determination of molecular concentration profiles," *J. Invest. Dermatol.*, vol. 116, no. 3, pp. 434–442, 2001.

[5] P. Caspers, *In vivo Skin Characterization by Confocal Raman Microspectroscopy*. 2003.

[6] A. C. Williams, H. G. M. Edwards, E. E. Lawson, and B. W. Barry, "Molecular interactions between the penetration enhancer 1,8-cineole and human skin," *J. Raman Spectrosc.*, vol. 37, no. 1–3, pp. 361–366, 2006.

[7] P. Caspers *et al.*, "Monitoring the Penetration Enhancer Dimethyl Sulfoxide in Human Stratum Corneum in Vivo by Confocal Raman Spectroscopy," *Pharm. Res.*, vol. 19, no. 10, pp. 1577–1580, 2002.

[8] P. Larkin, *Infrared and Raman Spectroscopy; Principles and Spectral Interpretation*. 2011.

[9] D. A. Long, *Introductory Raman Spectroscopy*, vol. 36, no. 10. 2005.

[10] M. Egawa and H. Iwaki, "In vivo evaluation of the protective capacity of sunscreen by monitoring urocanic acid isomer in the stratum corneum using Raman spectroscopy," *Ski. Res. Technol.*, vol. 14, no. 4, pp. 410–417, 2008.

[11] H. C. Broding, A. Van Der Pol, J. De Sterke, C. Monsé, M. Fartsch, and T. Brüing, "In vivo Monitoring of epidermal absorption of hazardous substances by confocal Raman micro-spectroscopy," *JDDG - J. Ger. Soc. Dermatology*, vol. 9, no. 8, pp. 618–627, 2011.

[12] W. F. Murphy, "Modern spectroscopy," *Vib. Spectrosc.*, vol. 4, p. 261, 1993.

[13] D.-W. Sun, *Infrared spectroscopy for food quality analysis and control*. 2009.

[14] E. Smith and G. Dent, *Modern Raman Spectrocopy: A Practical Approach*. 2005.

[15] R. S. Das and Y. K. Agrawal, "Raman spectroscopy: Recent advancements, techniques and applications," *Vib. Spectrosc.*, vol. 57, no. 2, pp. 163–176, 2011.

[16] R. Ian and G. M. Howell, "Handbook of Raman Spectroscopy," *Lewis, Ian R. Edwards, Howell G. M.* p. 1049, 2001.

[17] Imperial College London, "Raman Spectroscopy." [Online]. Available: http://www.bodyyouknow.org/raman-spectroscopy.

[18] J. A. McGrath, R. A. J. Eady, and F. M. Pope, “Anatomy and Organization of Human Skin,” *Rook’s Textb. Dermatology*, pp. 45–128, 2004.

[19] P. M. Elias, “Skin Barrier Function Peter,” *Curr Allergy Asthma Rep.*, vol. 14, no. 4, pp. 299–305, 2008.

[20] W. Montagna and P. F. Parakka, *The Structure and Function of Skin*, vol. 44, no. 1. 1974.

[21] R. R. Wickett and M. O. Visscher, “Structure and function of the epidermal barrier,” *Am. J. Infect. Control*, vol. 34, no. 10 SUPPL., pp. 98–110, 2006.

[22] J. M. Jungersted, L. I. Hellgren, G. B. E. Jemec, and T. Agner, “Lipids and skin barrier function – a clinical perspective,” *Contact Dermatitis*, vol. 58, no. 5, pp. 255–262, 2008.

[23] A. Idrissi, S. Longelin, and F. Sokolic, “Study of Aqueous Acetone Solution at Various Concentrations: Low-Frequency Raman and Molecular Dynamics Simulations,” *J. Phys. Condens. Matter*, vol. 16, no. 5, pp. S429–S453, 2001.

[24] Y. Numata, Y. Iida, and H. Tanaka, “Quantitative analysis of alcohol-water binary solutions using Raman spectroscopy,” *J. Quant. Spectrosc. Radiat. Transf.*, vol. 112, no. 6, pp. 1043–1049, 2011.

[25] M. S. C. S. Santos, J. Carlos, and R. Reis, “Thermodynamic evaluation of molar surface area and thickness of water + ethanol mixtures,” *J. Mol. Liq.*, vol. 255, pp. 419–428, 2018.

[26] J. Jayabharathi, K. Jayamoorthy, V. Thanikachalam, and R. Sathishkumar, “Fluorescence quenching of bovine serum albumin by NNMB,” *Spectrochim. Acta - Part A Mol. Biomol. Spectrosc.*, vol. 108, pp. 146–150, 2013.

[27] J. Clarkson, Z. Cui, and R. Darton, “Protein Denaturation in Foam.,” *J. Colloid Interface Sci.*, vol. 215, no. 2, pp. 333–338, 1999.

[28] S. Damodaran and K. B. Song, “Kinetics of adsorption of proteins at interfaces: role of protein conformation in diffusional adsorption,” *Biochim. Biophys. Acta (BBA)/Protein Struct. Mol.*, vol. 954, no. C, pp. 253–264, 1988.

[29] Malvern Panalytica, “Understanding the conformational stability of protein therapeutics using Raman spectroscopy,” 2014.

[30] H. Zhu, Y. Li, S. Vdović, S. Long, G. He, and Q. Guo, “Femtosecond coherent anti-Stokes Raman scattering spectroscopy of hydrogen bonded structure in water and aqueous solutions,” *Spectrochim. Acta - Part A Mol. Biomol. Spectrosc.*, vol. 151, pp. 262–273, 2015.

[31] K. Kamogawa and T. Kitagawa, “Raman Difference Spectroscopy of the C-H Stretching Vibrations : Frequency Shifts and Excess Quantities for Acetonelwater and AcetonitrilelWater Solutions,” vol. 395, no. 1978, pp. 1077–1081, 1986.

[32] S. Mitragotri *et al.*, “Mathematical models of skin permeability: An overview,” *Int. J. Pharm.*, vol. 418, no. 1, pp. 115–129, 2011.

[33] A. A. Mariod, B. Matthäus, Y. M. A. Idris, and S. I. Abdelwahab, “Fatty acids, tocopherols, phenolics and the antimicrobial effect of Sclerocarya birrea kernels with different harvesting dates,” *JAOCS, J. Am. Oil Chem. Soc.*, vol. 87, no. 4, pp. 377–384, 2010.

[34] M. Shatalebi and F. Ahmadraji, “Evaluation of the clinical efficacy and safety of an eye counter pad containing caffeine and vitamin K in emulsified Emu oil base,” *Adv. Biomed. Res.*, vol. 4, no. 1, p. 10, 2015.

[35] Horiba Jobin Yvon, “Raman Data and Analysis,” 2017. [Online]. Available: http://www.horiba.com/fileadmin/uploads/Scientific/Documents/Raman/bands.pdf.

Appendix I

Table I - Functional Groups in Raman Spectra by region and intensity. [35]

Functional Group/ Vibration	Region	Raman
Lattice vibrations in crystals, LA modes	10 - 200 cm^{-1}	strong
δ(CC) aliphatic chains	250 - 400 cm^{-1}	strong
υ(Se-Se)	290 -330 cm^{-1}	strong
υ(S-S)	430 -550 cm^{-1}	strong
υ(Si-O-Si)	450 -550 cm^{-1}	strong
υ(Xmetal-O)	150-450 cm^{-1}	strong
υ(C-I)	480 - 660 cm^{-1}	strong
υ(C-Br)	500 - 700 cm^{-1}	strong
υ(C-Cl)	550 - 800 cm^{-1}	strong
υ(C-S) aliphatic	630 - 790 cm^{-1}	strong
υ(C-S) aromatic	1080 - 1100 cm^{-1}	strong
υ(O-O)	845 -900 cm^{-1}	strong
υ(C-O-C)	800 -970 cm^{-1}	medium
υ(C-O-C) asym	1060 - 1150 cm^{-1}	weak
υ(CC) alicyclic, aliphatic chain vibrations	600 - 1300 cm^{-1}	medium
υ(C=S)	1000 - 1250 cm^{-1}	strong
υ(CC) aromatic ring chain vibrations	*1580, 1600 cm^{-1}	strong
	*1450, 1500 cm^{-1}	medium
	*1000 cm^{-1}	strong/medium
δ(CH3)	1380 cm^{-1}	medium
δ(CH2) δ(CH3) asym	1400 - 1470 cm^{-1}	medium
δ(CH2) δ(CH3) asym	1400 - 1470 cm^{-1}	medium
υ(C-(NO2))	1340 - 1380 cm^{-1}	strong
υ(C-(NO2)) asym	1530 - 1590 cm^{-1}	medium
υ(N=N) aromatic	1410 - 1440 cm^{-1}	medium
υ(N=N) aliphatic	1550 - 1580 cm^{-1}	medium
δ(H2O)	~1640 cm^{-1}	weak broad
υ(C=N)	1610 - 1680 cm^{-1}	strong
υ(C=C)	1500 - 1900 cm^{-1}	strong
υ(C=O)	1680 - 1820 cm^{-1}	medium
υ(C≅C)	2100 - 2250 cm^{-1}	strong
υ(C≅N)	2220 - 2255 cm^{-1}	medium
υ(-S-H)	2550 - 2600 cm^{-1}	strong
υ(C–H)	2800 - 3000 cm^{-1}	strong
υ(=(C-H))	3000 - 3100 cm^{-1}	strong
υ(≅(C-H))	3300 cm^{-1}	weak
υ(N-H)	3300 - 3500 cm^{-1}	medium
υ(O-H)	3100 - 3650 cm^{-1}	weak

Appendix II

Table II - APIs and solvents that were calibrated in this thesis to develop a methodology for penetration and permeation of topically applied compound with APIs.

Chemical Name	CAS.No	Purity	Distributor
		Solvents	
Acetone	67-64-1	≥ 99,9%	Lab Honeywell, Germany
MCT Oil			
Distilled water			
Ethanol	64-17-5	≥ 99,8% (v/v)	Acros Organics, Belgium
Glycerine	56-81-5		Sigma-Aldrich, The Netherlands
Propylene-glycol	57-55-6		Sigma-Aldrich, The Netherlands
		APIs	
2-Pyrrolidone-5-carboxylic acid	149-87-1		Sigma-Aldrich, The Netherlands
3-Methylsalicylic Acid	83-40-9	≥ 97%	Sigma-Aldrich, The Netherlands
4-Methylsalicylic Acid	50-85-1	≥ 99%	Sigma-Aldrich, The Netherlands
5-Methylsalicylic Acid	89-56-5	≥ 98%	Sigma-Aldrich, The Netherlands
β-carotene	7235-40-7		Sigma-Aldrich, The Netherlands
Bovine Serum Albumin	9048-46-8	≥ 98%	Sigma-Aldrich, The Netherlands
Caffeine	58-08-2		Sigma-Aldrich, The Netherlands
Hydrocortisone	50-23-7	≥ 98%	Sigma-Aldrich, The Netherlands
Ibuprofen	15687-27-1		Sigma-Aldrich, The Netherlands
Lidocaine	137-58-6		Sigma-Aldrich, The Netherlands
Methyl Salicylate	119-36-8	≥ 99%	Sigma-Aldrich, The Netherlands
Oleic Acid	112-80-1	≥ 99%	Sigma-Aldrich, The Netherlands
Retinol	68-26-8		Sigma-Aldrich, The Netherlands
Salicylic Acid	69-72-7	≥ 99%	Sigma-Aldrich, The Netherlands
Testosterone	58-22-0	≥ 99%	Sigma-Aldrich, The Netherlands
Ubiquinol			Kaneka Nutrients, Japan

Appendix III

General protocol was standardized for data collection for an API calibration experiment, following the steps of solutions preparations:

i. All the materials to be used in this experiment should be disinfected with 70% ethanol. Test tubes and pipette's tips should be sterile;

ii. The screws to be used as recipient of the API solution should be polish before the experiment. The ideal size of the screws is M4x6.

iii. The balance must be calibrated before the experiment.

iv. The calibration of a new material should be done, ideally, with at least three to four solutions with different mass ratios. All the solutions and the pure solvent should be measured in the same day for a good calibration of the material.

v. The material – API – should be weight first, avoid any material attached to the wall of the tube, leaving all at the bottom of the test tube (this is especially important for volatile materials). After weighting the material, the balance should stabilize before advance to the next step.

vi. Add the solvent to the test tube until the total solution mass is reached for the mass ratio chosen.

   a. The solutions prepared should have at least the minimum concentration higher than 0,5%. If not, the overall measurement time of the solutions should be higher - by increasing the number of frames collected - to increase the signal to noise ratio.

vii. The solution should be dissolved until it's homogenous.

   b. Depending on the material, it might be necessary to have the solutions on a roller block for a required time or to leave the solutions in a warm bath to increase solubility.

viii. A drop of the solution should be put inside the screw. The drop shouldn't be too big, otherwise it will spill out of the screw when in contact with the window. If it's too small, the drop might not be detected at 30 microns above the window or it'll evaporate during measurement.

ix. Between measurements, the window of the Skin Analyzer should be clean with two swipes of ethanol 70% and the screw should be clean inside with a tissue soaked with ethanol, then left for a few minutes in a goblet cup with 70% ethanol solution. After this disinfection step, the screws should be left to dry of completely, otherwise ethanol from the disinfection might contaminate the next measurement.

x. For conditions measurements, a fixed depth should be chosen, ideally 30 microns above window. All the solutions and solvent should be measured with 5 seconds exposure time to optimize the quality of the spectrum. Generally, if the solvent is water, data sets should have 100 or 200 frames, depending on the quality of each. Increasing the number of frames to 200 frames might be necessary to decrease the noise in the averaged measurements, depending on the material used. However, if the solvent has a very high intensity spectrum, e.g. ethanol or acetone, 100 frames per measurement should be sufficient.

c. All frames should have, approximately, the same intensity. For volatile solvents, such as ethanol, if the solvent starts to evaporate during the measurement, it's visible in the last frames that the solvent peaks start to diminish, and the material peaks might be higher because of the evaporation comparing to the first measurements.

   If this happens, the spectrum should be considered an outlier. If the second repetition of the measurement doesn't give a good quality spectrum, the drop in the screw might not be well placed or the number of frames might need to be diminished to guarantee that the measurement is done before the solvent starts to evaporate.

xi. Evaluate each spectrum of the measurements, if the spectrum has bad quality repeat the measurement with a new drop of the solution prepared. If the problem is persistent with the repetition of the measurement, a new solution should be prepared or the chosen mass ratio should be reviewed.

xii. As an extra step, the pure material can be measured with the same conditions as the API solutions to help in the data analysis of the calibration.

Additional Remarks

The BSA Solutions need an extra step in the general API Protocol, since there's the risk of protein denaturation during the preparation of these solutions.

While adding water to achieve the total mass of the solution, the tip of the pipette should be pointed to the wall of the test tube to avoid any foam or bubbles. The BSA solutions should be left on a roller block for 24 hours to dissolve the material. Avoid rough or abrupt handling of the test tube to avoid denaturation of the protein. When foam is formed, it's an indicative of the denaturation of the protein.

After the dissolution, the solution should be completely homogenous before the measurements. And before each measurement, the solution should rest still for at least 20 min in the rack to avoid any collection of any particles in suspension.

Appendix IV

A few quality requirements must be taken into consideration to achieve a good quality API reference spectrum.

1. The difference spectrum, which will be the API reference spectrum, should not contain any negative intensity. If so, the value of the solvent factor is too high and should be decreased;
2. If the solvent doesn't have any common peaks with the API, a good range of values for the solvent scaling factor should represent in the spectrum no peaks in the same Raman shift. And if there is no contribution of background in the solution spectrum, in theory, in the Raman shifts of those peaks, the reference spectrum should have, approximately, zero in intensity;
3. If there is a significant presence of background in the difference spectrum, that spectrum can be used as a start point for extraction of the reference spectrum, however, the spectrum would need an extra manually step of processing in Matlab that takes out the background in the spectrum;
4. The highest concentration solution should be used to extract the API reference spectrum, because it results in a spectrum with a least amount of noise, since it has the highest intensity contribution of API from all the solutions of the data set. A few exceptions should be considered:
    a. Depending on the solvent used, especially for organic solvents such as ethanol or acetone, there might be shifts between the solution and the solvent measurements, which lead to two high steeps in the difference spectrum in the same Raman shift as the main peaks of the solvent. Depending on the data set, choosing a lower concentration solution as a new reference, might not display as many shifts, leading to a good quality API reference spectrum. However, this API reference spectrum from a lower concentration solution should still meet the requirement of having very low amount of noise to API signal ratio, therefore is not advised to choose the lowest concentration solution of the data set.
    b. The solution should result in a good fit for the API solutions, but if it doesn't then this step should be repeated to extract a different API reference;
5. If none of the solutions leads to a good quality API reference spectrum, the difference spectrum of the highest concentration should be further processed in Matlab to remove the high steeps from the solvent's shifts or any other artefact and background from the spectrum or it should be processed like BSA and ethanol, the user must choose which way does the reference need to be edited.
6. Remarks: The general approximation done with this method compared to the BSA and ethanol calibration was not treating the solvent and quartz intensity contribution as independent factors in the API solution. This way it's assumed that the quartz of the solvent measurement will be, approximately, the same as the API solution measurement. Therefore, by subtracting the solvent measurement from the API solution spectrum, there's a simultaneous subtraction of solvent and quartz from the API solution.

Appendix V

Table III - Summary of all materials calibration studied in this thesis

Chemical Name	*Solvent*	$\frac{c_{RefAPI}}{c_{RefSolvent}}$	$\frac{c_{RefAPI}}{c_{RefKeratin}}$	$Quant.Factor_{API}$	$Error_{Q.F.}$
			Solvents		
Acetone	Water	23,238	$8{,}569 \times 10^{5}$	$1{,}167 \times 10^{-6}$	$\pm 24{,}59\%$
MCT Oil	Ethanol	0,767	$5{,}441 \times 10^{5}$	$1{,}838 \times 10^{-6}$	$\pm 27{,}33\%$
Water	--	0,089	$3{,}036 \times 10^{4}$	$3{,}294 \times 10^{-5}$	$\pm 19{,}80\%$
Ethanol	Water	23,378	$7{,}097 \times 10^{5}$	$1{,}409 \times 10^{-6}$	$\pm 22{,}53\%$
Glycerine	Water	11,828	$3{,}591 \times 10^{5}$	$2{,}785 \times 10^{-6}$	$\pm 24{,}59\%$
Propylene-glycol	Water	15,030	$4{,}562 \times 10^{5}$	$2{,}192 \times 10^{-6}$	$\pm 24{,}59\%$
			APIs		
2-Pyrrolidone-5-carboxylic acid	Water	14,591	$4{,}429 \times 10^{5}$	$2{,}258 \times 10^{-6}$	$\pm 24{,}59\%$
3-Methylsalicylic Acid	Ethanol	1,990	$1{,}412 \times 10^{6}$	$7{,}081 \times 10^{-7}$	$\pm 27{,}33\%$
4-Methylsalicylic Acid	Ethanol	2,505	$1{,}778 \times 10^{6}$	$6{,}626 \times 10^{-7}$	$\pm 27{,}33\%$
5-Methylsalicylic Acid	Ethanol	2,253	$1{,}599 \times 10^{6}$	$6{,}254 \times 10^{-7}$	$\pm 27{,}33\%$
β-carotene	Ethanol	203,235	$1{,}442 \times 10^{8}$	$6{,}934 \times 10^{-9}$	$\pm 27{,}33\%$
Bovine Serum Albumin	Water	11,256	$3{,}417 \times 10^{-5}$	$2{,}927 \times 10^{4}$	$\pm 15{,}00\%$
Caffeine	Water	46,021	$1{,}397 \times 10^{6}$	$7{,}158 \times 10^{-7}$	$\pm 24{,}59\%$
Chemical UV filter I	MCT Oil	28,151	$1{,}532 \times 10^{7}$	$6{,}529 \times 10^{-8}$	$\pm 32{,}13\%$
Chemical UV filter II	Ethanol	6,024	$4{,}275 \times 10^{7}$	$2{,}339 \times 10^{-6}$	$\pm 27{,}33\%$
Hydrocortisone	Ethanol	1,522	$1{,}080 \times 10^{6}$	$9{,}257 \times 10^{-7}$	$\pm 27{,}33\%$
Ibuprofen	Ethanol	1,168	$8{,}287 \times 10^{5}$	$1{,}207 \times 10^{-6}$	$\pm 27{,}33\%$
Lidocaine	Ethanol	1,007	$7{,}148 \times 10^{5}$	$1{,}399 \times 10^{-6}$	$\pm 27{,}33\%$
Methyl Salicylate	Ethanol	3,168	$2{,}248 \times 10^{6}$	$4{,}448 \times 10^{-7}$	$\pm 27{,}33\%$
Oleic Acid	Ethanol	0,925	$6{,}564 \times 10^{5}$	$1{,}524 \times 10^{-6}$	$\pm 27{,}33\%$
Retinol	Ethanol	35,794	$2{,}540 \times 10^{7}$	$3{,}937 \times 10^{-8}$	$\pm 27{,}33\%$
Salicylic Acid	Ethanol	2,631	$1{,}867 \times 10^{6}$	$5{,}356 \times 10^{-7}$	$\pm 27{,}33\%$
Testosterone	Ethanol	1,888	$1{,}340 \times 10^{6}$	$7{,}464 \times 10^{-7}$	$\pm 27{,}33\%$
Ubiquinol	Acetone	2,070	$1{,}774 \times 10^{6}$	$5{,}536 \times 10^{-7}$	$\pm 29{,}39\%$

Appendix VI

This appendix has all other APIs reference spectra that were studied in this thesis, but its results were not shown in chapter 4.

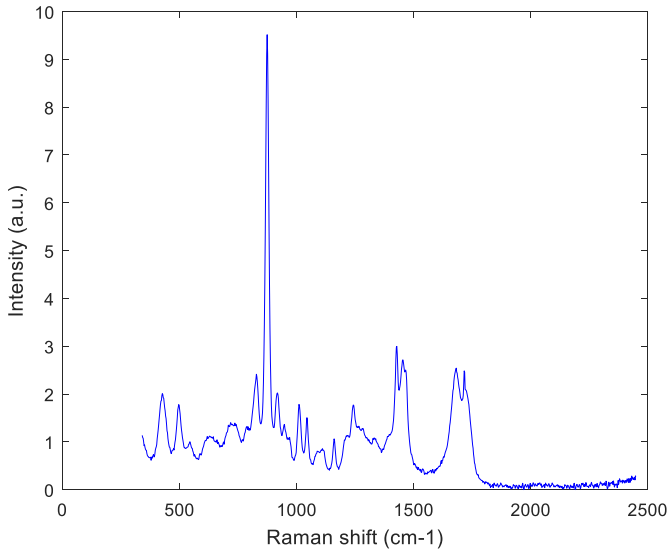

Figure I - 2-Pyrrolidone-5-carboxylic acid normalized reference spectrum.

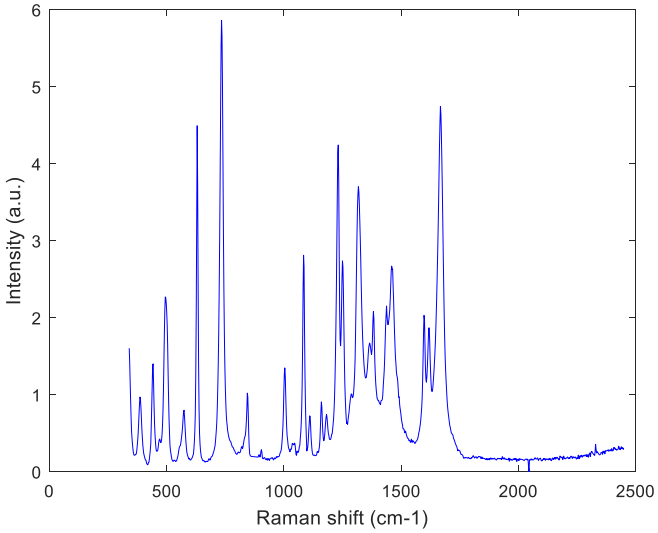

Figure II - 3-Methyl Salicylic Acid normalized reference spectrum.

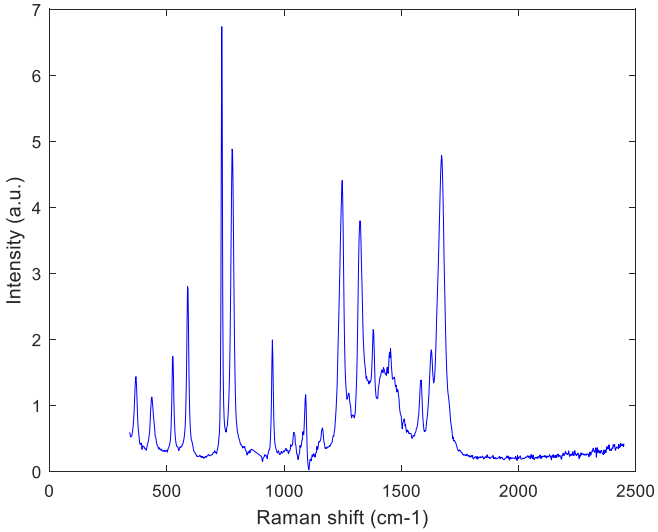

Figure III - 4-Methyl Salicylic Acid normalized reference spectrum.

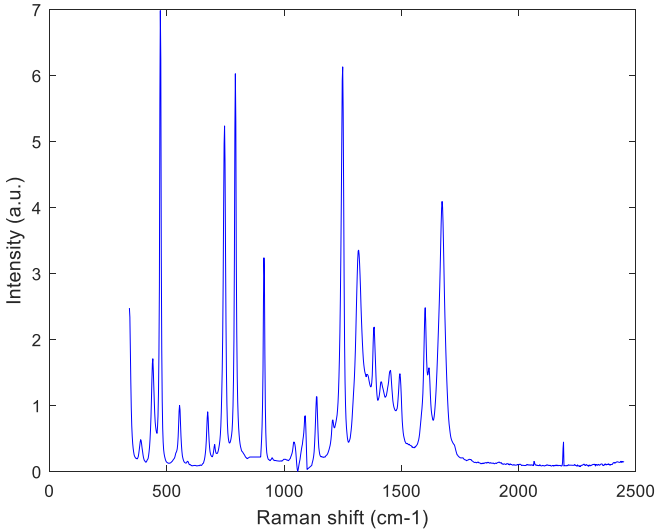

Figure IV - 5-Methyl Salicylic Acid normalized reference spectrum.

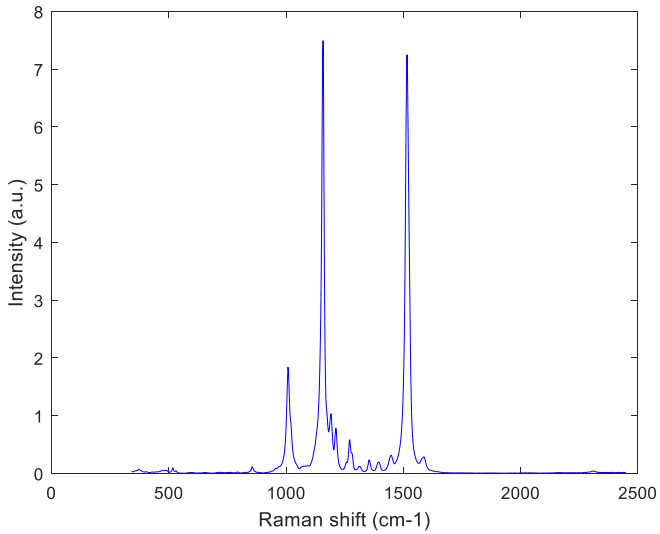

Figure V – beta-carotene normalized reference spectrum used in calibration.

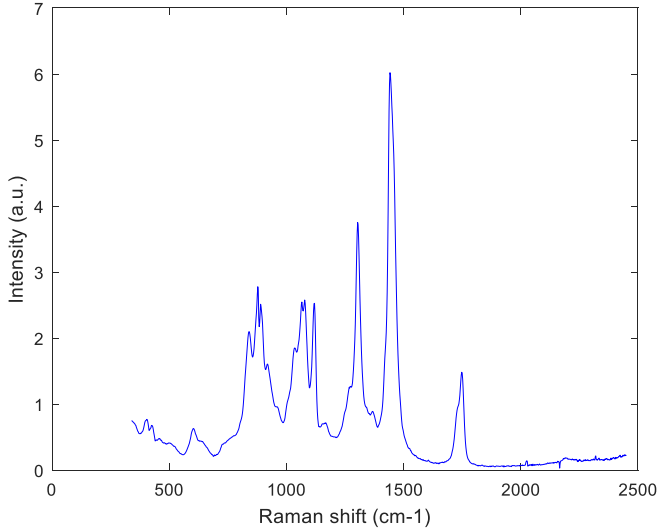

Figure VI – MCT oil normalized reference spectrum used in calibration.

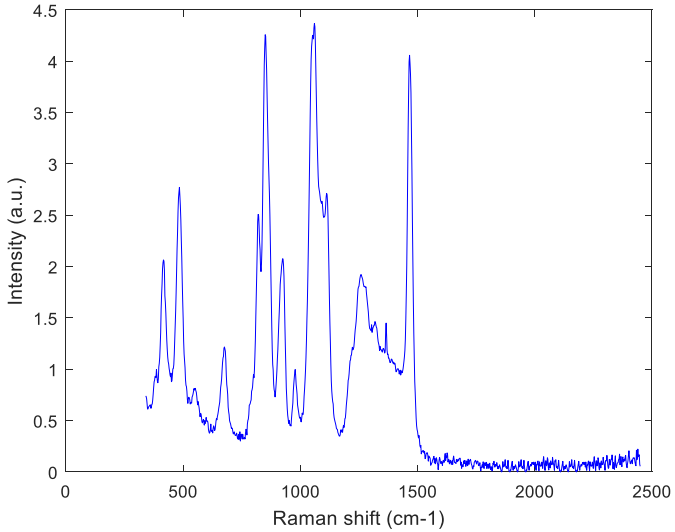

Figure VII – Glycerol normalized reference spectrum used in calibration.

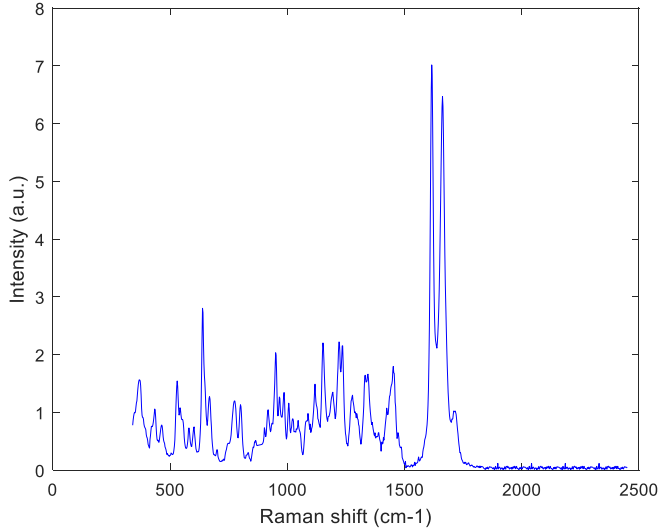

Figure VIII – Hydrocortisone normalized reference spectrum used in calibration.

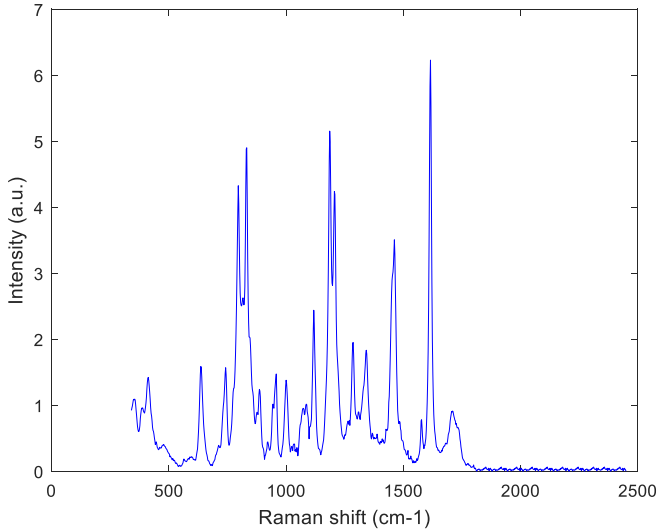

Figure IX – Ibuprofen normalized reference spectrum used in calibration.

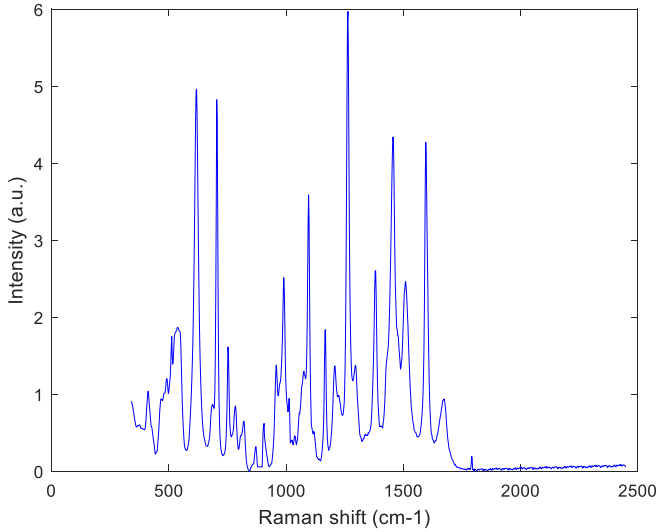

Figure X – Lidocaine normalized reference spectrum used in calibration.

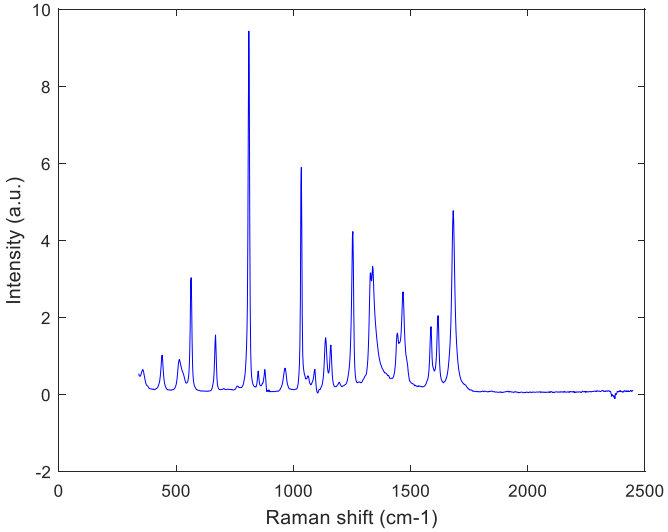

Figure XI – Methyl Salicylate normalized reference spectrum used in calibration.

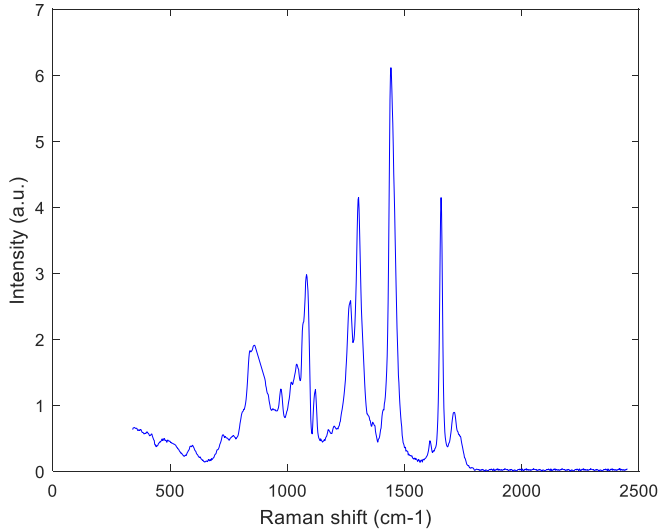

Figure XII – Oleic Acid normalized reference spectrum used in calibration.

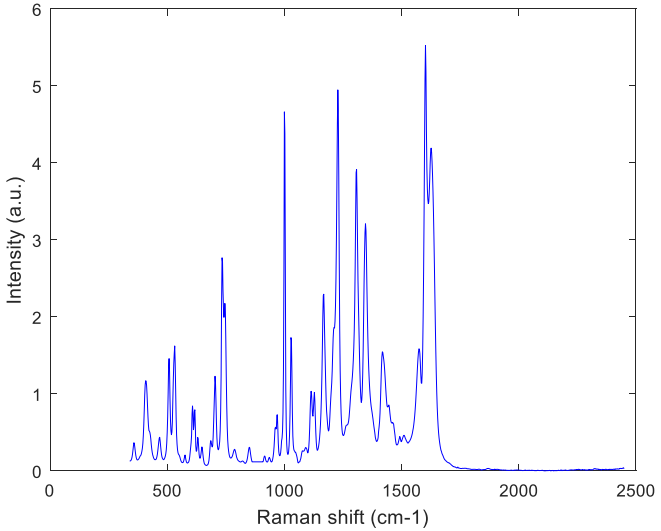

Figure XIII – Chemical UV filter II normalized reference spectrum used in calibration.

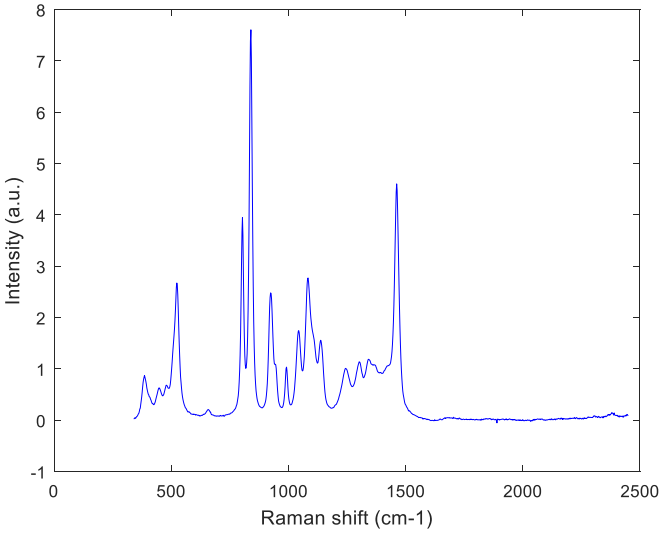

Figure XIV – PG normalized reference spectrum used in calibration.

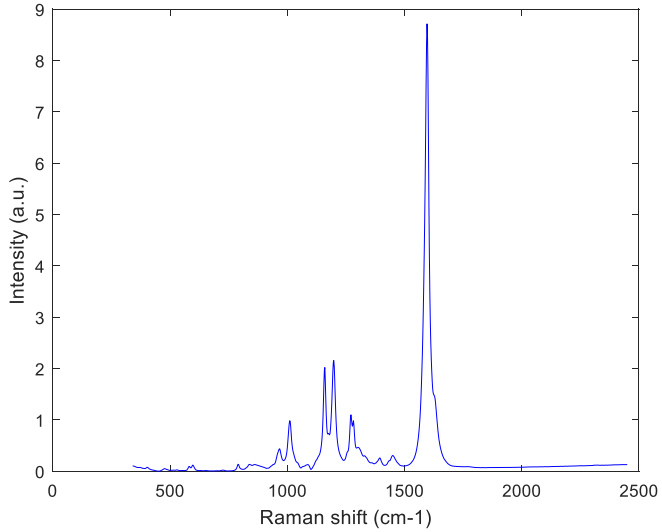

Figure XV – Retinol normalized reference spectrum used in calibration.

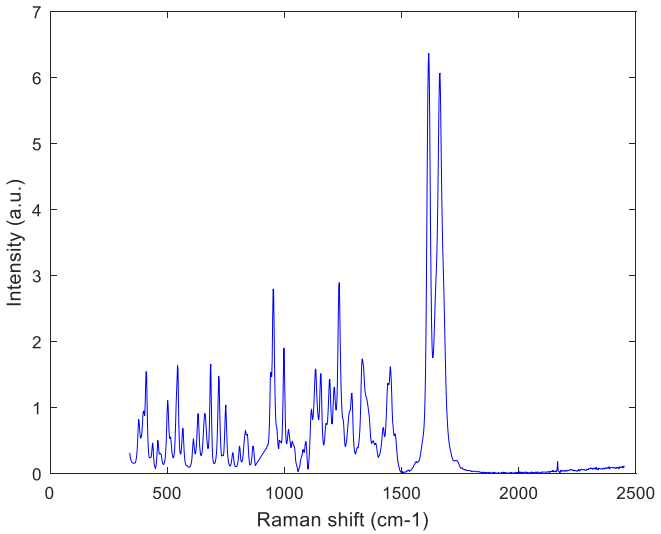

Figure XVI – Testosterone normalized reference spectrum used in calibration.